Report 2

Object: Targeting, exploration, interpretation and understanding of geothermal sites in Tasmania, Australia, including the area known as the Tamar Conductivity Zone (TCZ).

by Adele Manzella Pisa, 10th January 2008

Introduction

I received data in the form of edi files, containing the sprecta resulting from the already performed data analysis, and time series data. Data have been recorded in difficult condition, because the natural signal has been very weak in the recording period, as I experienced myself in my fieldwork. By luck, the noise sources have been not so extensive and the noise only seldom covered the natural signal. As long as the signal is periodic and in form of spikes, codes such as the one used for the standard analysis provide good result. In the few cases where the noise has been particularly strong, such as for some of the eastern sites in the Northern Profile it would be useful to test some other code performing a very robust analysis in remote reference mode. I tried to read and process data but the routine I have for reading refer to an old version of the software and I could not do any test. If one troublesome site data (such as NTL033) and the corresponding remote site data can be provided in ascii format I could try to test if the code I usually use is able to provide better data.

However, data are in most case of such an excellent quality that I could perform this study even without applying a specific robust processing.

Decomposition: theory in brief

In a stratified medium, the 1D case, resistivity changes only with depth and the impedance tensor is independent of the measurement orientation of the field components, the two polarization curves, i.e., *xy* or *yx* curves, are the same.

In the 2D case, geoelectrical changes occur with depth as well as in a direction perpendicular to the geologic strike direction. Maxwell equation's can be decoupled into two different polarization modes, TE and TM with respect to the electrical strike direction. The TE mode (transverse electric) is defined when the horizontal component of the electric field E is parallel to the strike direction and the horizontal magnetic field H is perpendicular. Conversely, the TM mode (transverse magnetic) is defined when the horizontal magnetic field H is parallel to the strike direction and E is perpendicular.

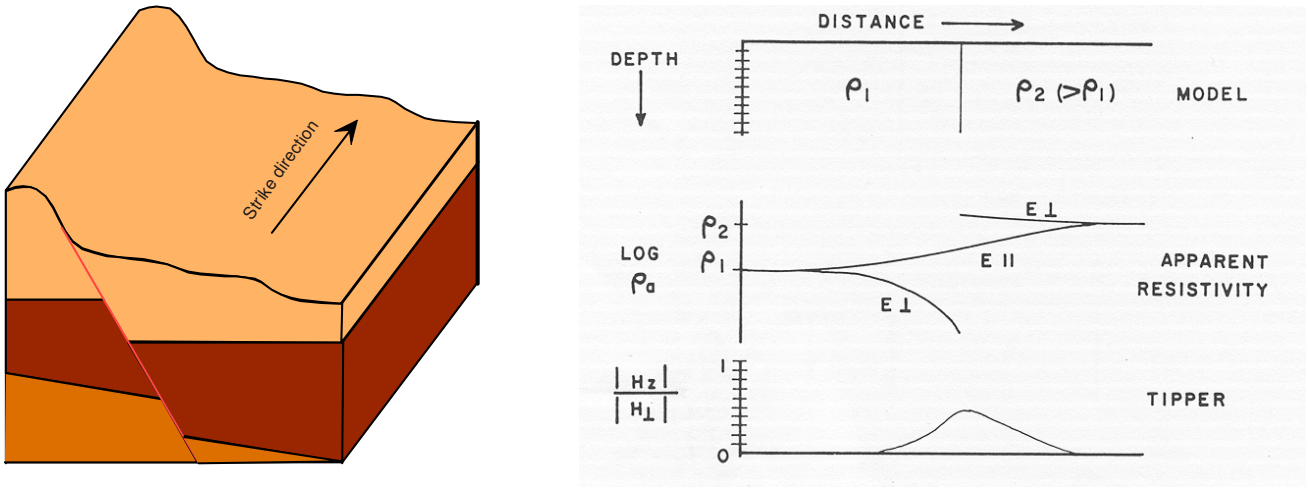

Figure 1. An example of 2D structure and strike direction (left) and a schematic variation of E field amplitude around a lateral discontinuity.

Thanks to the 2D boundary conditions many information may be achieved with few data site. The current density of E parallel to the strike ($E_{||}$, corresponding to TE) is continuous, whereas the current density of E orthogonal to strike ($E_{\perp}$, corresponding to TM) is not. The same for impedance and hence for resistivity. Therefore, the situation may be depicted as in Fig. 1. In principle, with just one site it is possible to define the strike direction, the resistivity distribution below the site as well as a rough estimation of the resistivity beyond the lateral discontinuity.

When measurements are not performed along the electrical strike direction, the latter can be defined computing the direction for which the diagonal impedance values are maximum(Swift 1967) and by trigonometric rotation TE and TM curves can be retrieved. Starting from a tensor impedance which is derived from measurements, and assuming 2D conditions, several different means have been used to find the rotation angle θ_0 between measurement direction and strike. One of these is to rotate the impedence in steps (say 5 degrees), plot them on a polar diagram, and pick an optimum angle from the plots. An optimum angle maximizes or minimizes some combination of the impedence components. These interesting diagrams, called *polar figures* or *impedance polar diagrams,* are usually plotted at many frequencies, because in practice the strike direction often changes with depth. When polar diagram ellipses show a round shape they define an almost 1D condition, whereas elongated magnitude polar diagrams define 2D or 3D condition. Figure 2 shows polar plots for almost 1D (polar diagrams 1 and 4) and a 2-D (polar diagrams 2 and 3) structure.

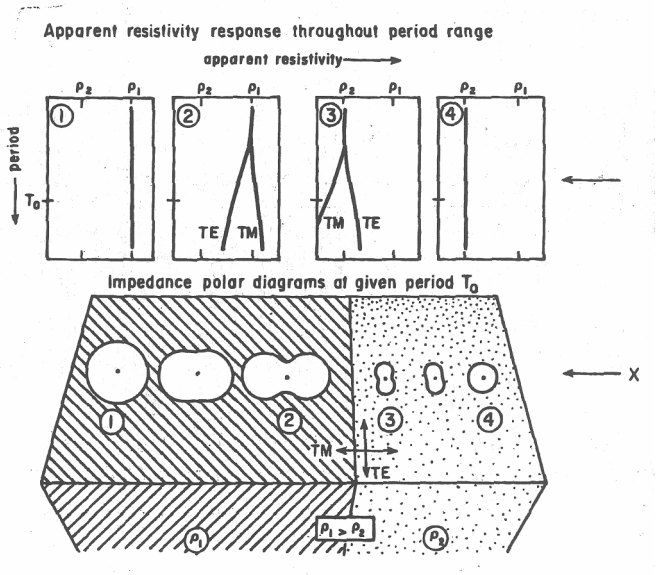

Fig. 2 Impedance polar diagrams (Z_{xy} only, *at one frequency) and apparent resistivities, at four sites on a simple 2-D contact model. (TE and TM refer to Transverse electric (**E** parallel to strike) and Transverse Magnetic (**H** parallel to strike) field polarizations, respectively.*

The 3D case represents the most general type of geoelectrical structure where resistivity changes in all directions and the impedance tensor contains all the horizontal electric and magnetic field components independently of the measurement direction. In this case there are no special directions along which the modes decouple in the sense they do in 2D structures, and a strike direction cannot be clearly defined. A linearly polarized magnetic field will induce an elliptically polarized electric field in this case, and special directions will be replaced by polarization states, that can be retrieved by tensor analyses like those of La Torraca et al. (1986), Groom and Baley (1989) or Smith (1995). Tensor analysis provide smooth data, which are easier to interpret. I do not enter here in the details.

In order to improve 2D inversion results, the mean values of apparent resistivity and phase data can be computed and used for inversion, especially when, such as for Tasmania data, the data scatter and error bars are very small. This averaging process is done manually, after discarding the main outliers, i.e., those points which are more than 2 standard deviations from the median. This phase, called editing of curves, is performed after rotation/decomposition.
Instead of using a geometric mean, or even a median, I use the D+ method (Beamish and Travassos, 1992), which allows to check also the consistency of apparent resistivity and phase data by finding the one-dimensional earth which best fits both parameters.

A problem very common in MT is data distortion produced by the presence of three-dimensional local scale structures, located in the shallow subsurface, producing an anomalous charge distribution over its surface area. Distortion may be galvanic or inductive, but the inductive distortion can generally be ignored due to its small magnitude. Galvanic distortion is frequency independent and its effect on the electric field may be of the same order of magnitude as that of the regional electric field, and is thus considered as an additional anomalous electric field. Galvanic distortion is a complex problem in MT field surveys, where the impedance tensor is affected by a distortion matrix. In the simplest cases in 1D, and in some 2D cases where measurements are performed in the TE and TM directions, its effect is called static shift. In practice, static shift is a vertical displacement of the apparent resistivity curves, where the phase angle curve is not affected.

There is no numerical method to correct for the static shift and it is necessary to use information from other geophysical methods that are not affected by static shift, using the vertical magnetic field component data, or comparing all the survey responses with a priori geological or geophysical information.

Decomposition and editing of Tasmania MT data

The first step of my analysis has been data rotation and decomposition.

Decomposition performed with different algorithms provided very similar results, and error bars were very small in most cases, showing a clear difference between the two polarization modes on most sites, proving that there is clear sign of lateral discontinuities. It was therefore very important to define a strike direction and to distinguish between TE and TM mode in order to proceed to 2D modeling phase.

In most sites the vertical magnetic signal has provided very good data, and the tipper strike was clear. In order to distinguish the two modes, and therefore the strike direction, I have used mostly the information provided by the tipper strike. The strike proved to be variable along both the two profiles. In Figure 3 I show the strike direction for sites on Northern Profile at high frequency (10 Hz) and low frequency (0.01 Hz), and in Figure 4 the same for the Southern profile.

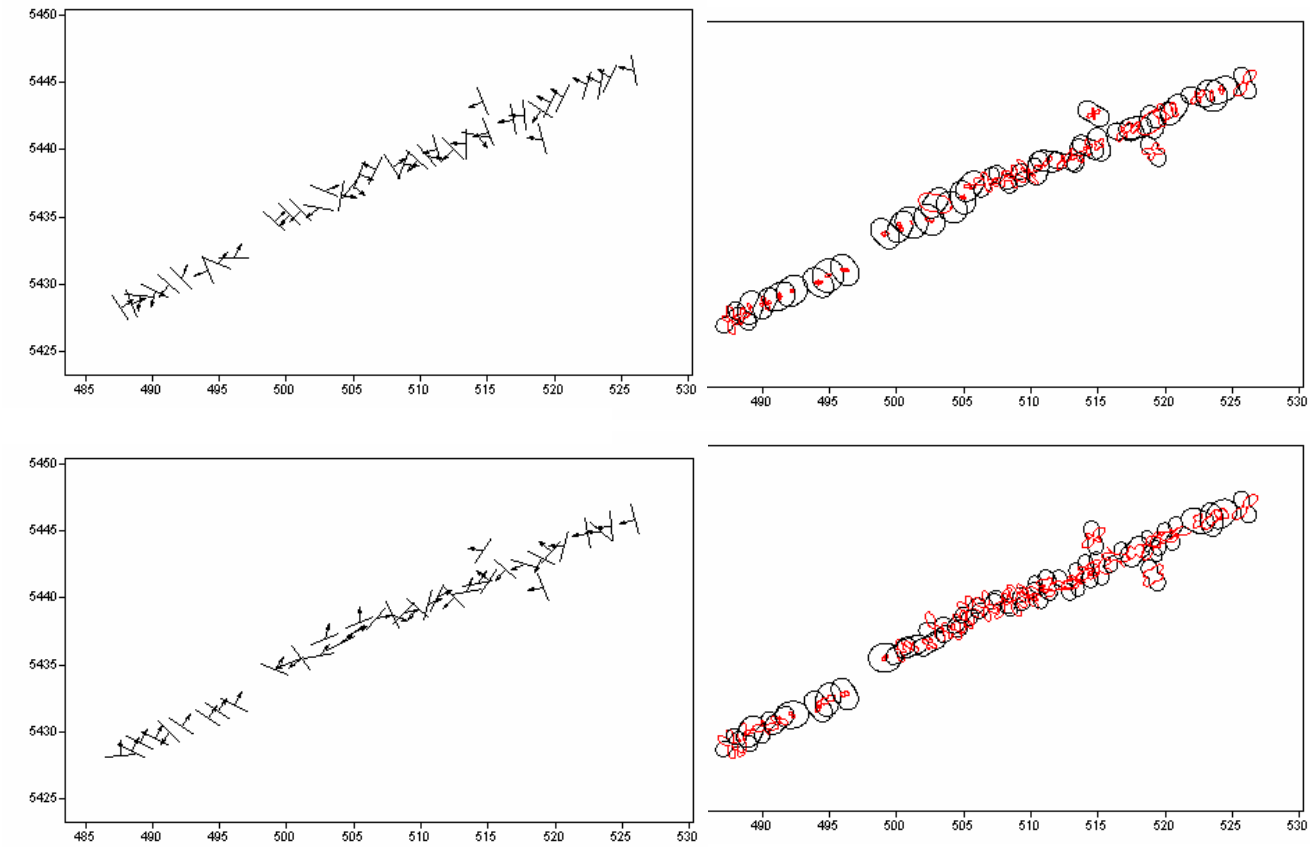

Figure 3. On the left: tipper strike and induction arrow (pointing toward the conductor) for sites on Northern Profile. Data are shown at 10 Hz (top) and 0.01 Hz (bottom). On the left: magnitude polar diagrams of impedance tensor (Zxx in red, Zxy in black) at 10 Hz (top) and 0.01 Hz (bottom). The round shape at high frequency implies an almost-1D structure at shallow depth. At higher depth a definite strike direction is testified by the direction of elongated magnitude polar diagrams on most sites.

I observe that the strike, in most cases, is not orthogonal to the profile directions. Most probably the condition is a 3D structure, and lateral discontinuities are present not only along the profiles but also adjacent to them. However, 3D modeling is not possible when data sites are aligned along distant profiles. In order to retrieve the maximum number of information from the 2D modeling, I preferred to decompose data instead of rotate them to a fixed direction. I used in most cases La Torraca decomposition, but checking also the results of the other decompositions.

The statistical error of apparent resistivity and phase data are lost in La Torraca decomposition, and this can be a problem when data are noisy. This is not a problem here since data are very good in most cases and the few bad data segments can be simply masked during editing of curves without loosing too much information. For example, a bad (NTL035) and a good (NTL007) data curves rotated to the main strike direction and decomposed reveal that the quality is fairly consistent and high (Figure 5). A simple masking of biased data and smoothing of data allows to retrieve most of the information.

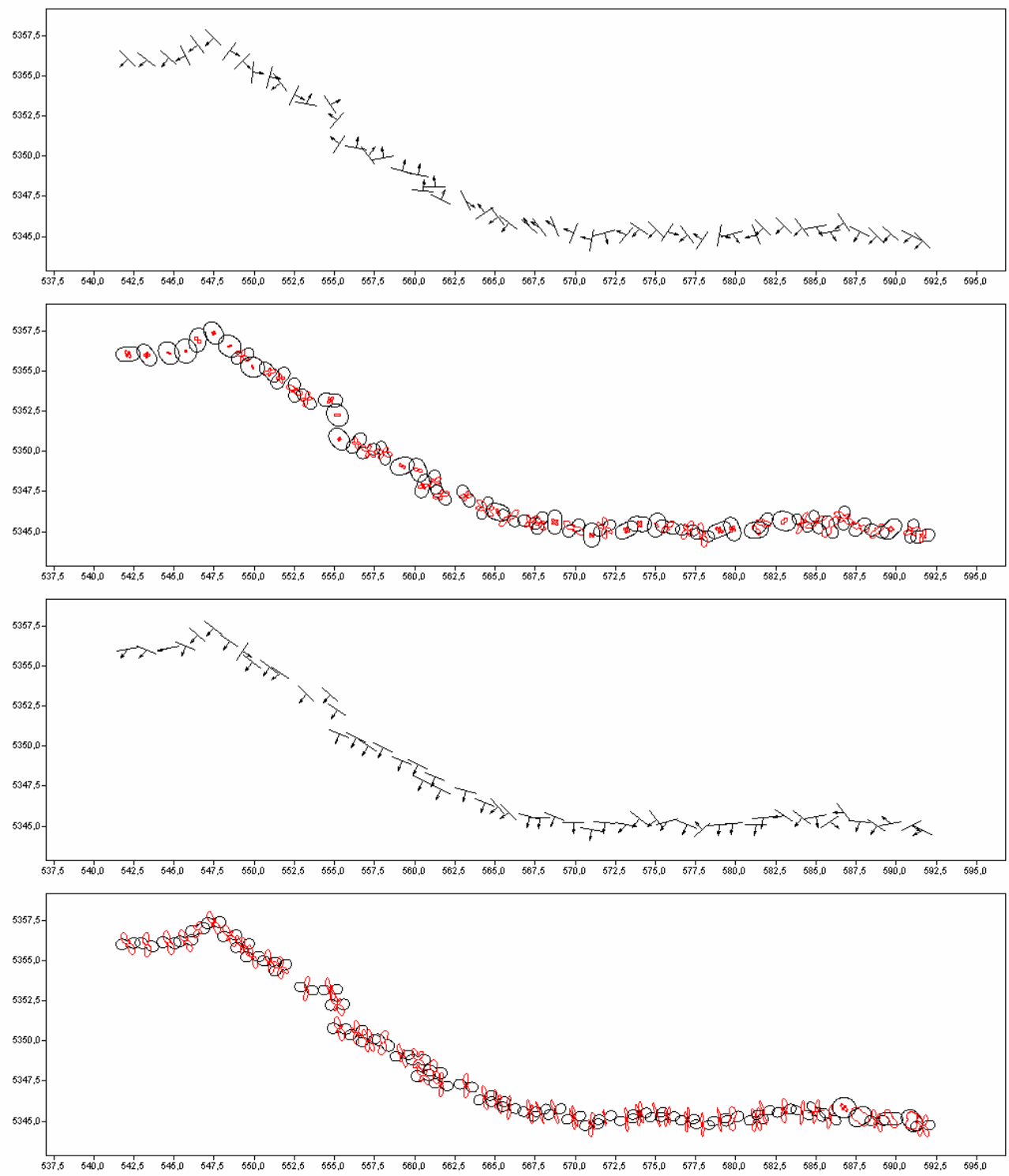

Figure 4. Southern Profile, from the top: a) tipper strike and induction arrow (pointing toward the conductor) at 10 Hz; b) magnitude polar diagrams of impedance tensor at 10 Hz; c) tipper strike and induction arrow (pointing toward the conductor) at 0.01 Hz and d) magnitude polar diagrams of impedance tensor at 0.01 Hz. The round shape at high frequency implies an almost-1D structure at shallow depth. At higher depth a definite strike direction is testified by the direction of elongated magnitude polar diagrams on most sites.

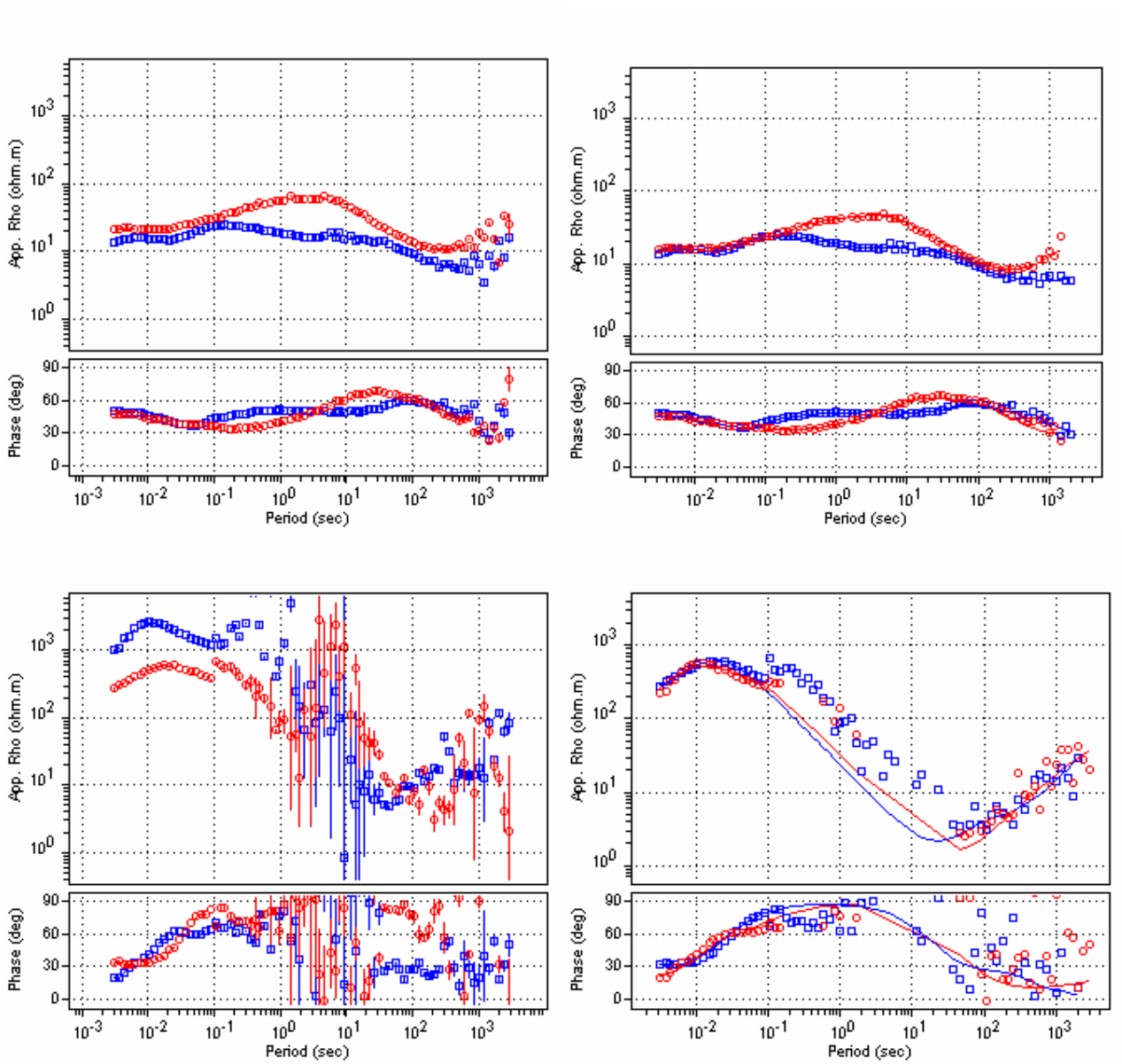

Figure 5. Examples of a good (Site NTL007, on the top) and a bad (Site NTL035, on the bottom) data. Data curves are rotated to the main strike direction (left) and decomposed with La Torraca algorithms and smoothed (right).

Only in a few case I could not use La Torraca decomposition. In four sites of the northern profile (N050, N051, N053, N054) La Torraca decomposed data resulted in a not credible jump from one mode to another at low frequency. Figure 6 shows the situation for site N050. The closest sites, i.e., 49, 52 and 55 show a main E axis rotated to 90 degrees, and I used a rotation angle of 90 for these four sites.

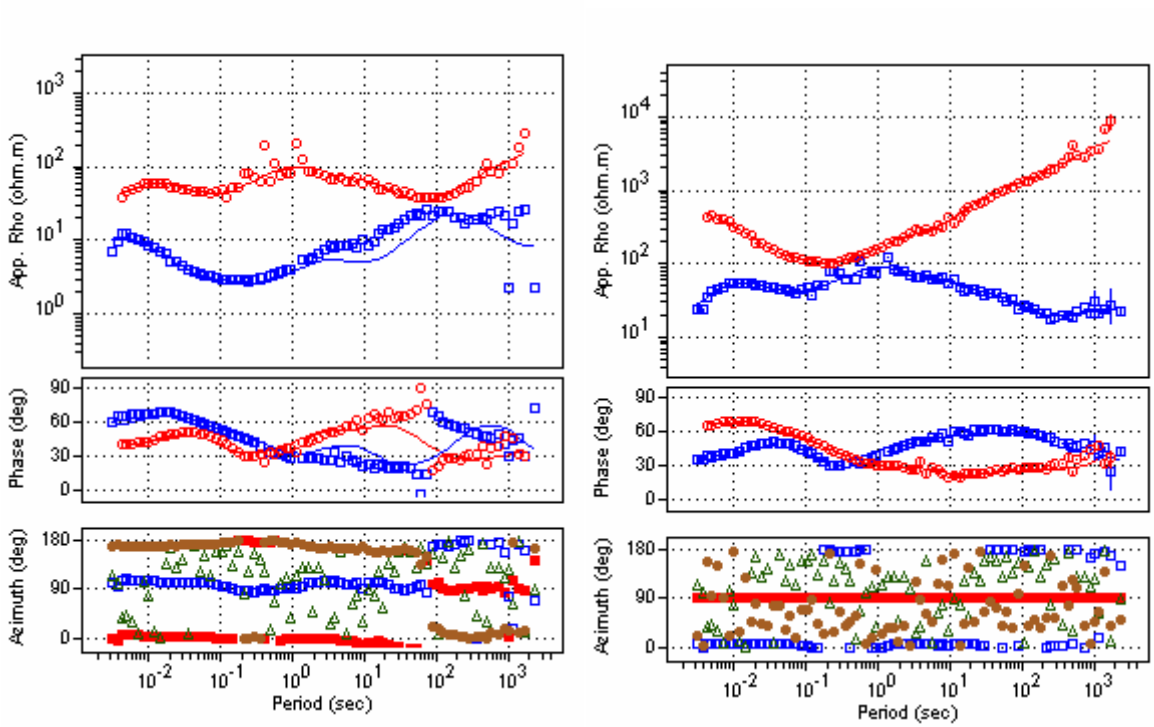

Figure 6. N050 data decomposed using La Torraca code (left) and rotated to 90 degrees North (right).Note the swapped decomposed data in the low frequency.

After decomposition, data at each site were edited by removing biased data (point located more than 2 standard deviation off the median) and smoothing the curves using D+ algorithm. The resulting curves are presented in Appendix 1.

On the base of tipper strike direction, the TE and TM modes were defined for each site. Since apparent resistivity data on most sites showed significant difference between the two polarization curves at high frequencies, testifying a probable galvanic distortion, a manual static shift correction was also attempted based on comparison of adjacent sites and check of geological outcropping formations. Data were then inverted using both the original, although edited, data and the shifted data.

The resulting pseudosection of Northern and southern profiles are given respectively in Figure 7 and Figure 8.

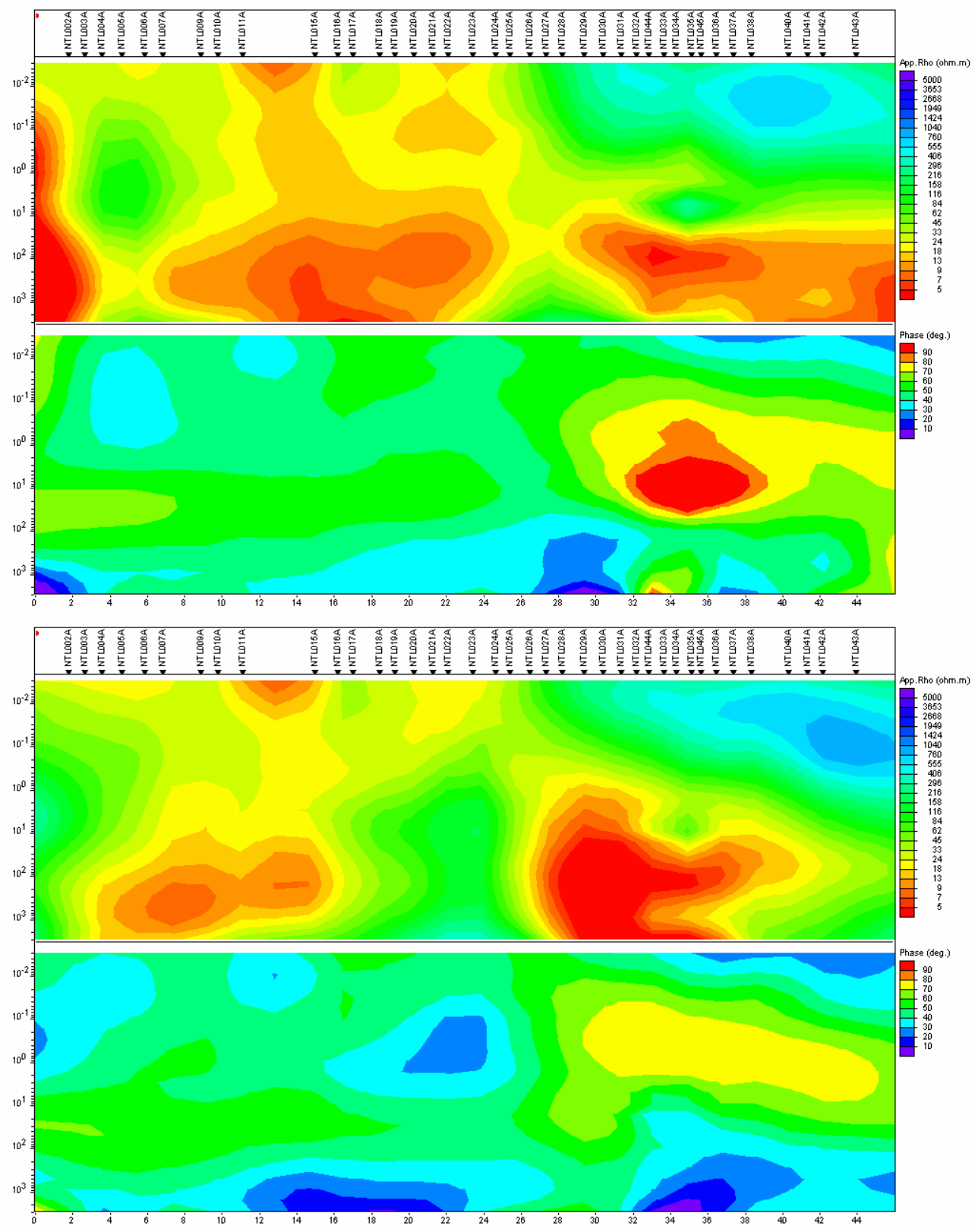

Figure 7. Northern Profile: pseudosection of shifted TM (top) and TE (bottom) data.

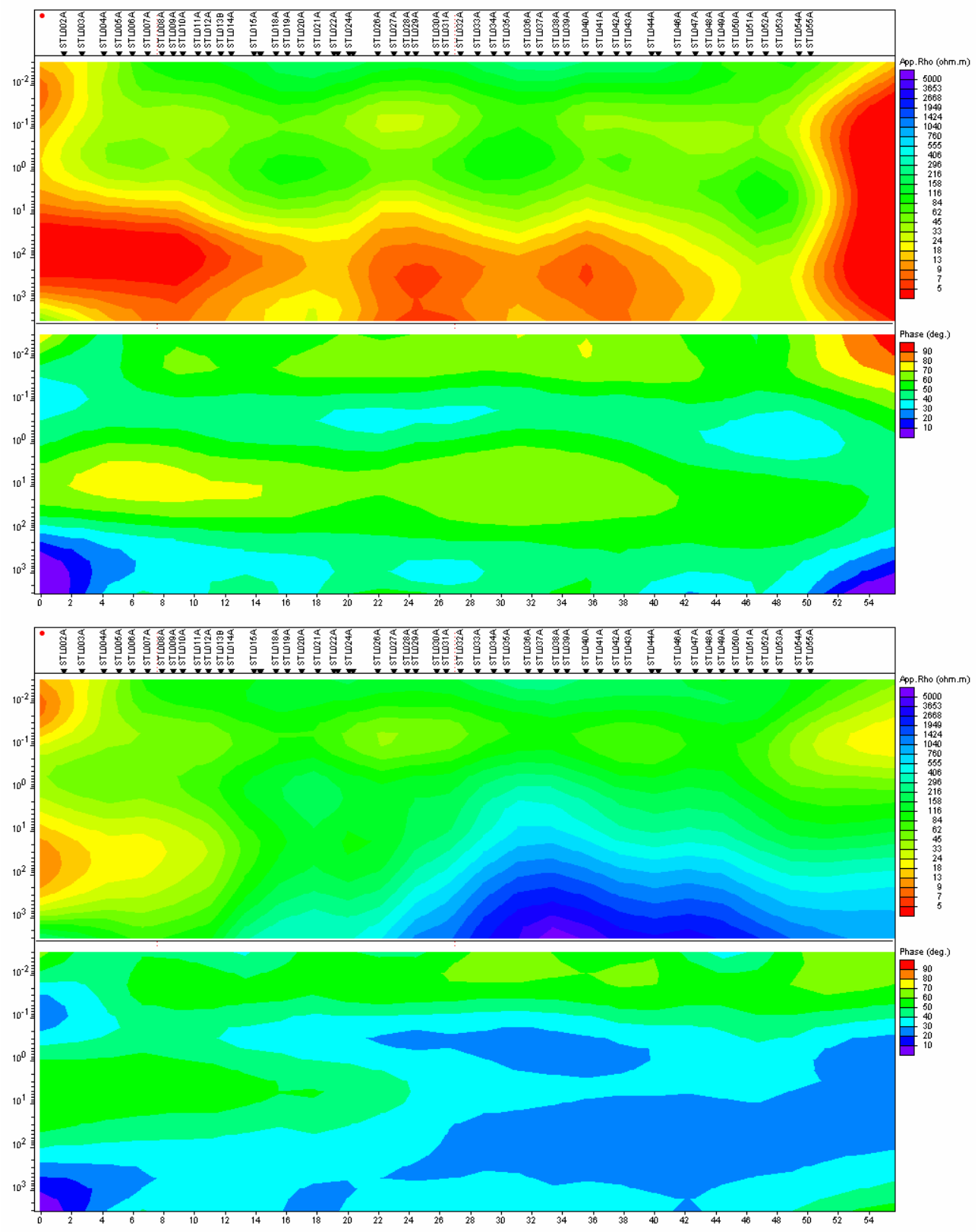

Figure 8. Southern Profile: pseudosection of shifted TM (top) and TE (bottom) data.

Inversion

1D inversion of the determinant (DET) data as well as 2D inversion of TE-, TM-, TE+TM data was performed using various algorithms.

Inversion of 3D structures with 1D and 2D modeling can lead to misinterpretation, and the use of the determinant of the impedance tensor was proposed as a useful tool for computing routine inverse models, given that the determinant is invariant under rotation. The determinant mode reduces the distortion effects caused by shallow heterogeneities and non-finite lateral structures, and the phase is not affected by galvanic distortions. The determinant inversion generally allows a good data fit while at the same time resolving reasonably well both resistive and conductive structures along any profile. Estimated resistivity values lie much closer to the true subsurface resistivity in between the extreme resistivities predicted by individual TE and TM mode inversions.

At all sites 1D Bostick, Occam and layered inversion was performed, while all data along the two profiles were 2D inverted using the algorithm of Rodi and Macie (2001). Since apparent resistivity and phase data on most sites showed significant difference between the two polarization curves at low frequencies, proving that the structure is not a 1D one, 1D inversion of TE or TM mode would have produced a biased result. Regardless of the true dimensionality, 1D inversion of MT data and, in particular, inversion of rotationally invariant data like the determinants, provides an overview of the subsurface conductivity in a feasible sense. Since geological information of the subsurface were scarce, a reasonable starting model and strategy could be constructed for 2D inversions based on the results of 1D inversion.

I show here the inversion results for the two profiles.

Northern Profile modeling results

Figure 9 shows the inversion results of 1D modeling of Northern profile's sites. I do not include Bostick inversion, which always resolves in a very smooth and too simplified picture of the subsurface.

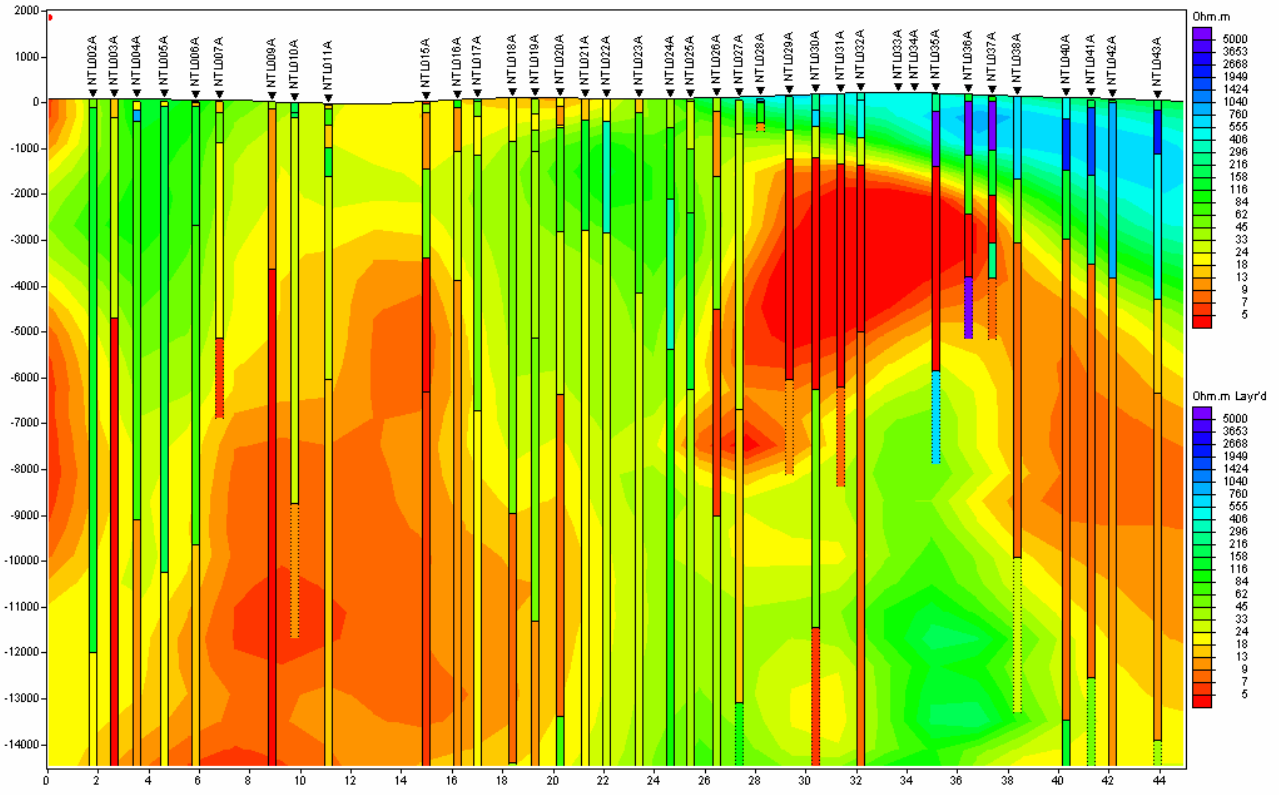

Figure 9: Northern Profile 1D inversion result. Occam inversion interpolation on the back, 1D layered inversion as geoelectrical columns.

2D geoelectrical models are correctly retrieved by the combined inversion of TE and TM modes. However, in the real three-dimensional world the resulting 2D models may fail on the good correspondence between the measured data and model response. The use of only one of the two modes (TE or TM) in the inversion process may provide information regarding the robustness of the results. TM is the mode less affected by 3D, off-profile effects but results in a overestimation of conductive features. On the contrary, TE effect is more affected by 3D, off-profile effects.

Due to lack of geological constrains, 2D inversion was originally done using a homogeneous subsurface of 100 ohm.m resistivity as a priori model. Figure 10 shows the TM mode data inversion results using the original, although edited, data, inverted taking care of the static shift (an option allowed from the Rodi&Mackie code). When data are manually shifted so to reduce high frequency inconsistency created by galvanic distortions, producing a smoother change of high frequency resistivity from one site to the adjacent ones, the inversion results do not change sensibly (Figure 11). I consider better to use shifted data, but I always tested inversion results with all data set. What I show in the rest of the more robust data I obtained, checked both by making changes to see what features were really required by data and not bias effects produced by inversion, and producing sensitivity maps of inversions.

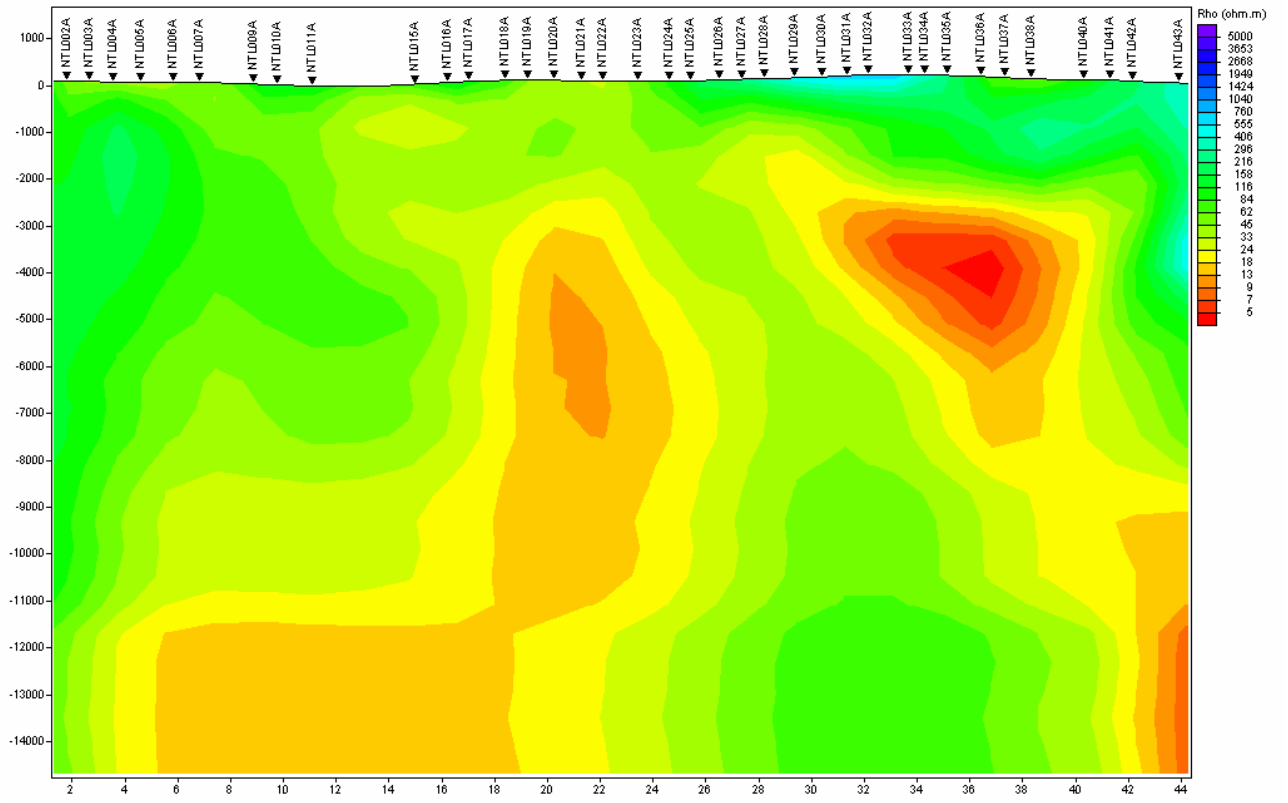

Figure 10. Northern Profile 2D inversion of TM unshifted data using a homogeneous a priori model of 100 ohm.m. RMS=10.1.

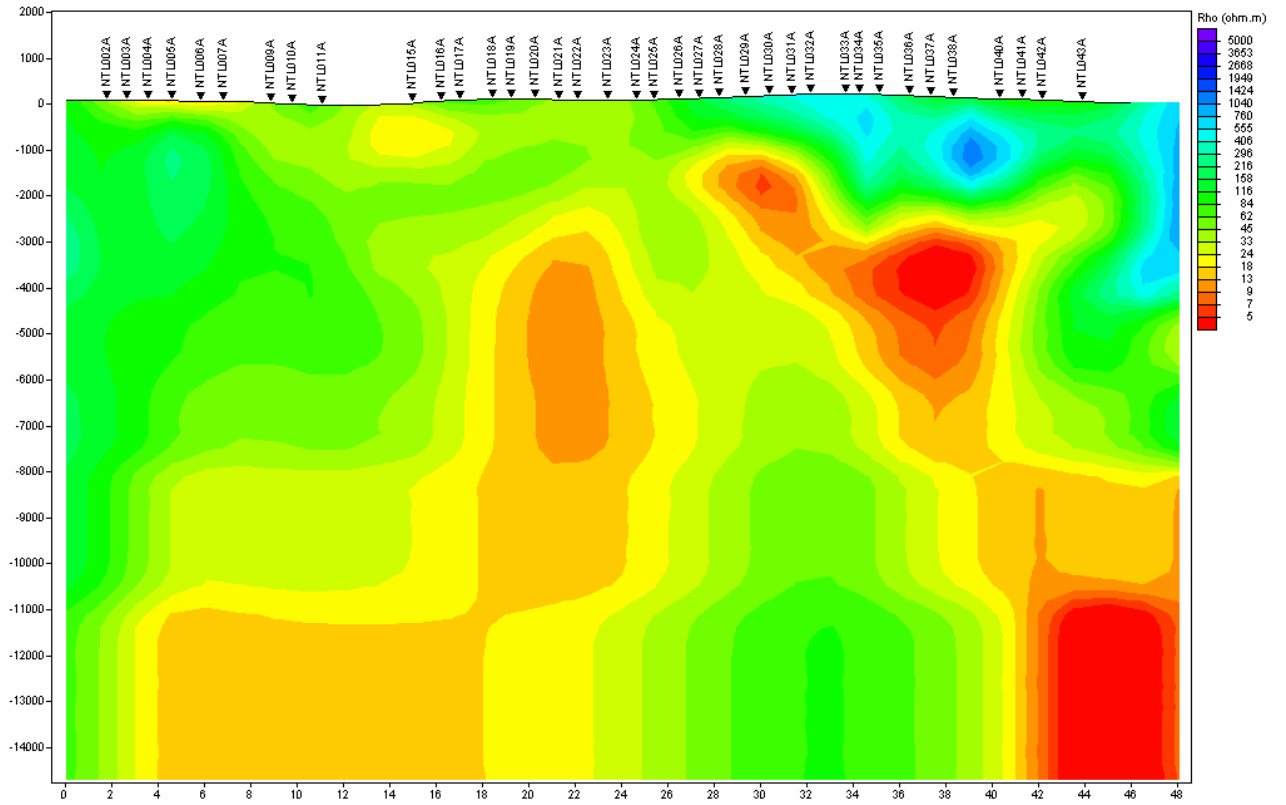

Figure 11. Northern Profile 2D inversion of TM shifted data using a homogeneous a priori model of 100 ohm.m. RMS=10.0.

The same procedure has been followed for joint TE and TM inversion, as shown in Figures 12 and 13.

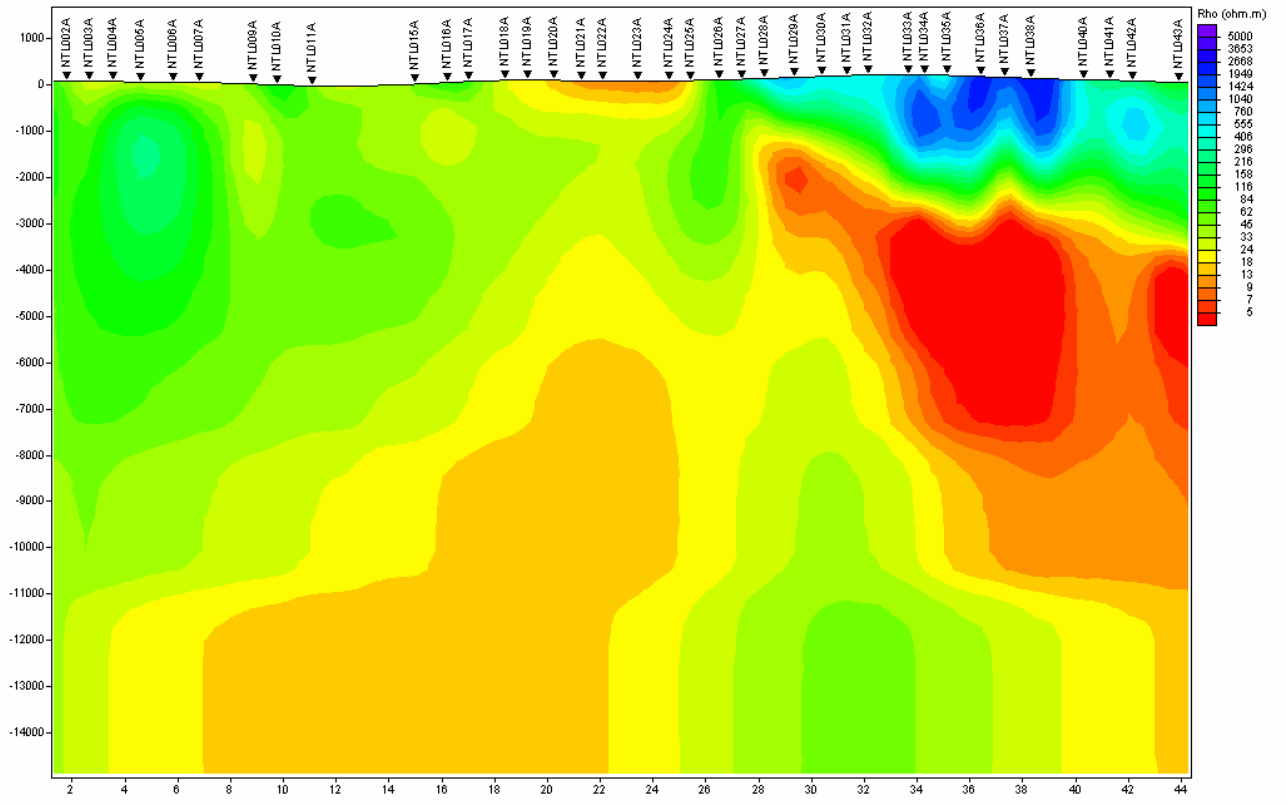

Figure 12. Northern Profile 2D inversion of TM-TE unshifted data using a homogeneous a priori model of 100 ohm.m. RMS=19.9.

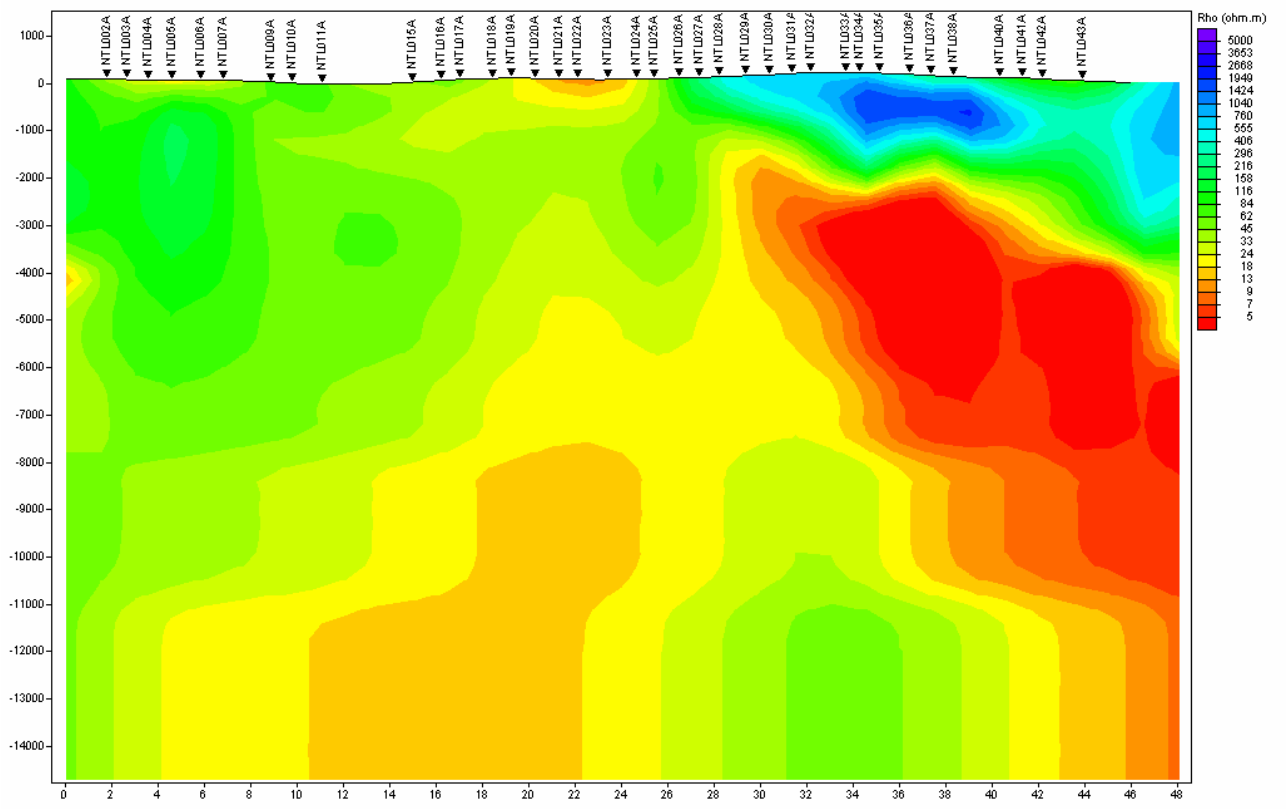

Figure 13. Northern Profile 2D inversion of TM-TE shifted data using a homogeneous a priori model of 100 ohm.m. RMS=20.0

RMS values are around 10 for TM inversions and 20 for TE-TM inversions. These relatively high values are mainly due to the very low error floor I used for inversion, since I set 2% for resistivity and 1% for phase. Actually, inversion results are very good in most cases. Figure 14 shows a comparison of real data and computed data in the form of apparent resistivity and phase pseudosections. The difference between experimental and computed data is most probably due to 3D effects that cannot be resolved by 2D modeling. TE-TM experimental and computed data are provided in Appendix 2.

Usually when a more refined a priori model is provided also the inversion results are more refined. The lack of other data such as deep geological information and other geophysical data did not allow me to perform a better inversion. I tried therefore to introduce some features that were evident in the 1D inversion results and I built a little more complex subsurface where a more resistive unit was inserted outcropping in the eastern portion of the profile. I did not introduced any conductive anomaly, although two anomalies are clearly shown in Figure 9, because conductors are our target and I wanted them to be purely defined by 2D inversions. A comparison of the homogeneous a priori model and the model based on 1D inversion results is shown in Figure 15.

Results remained essentially the same, as shown in Figure 16.

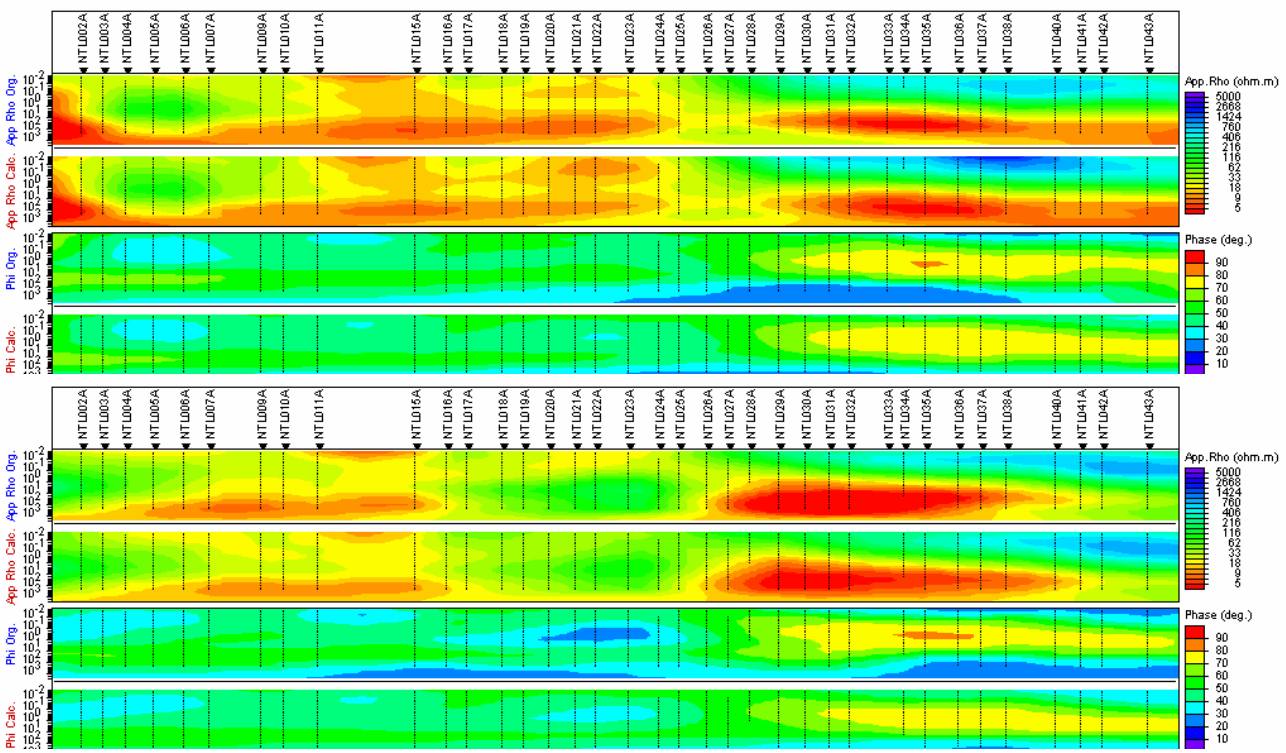

Figure 14. Northern Profile pseudosections of TM (top) and TE (bottom) mode data comparing experimental and calculated data from 2D inversion.

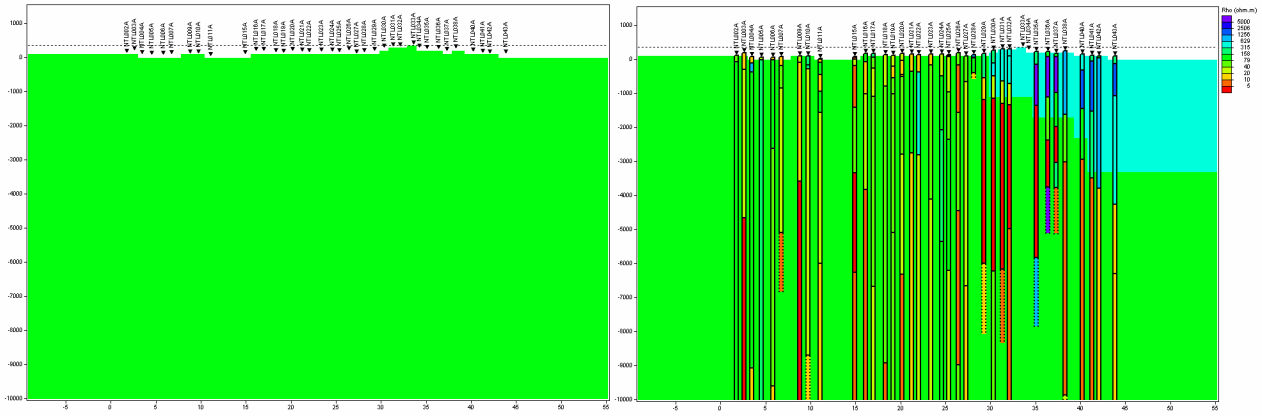

Figure 15. Northern Profile a priori models used for the inversion. On the left the homogeneous a priori model used for the first inversions, on the left the a priori model built on the base of 1D inversion information, and compared to 1D layered models.

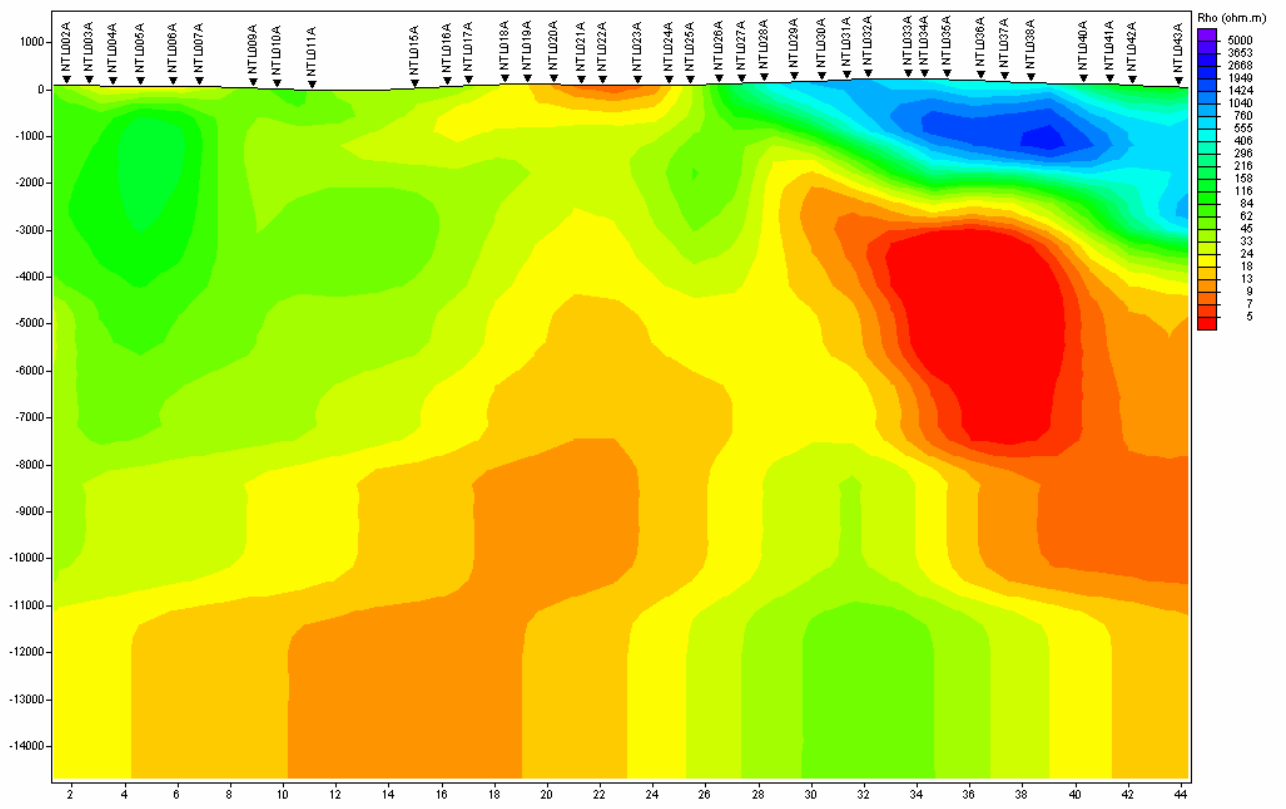

Figure 16. Northern Profile 2D inversion of TM-TE shifted data using an a priori model built on the base of the 1D inversion results. RMS=18.4

Northern Profile: preliminary considerations and interpretation

For this report I restricted my analysis to the first 12 km.

Comparing results from 1D, 2D TM and 2D TE-TM inversion the models do not change sensibly (Figure 17 for comparison of 1D and joint TE-TM inversion results). This is probably due to two factors: on one side the strike direction is in most cases almost orthogonal to the profile direction, so that the 2D inversion may work in the best possible condition. Moreover, the similar models obtained for 2D TM and TE-TM inversion let me think that 3D effects are very limited. This is also confirmed by observed low skew data (not shown).

All models reflect the presence of a main conductive body in the eastern portion of the profile at a depth of about 2.5 km below sea level (b.s.l.). MT may resolve well the top and lateral boundaries, provided the uncertainties due to a possibly not completely corrected static shift effect, but it does never resolve well the bottom, i.e., the thickness of the anomalous body. In a first approximation I can say that the anomaly is very visible and the body should have a thickness of no less than 2 km, otherwise it could not produce such a strong effects on data. This was checked also by forward models changing the thickness of the conductor.

Another conductor is also defined in the central-western deep part of the profile. Resistivity appears higher than for the previous body but this could be due to the smoother response at high depth. The top of this body is deeper than the other, 5 km b.s.l.. These two conductive bodies are separated by a more resistive section, whose explanation requires some more geological information.

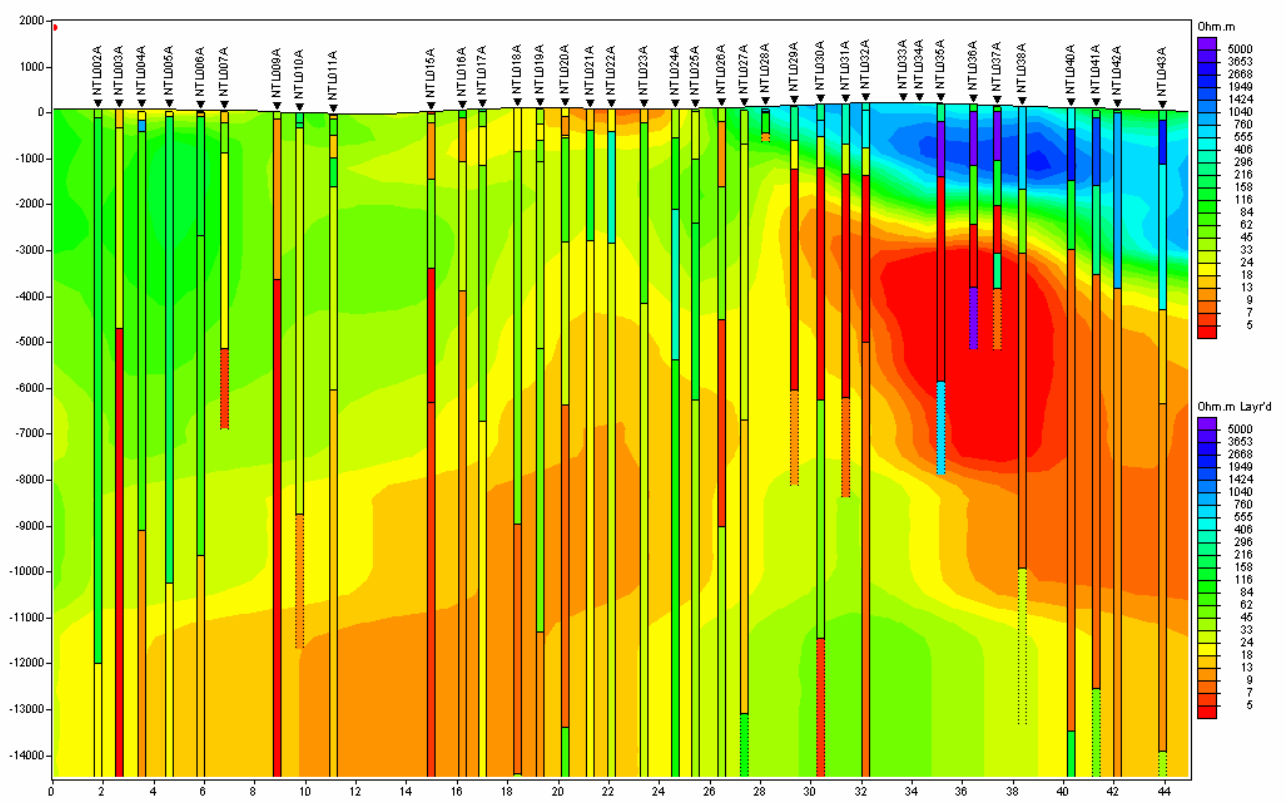

Figure 17. Northern Profile: comparison of 2D joint TE and TM inversion (on the background) and 1D inversion (geoelectrical columns) results.

Southern Profile modeling results

For this profile I did the same kind of inversions and tests I did for the Northern Profile.

Figure 18 shows the 1D inversion results for determinant data. Data were inverted both as they were and shifted in order to reduce static shift effects. Here I show just the results referred to the shifted data since the models are very similar to those obtained from unshifted data, as for the Northern profile.

2D inversions results are shown in Figures 19-24. TM data (Figure 19) and joint TE-TM data (Figure 20) were inverted using a homogeneous a priori model of 100 ohm.m. Then, as described for the Northern Profile, an a priori model was built on the base of information retrieved from 1D inversion, as shown in Figure 21. The corresponding inversion results for TM, TE-TM and TE are shown respectively in Figures 22, 23 and 24. RMS for these last models is slightly lower and sensitivity higher, therefore the resistive body defined in the center of the profile is a robust feature.

The pseudosections resulting from 2D inversion of joint TE and TM data in Figure 25 shows the good fit of TM data and the more difficult fit of TE data, as will be discussed in the following paragraph. Results of inversion are provided in Appendix 2.

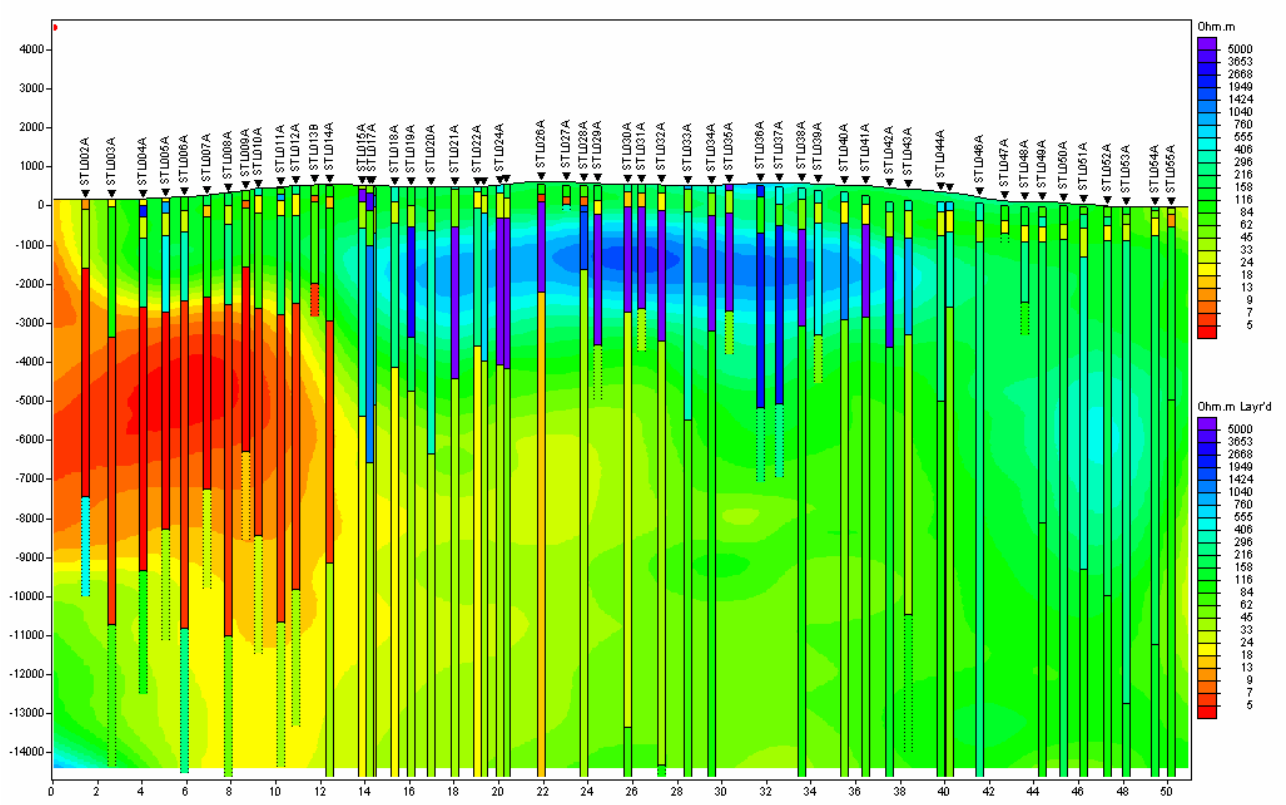

Figure 18. Southern Profile: 1D inversion result. Occam inversion interpolation on the back, 1D layered inversion as geoelectrical columns.

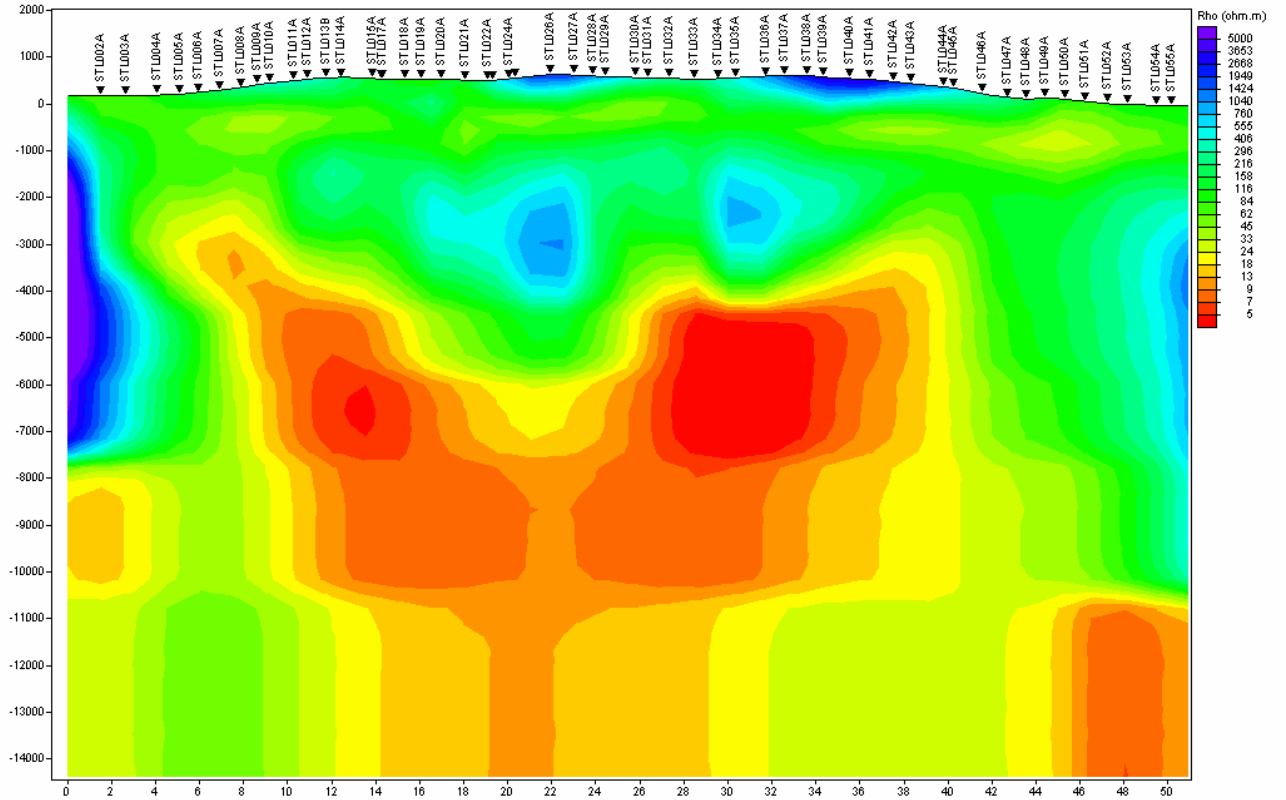

Figure 19. Southern Profile 2D inversion of TM shifted data using a homogeneous a priori model of 100 ohm.m. RMS=8.9.

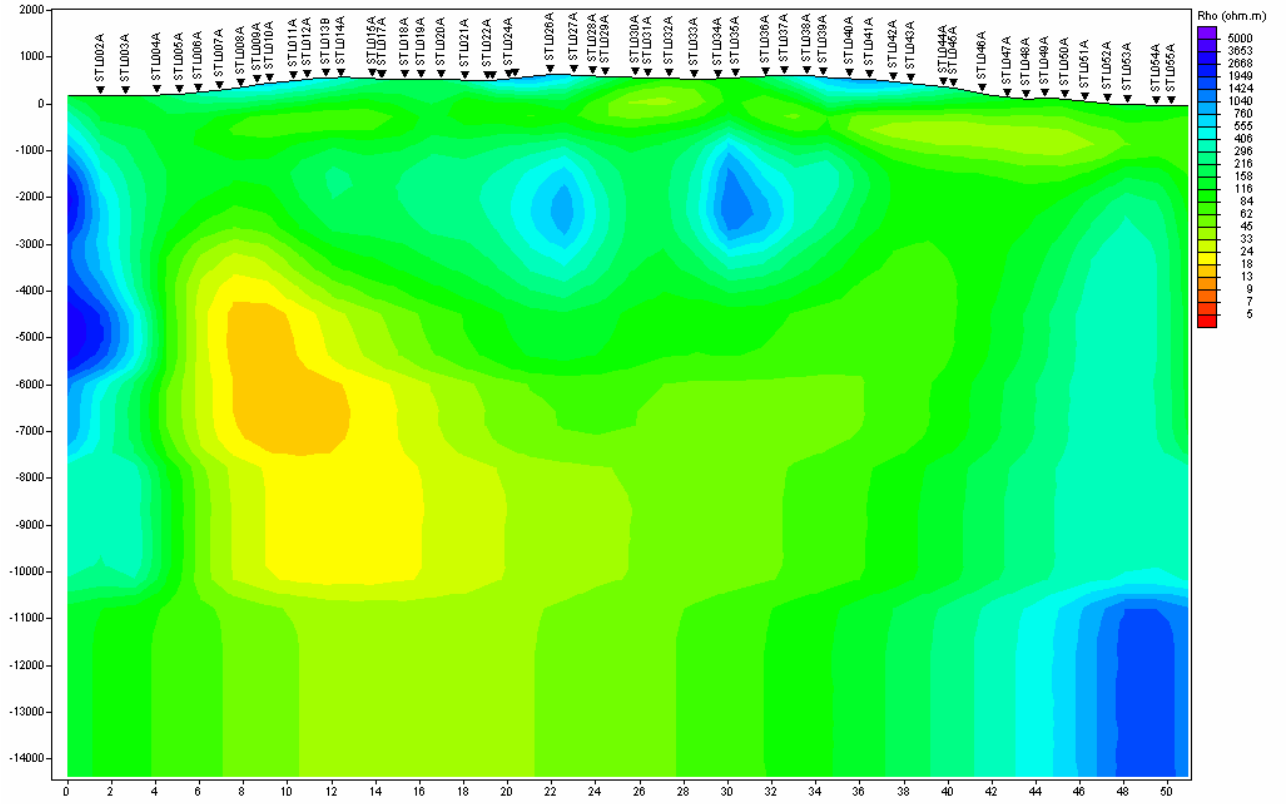

Figure 20. Southern Profile 2D inversion of TM-TE shifted data using a homogeneous a priori model of 100 ohm.m. RMS=18.8.

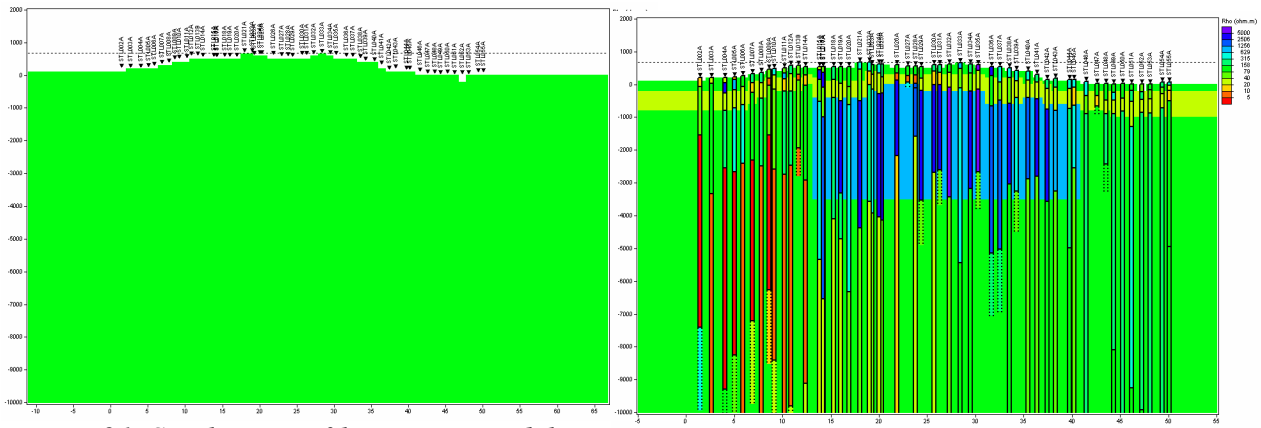

Figure 21. Southern Profile a priori models used for the inversion. On the left the homogeneous a priori model used for the first inversions, on the left the a priori model built on the base of 1D inversion information, and compared to 1D layered models.

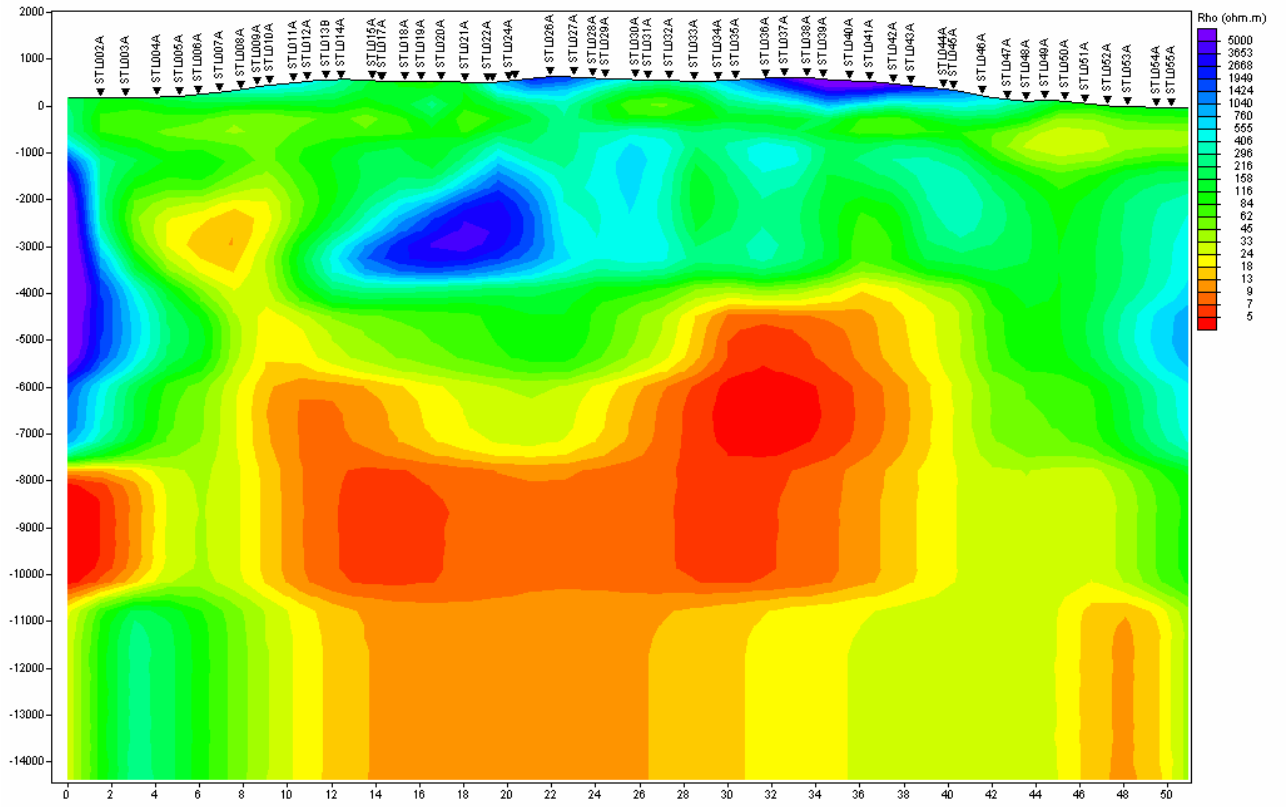

Figure 22. Southern Profile 2D inversion of TM shifted data using an a priori model built on the base of the 1D inversion results. RMS=9.5

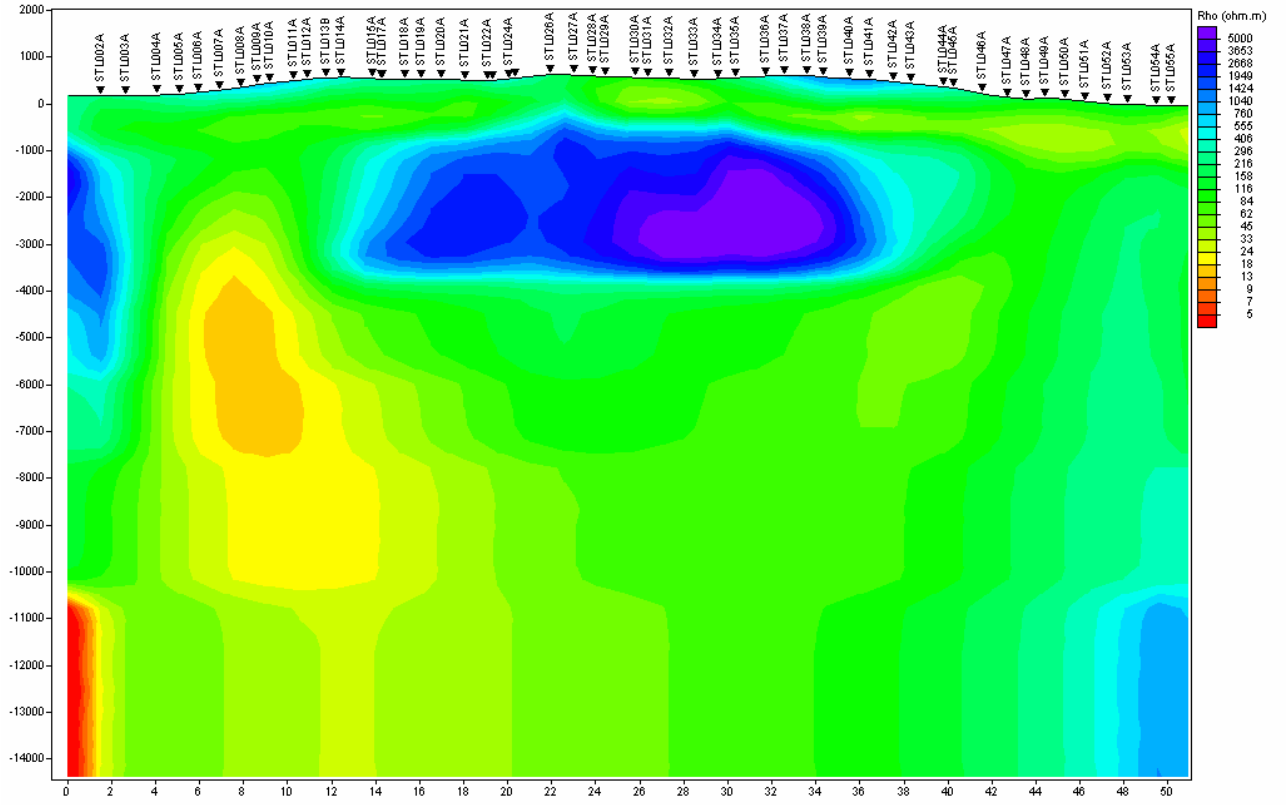

Figure 23. Southern Profile 2D inversion of TM and TE shifted data using an a priori model built on the base of the 1D inversion results. RMS= 19.0.

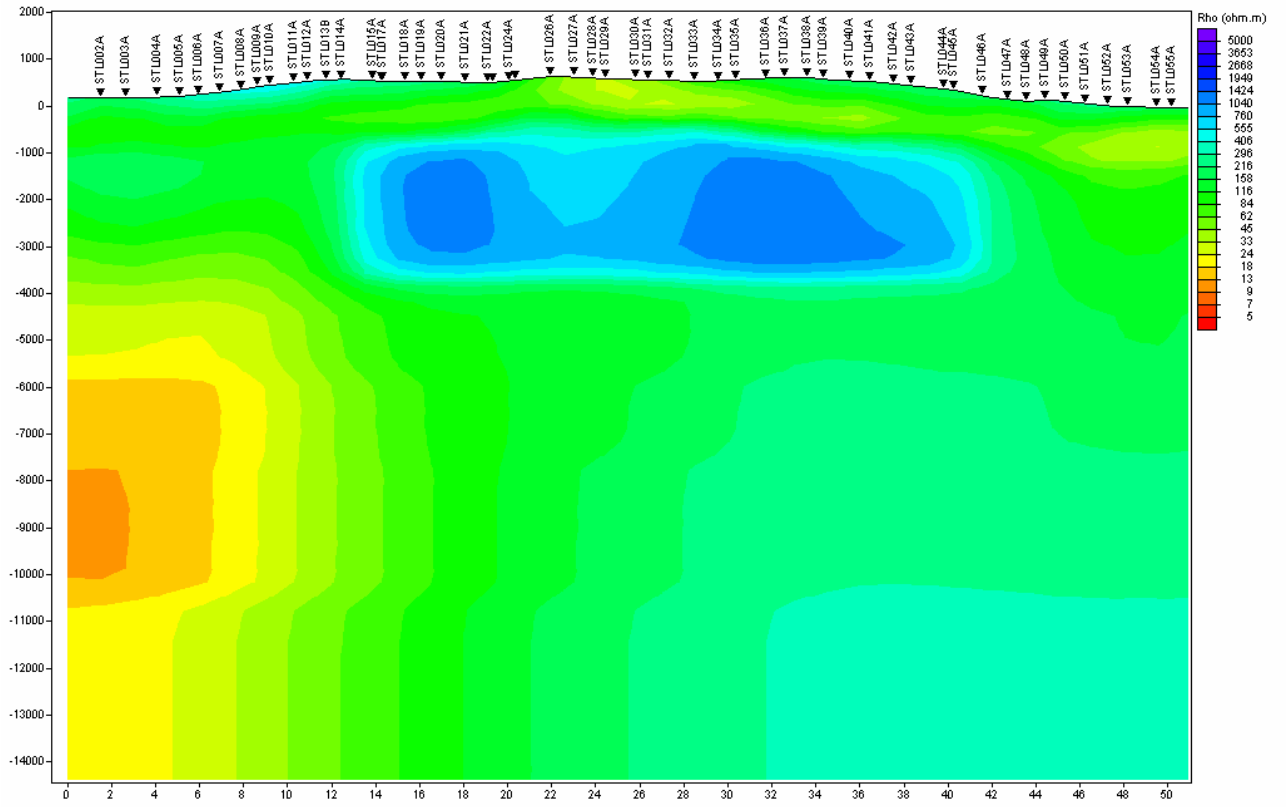

Figure 24. Southern Profile 2D inversion of TE shifted data using an a priori model built on the base of the 1D inversion results. RMS=17.8.

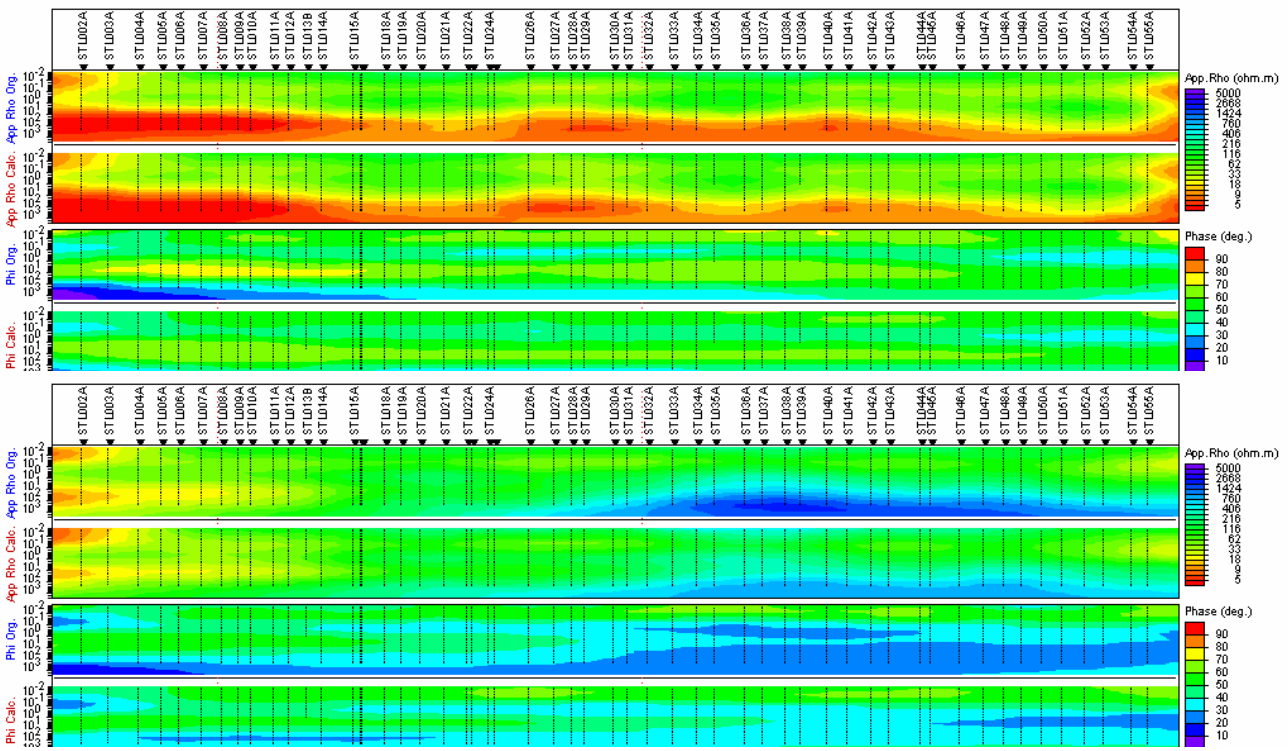

Figure 25. Southern Profile pseudosections of TM (top) and TE (bottom) mode data comparing experimental and calculated data from 2D inversion.

Southern Profile: preliminary considerations and interpretation

For this profile the situation is different from what has been discussed for the Northern profile. In this case 1D inversion results are comparable to 2D joint TE-TM data inversion results (Figure 26), but TM inversions appear very different (see Figures 19 and 22). This is most probably due to strong 3D effects, that cannot be completely resolved by 2D inversions, and by a strike direction parallel to the profile (see Figure 4). TE inversion results are comparable to 1D and 2D TE-TM inversions, proving that most probably surrounding structure are more resistive than structure crossed by the profile, in particular in the east.

All models define a conductive anomaly in the western part of the profile, at a depth of 3.5-4 km. This body seems more resistive and limited with respect to the first one described for the Northern profile, but it is hard to say for sure due to 3D effects. TM data inversion model describe a much broader conductive feature spanning almost 30 km as lateral extent, but this features, if of interest, should be defined in more detail with transversal profiles crossing the main Southern profile.

Finally, the very resistive feature defined at a depth of about 2 km in the central part of the profile is confirmed by all inversions.

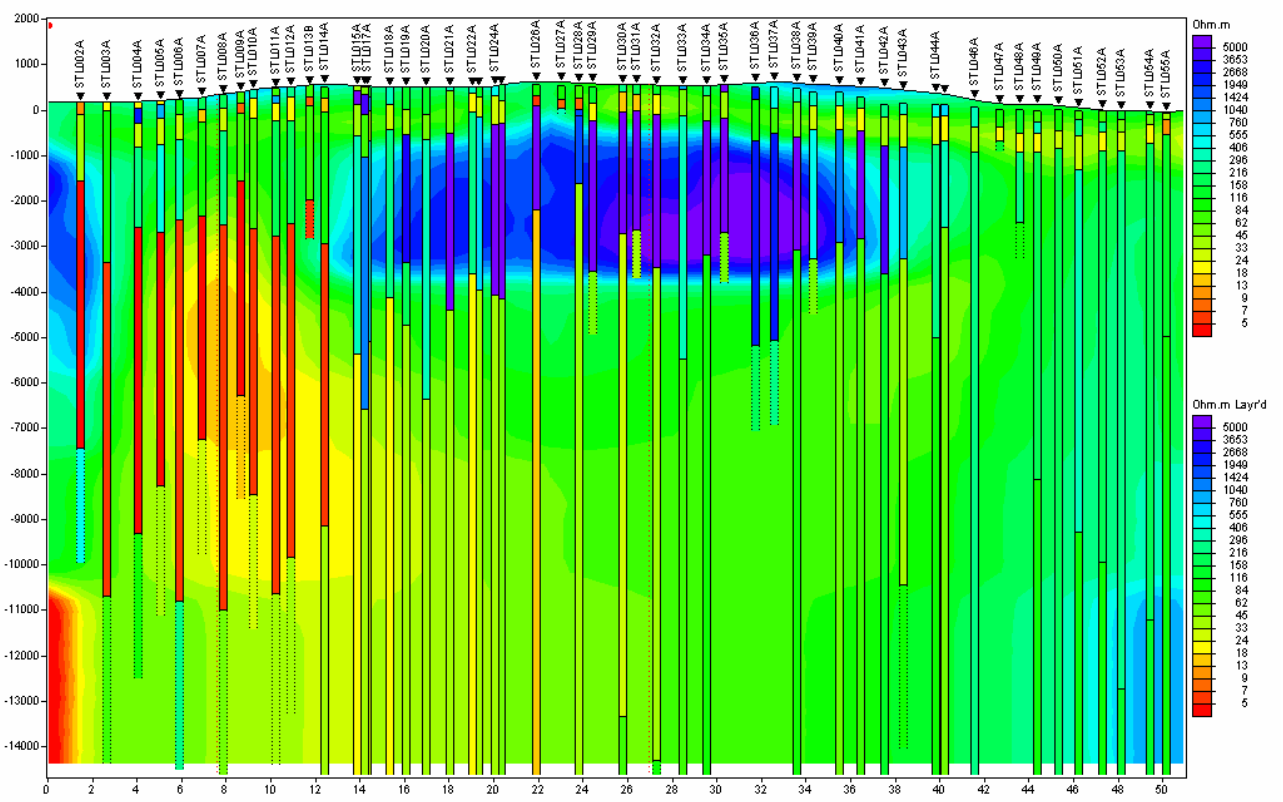

Figure 26. Southern Profile: comparison of 2D joint TE and TM inversion (on the background) and 1D inversion (geoelectrical columns) results.

Bibliography

Beamish, D., and Travassos, J.M., (1992) The use of the D+ solution in magnetotelluric interpretation. J. Appl. Geophys., 29, 1-19

Groom R.W and Baley R.C. (1989) Decomposition of magnetotelluric impedance tensors in the presence of three-dimensional galvanic distortion. J. Geophys. Res. 94B, 1913-1926.

La Torraca G.A, Madden T.R, Korringa J. (1986) An analysis of the magnetotelluric impedance for three dimensional conductivity structures. Geophysics 51:1819–1829.

Rodi, W. and Mackie, R.L. (2001) Nonlinear conjugate gradients algorithm for 2-D magnetotelluric inversion, Geophysics, 66, 174-187.

Smith T (1995) Understanding telluric distortion matrices. Geophys. J. Int. 122:219–226.

Swift JR (1967) A magnetotelluric investigation of an electrical conductivity anomaly in the southwestern United States. PhD Thesis, MIT, Boston.

Appendix 1

Apparent resistivity and phase data after decomposition, editing and smoothing. Symbols are experimental data (xy in red, yx in blue), curves are smoothed data used for inversions.

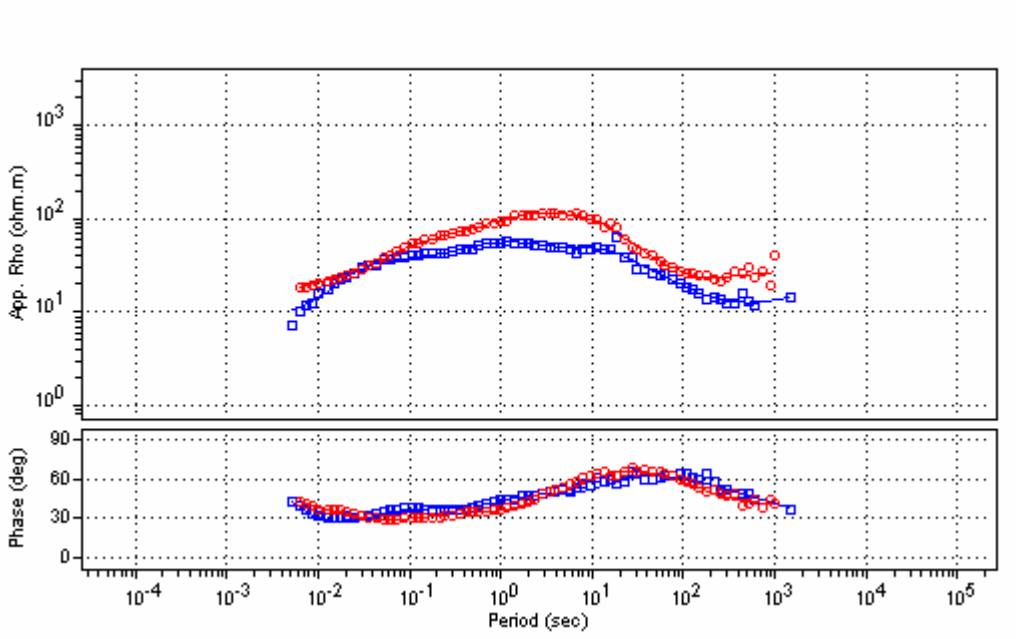

NTL002

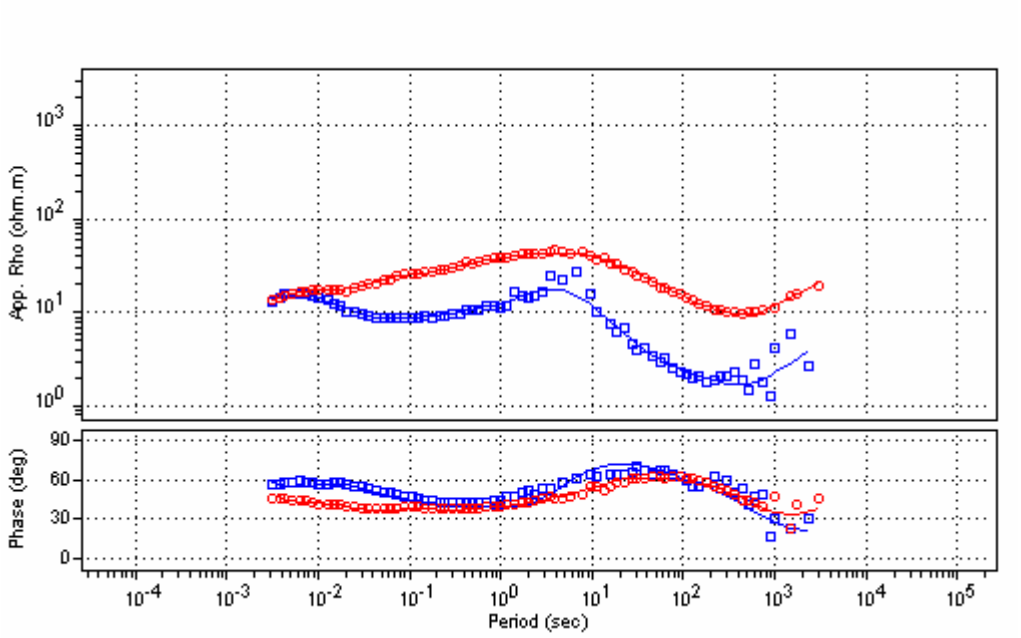

NTL003

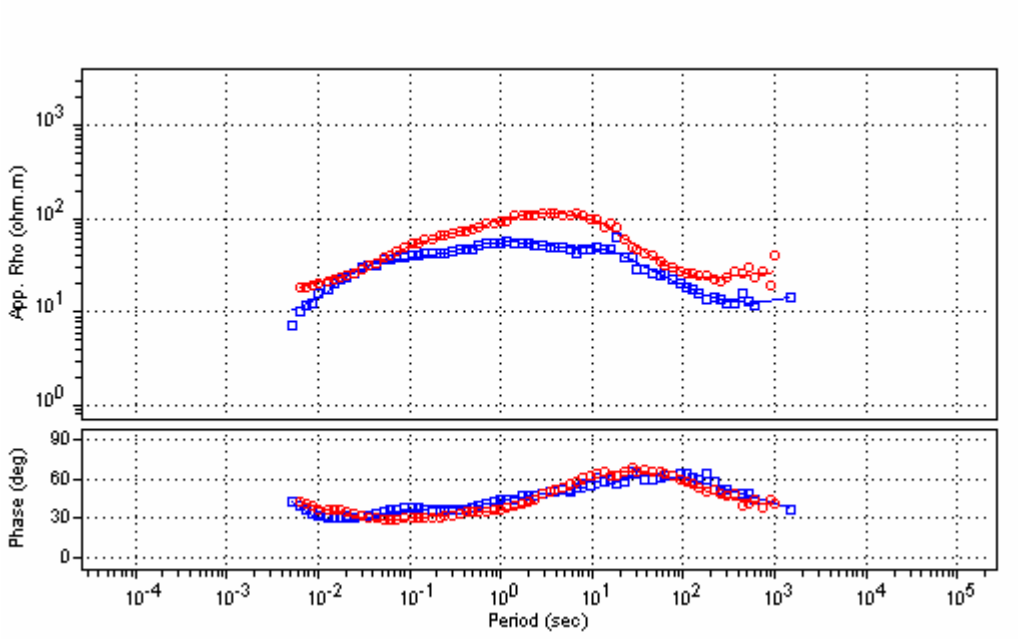

NTL004

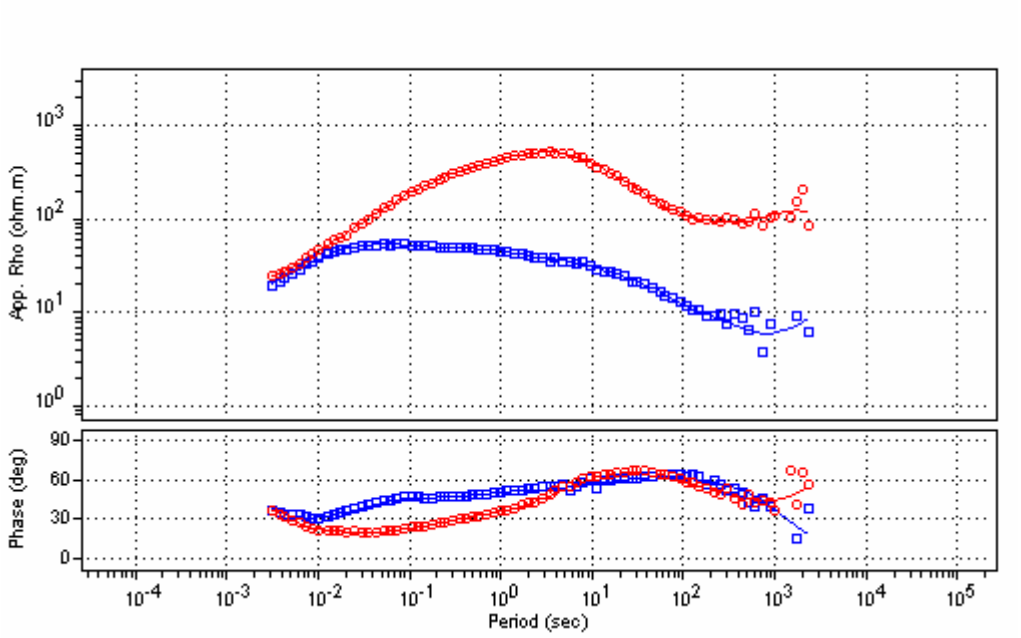

NTL005

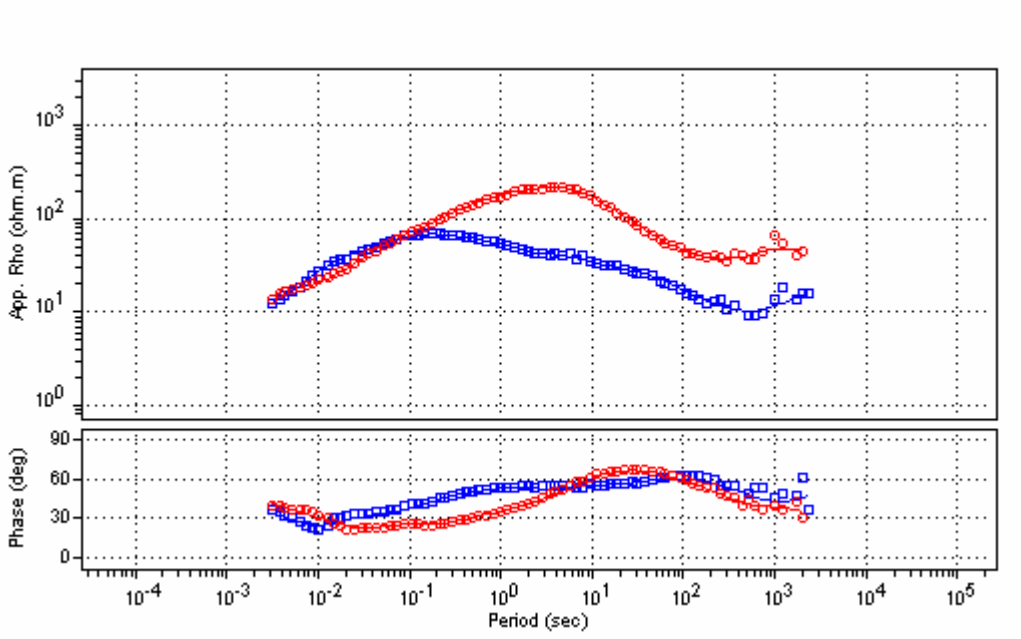

NTL06

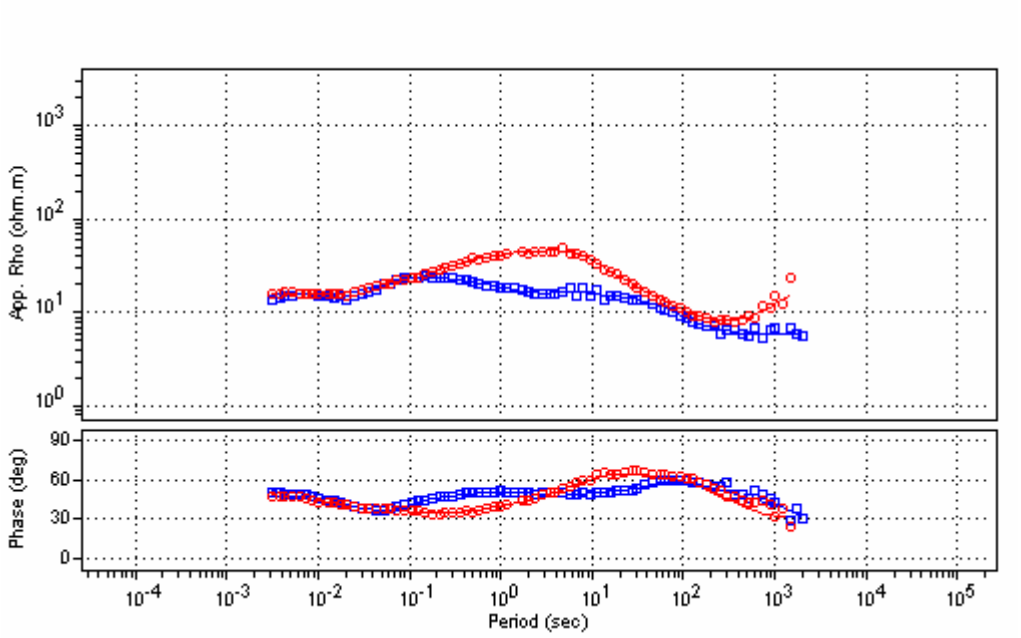

NTL007

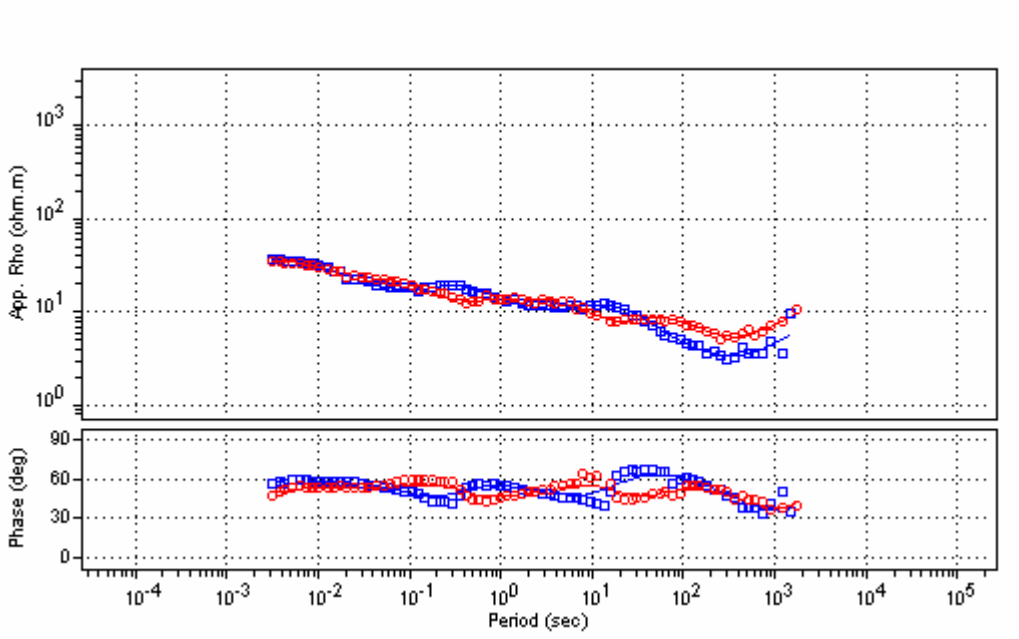

NTL009

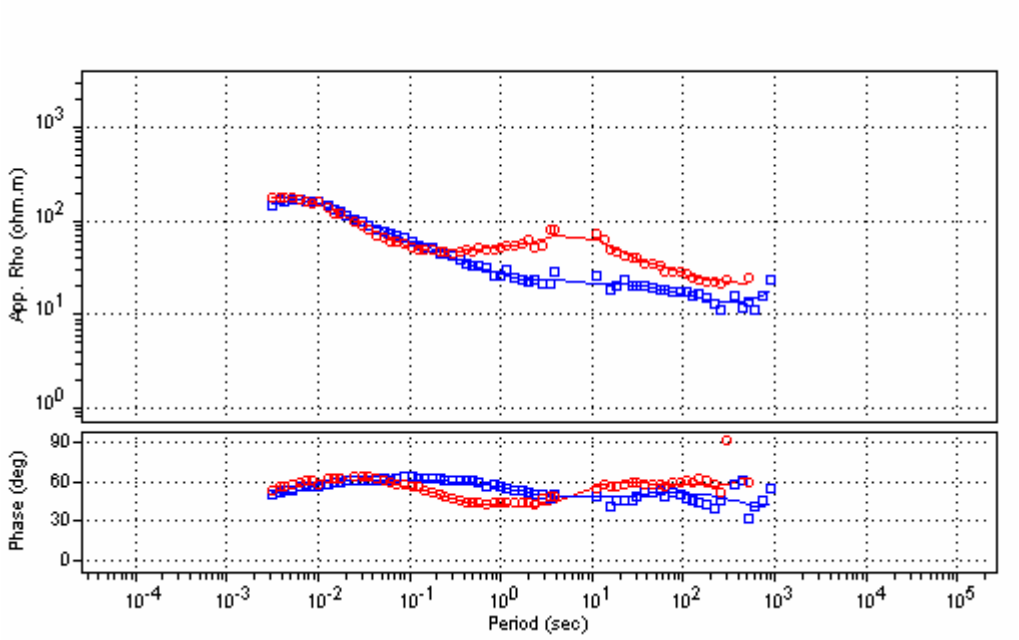

NTL010

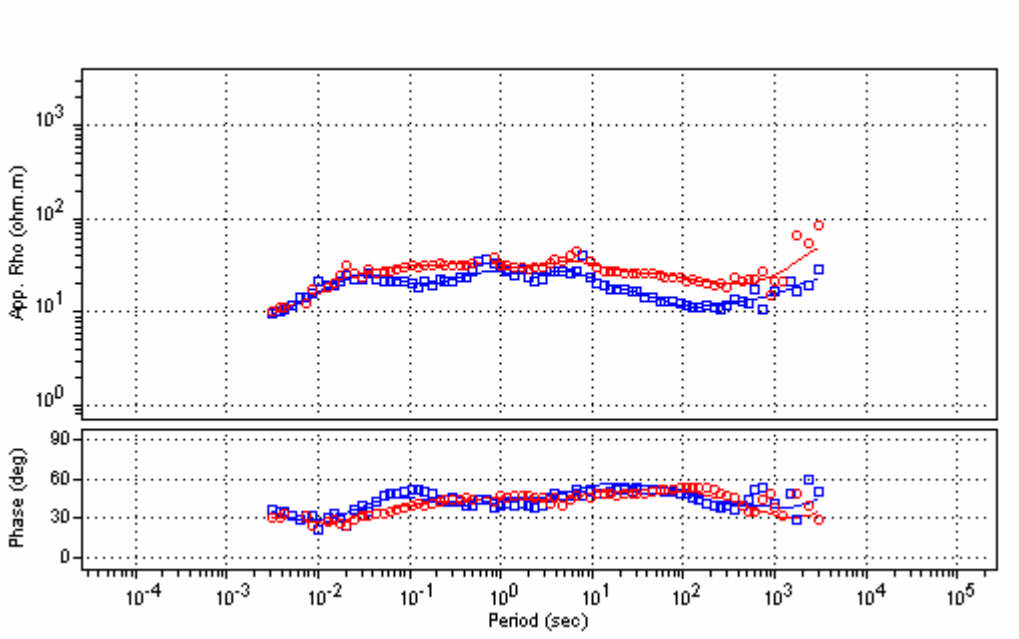

NTL011

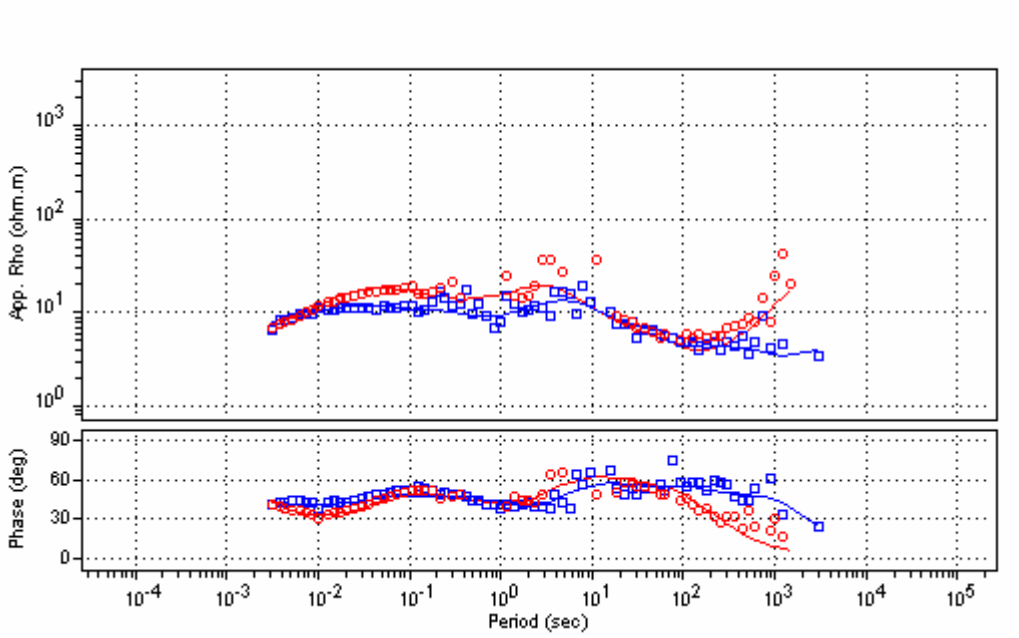

NTL015

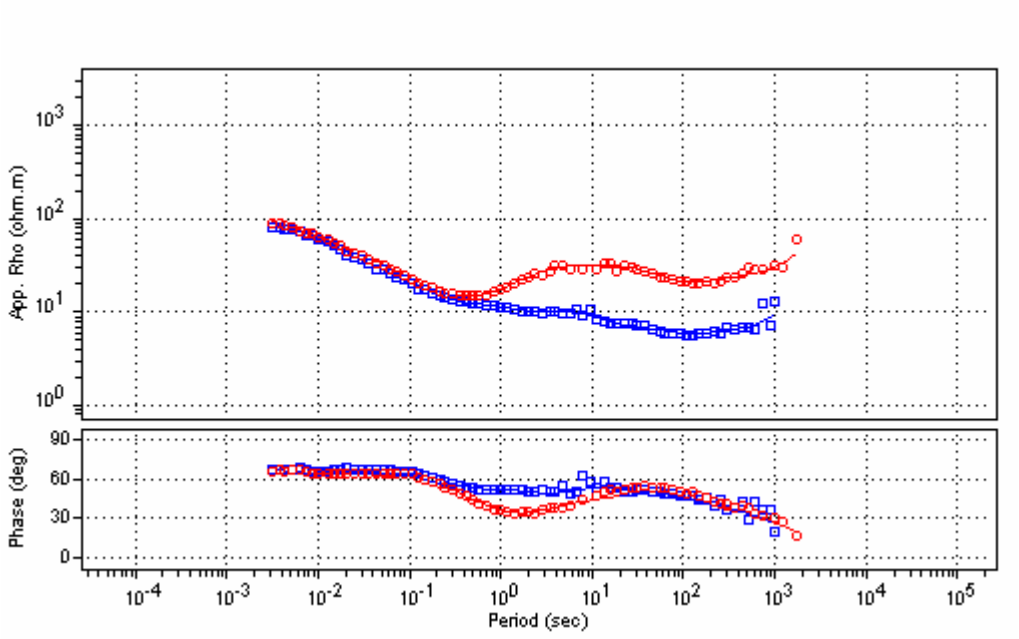

NTL016

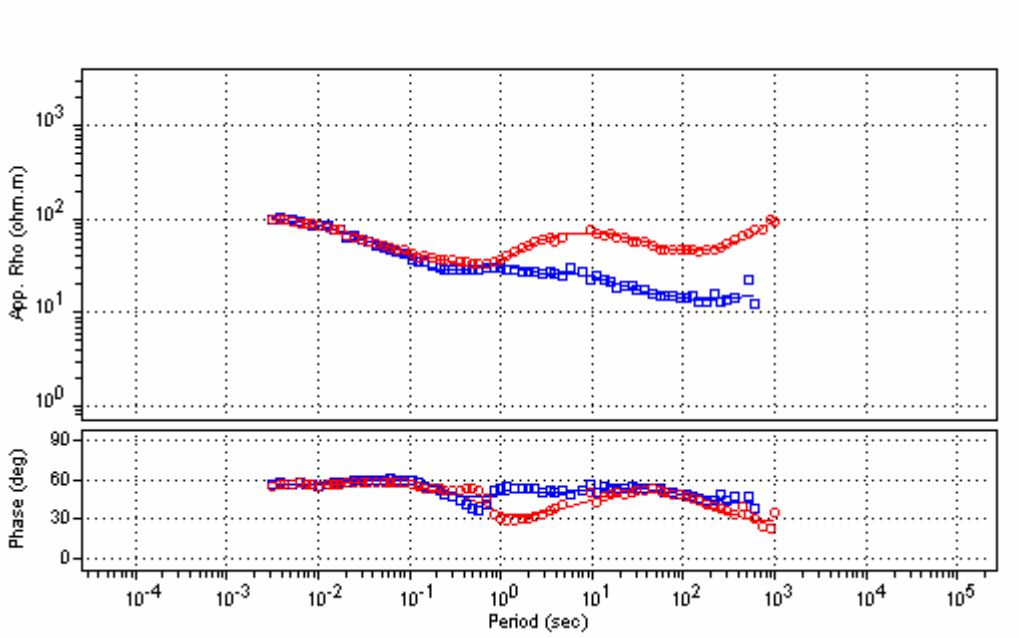

NTL017

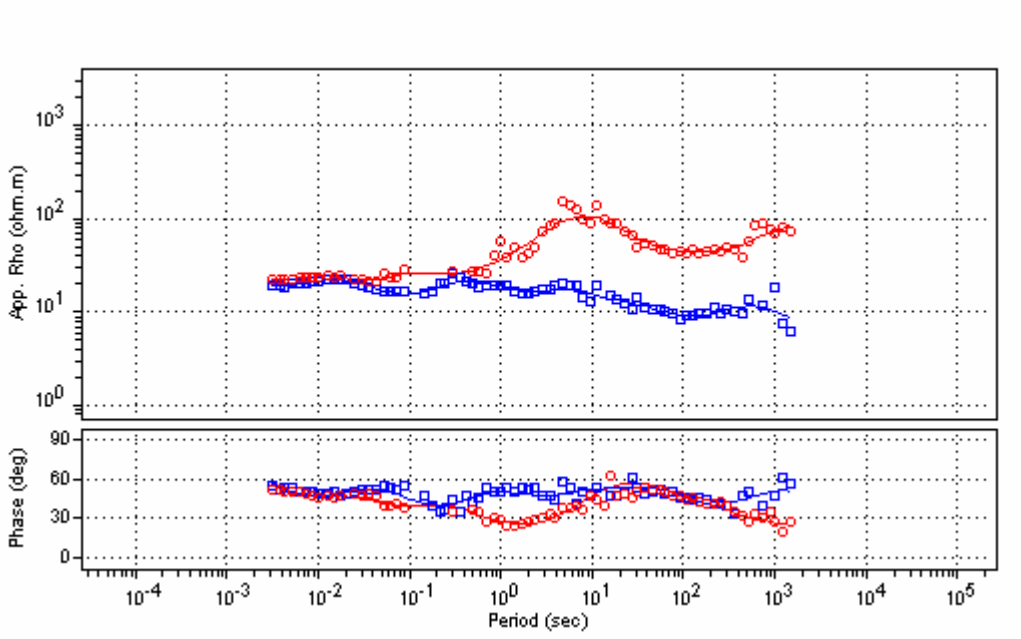

NTL018

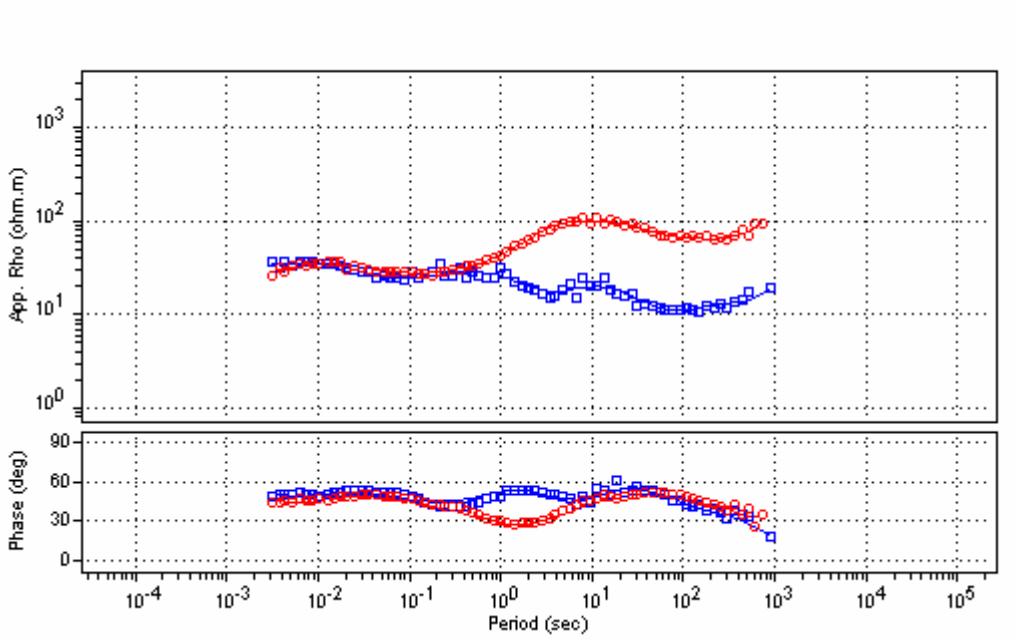

NTL019

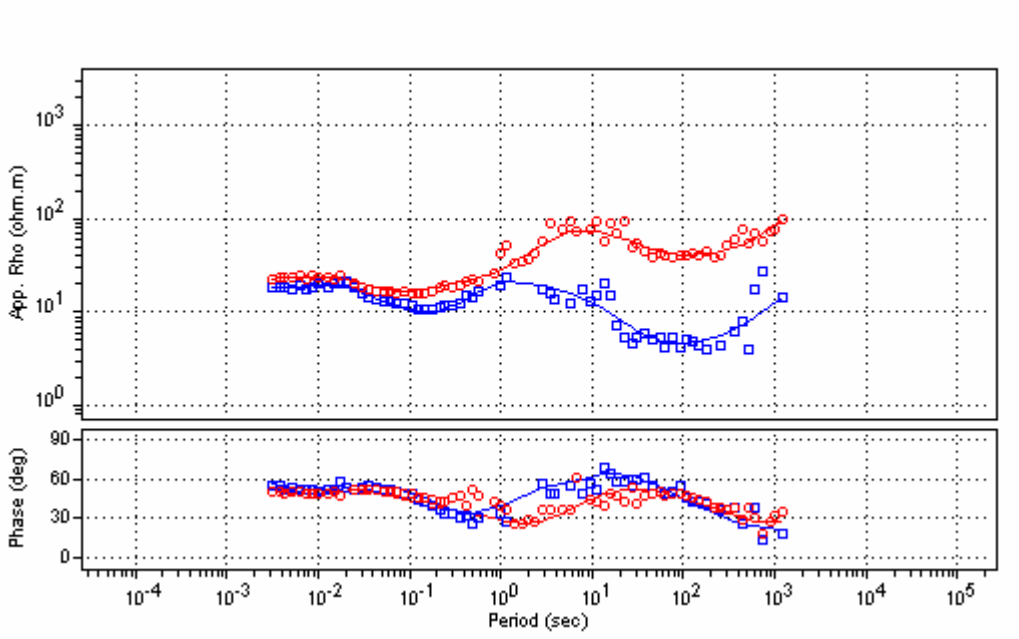

NTL020

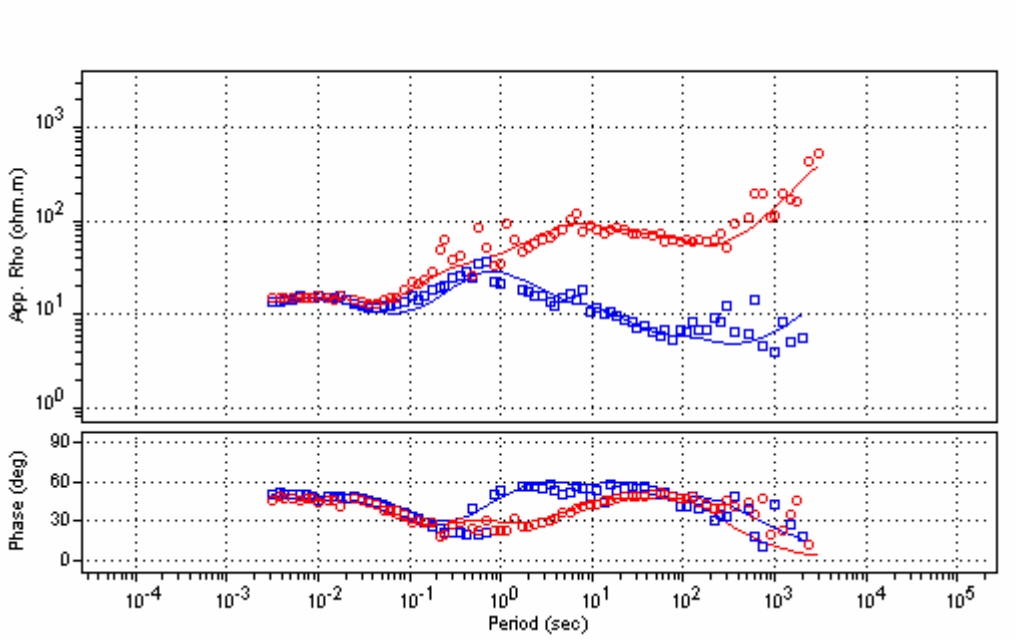

NTL021

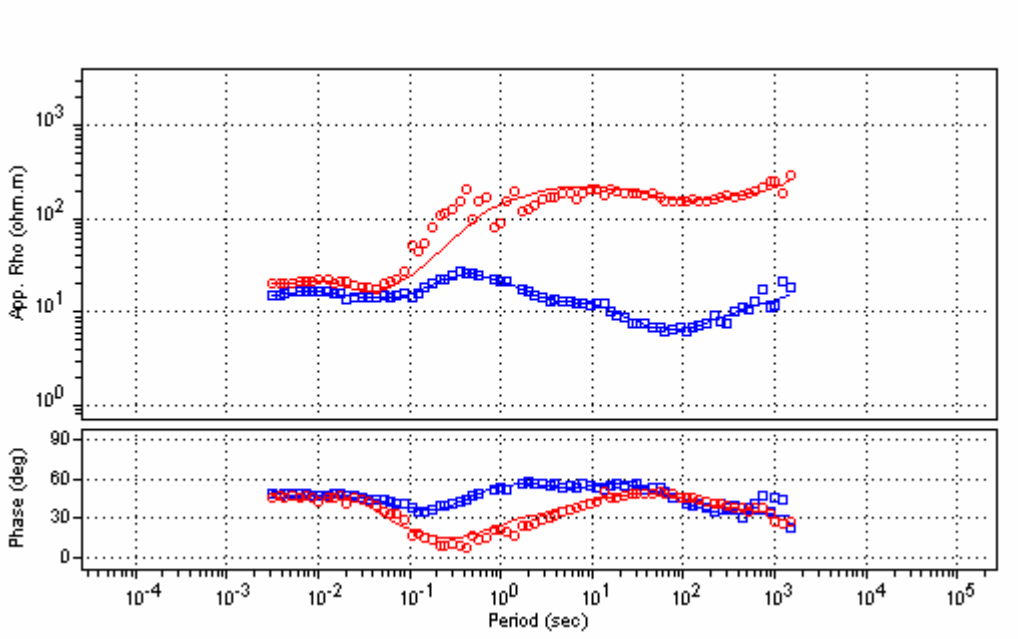

NTL022

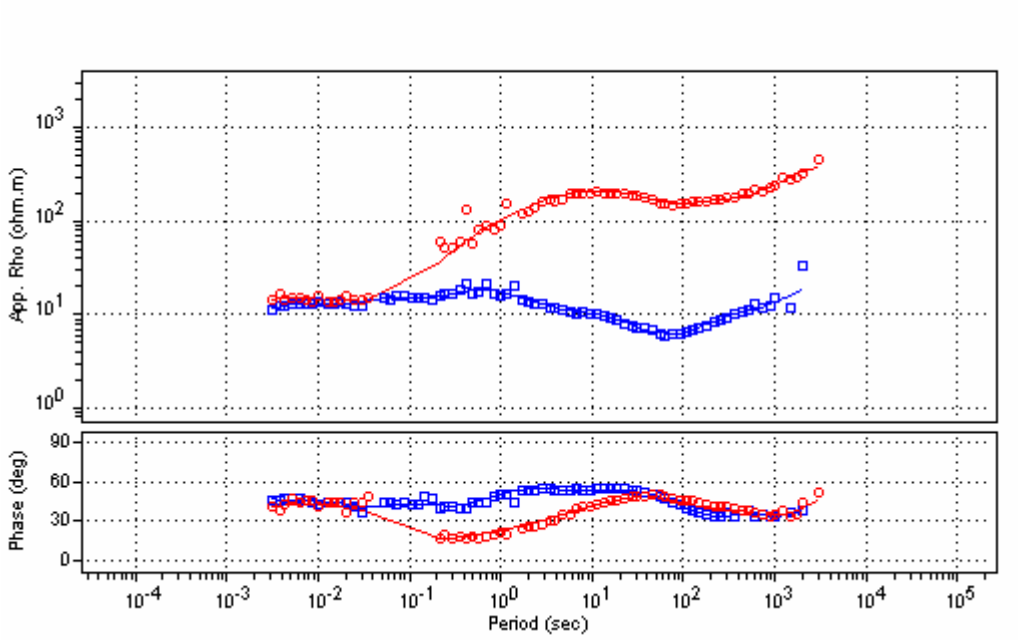

NTL023

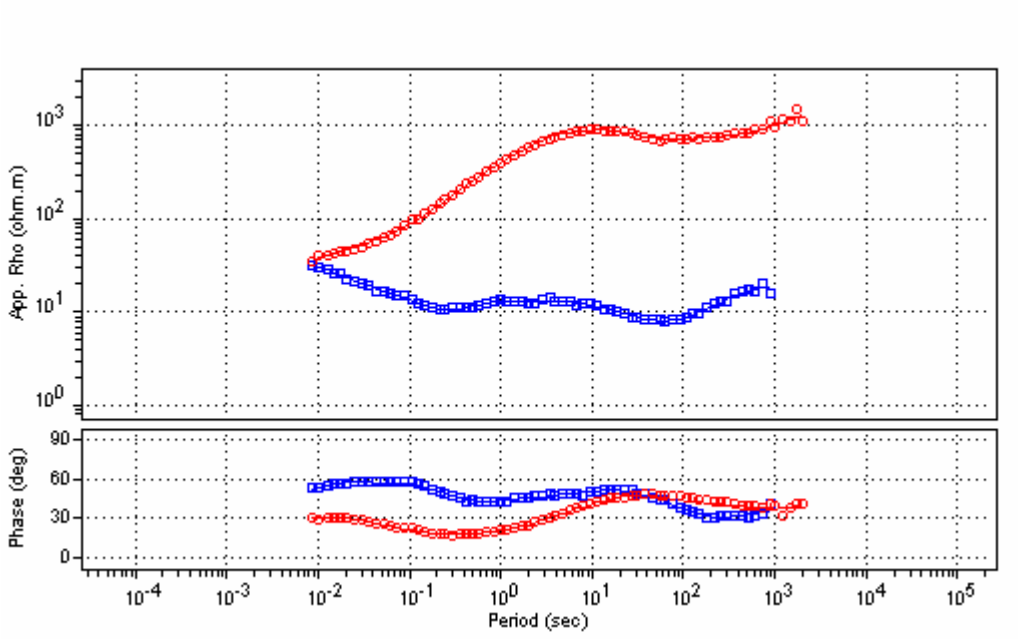

NTL024

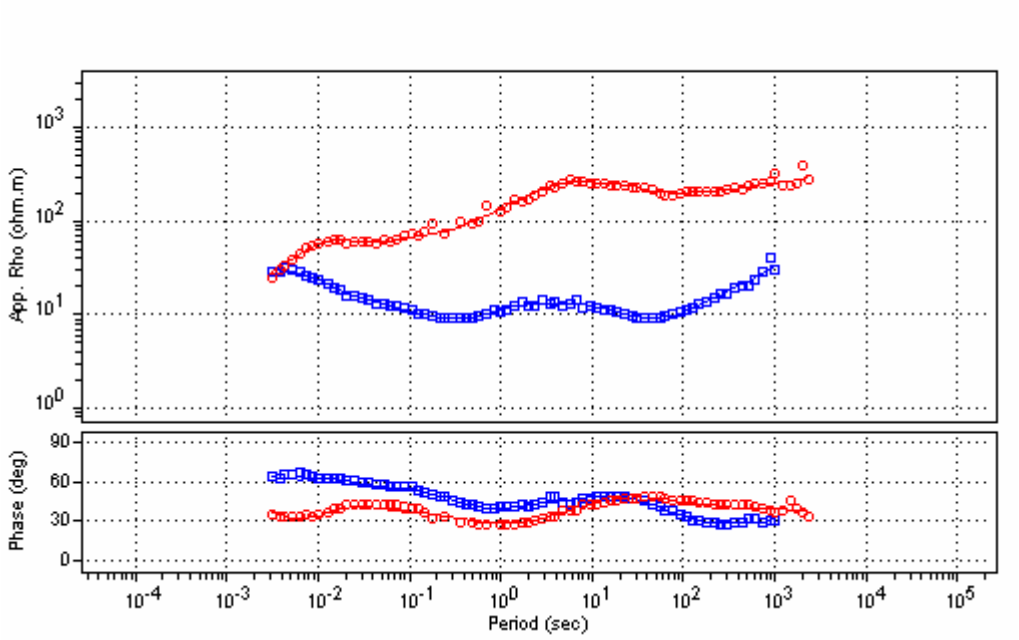

NTL025

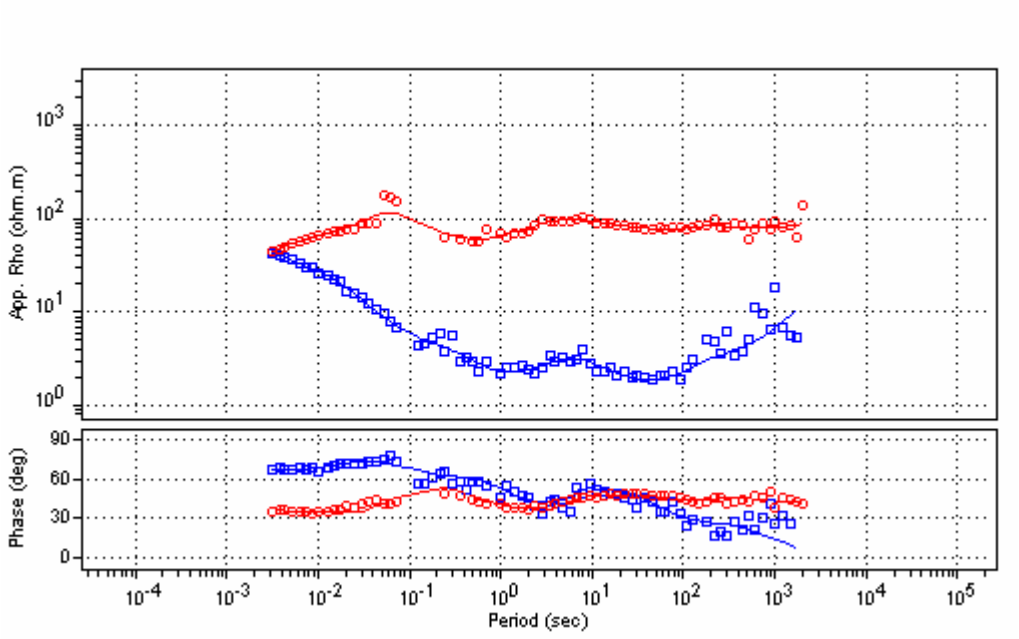

NTL026

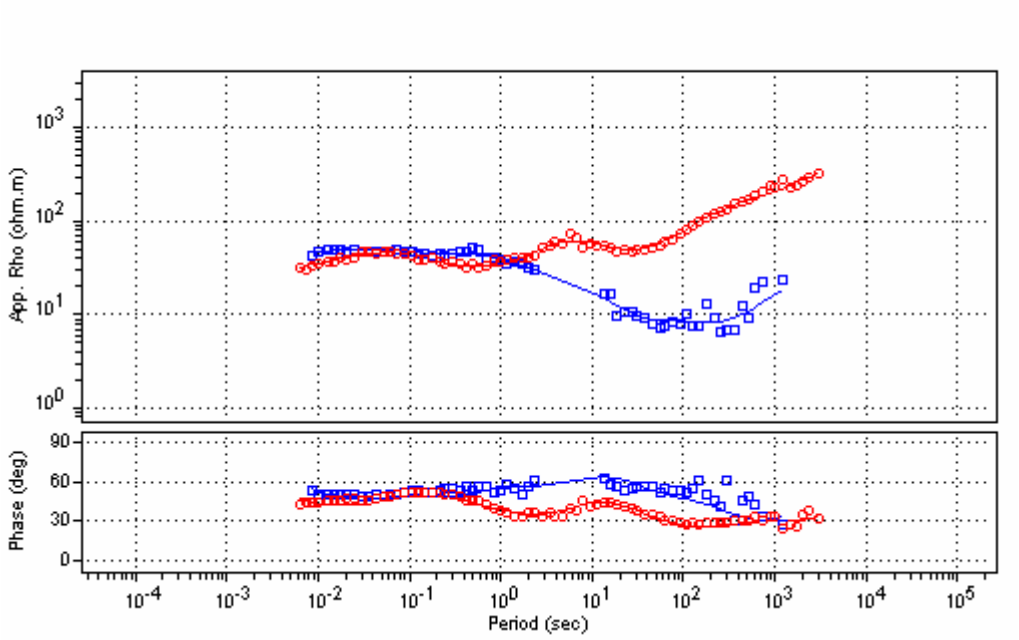

NTL027

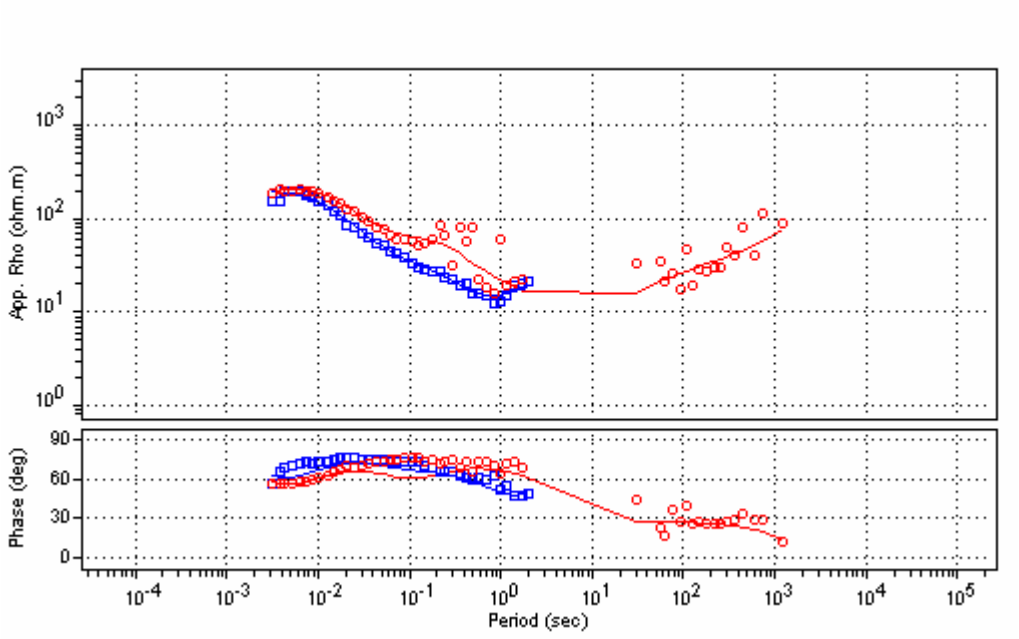

NTL028

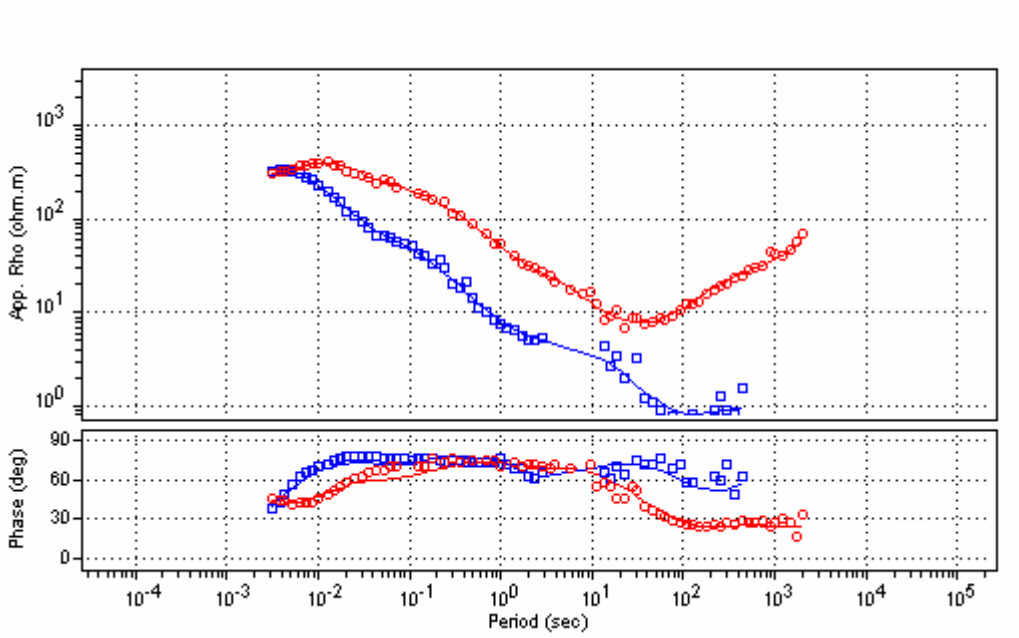

NTL029

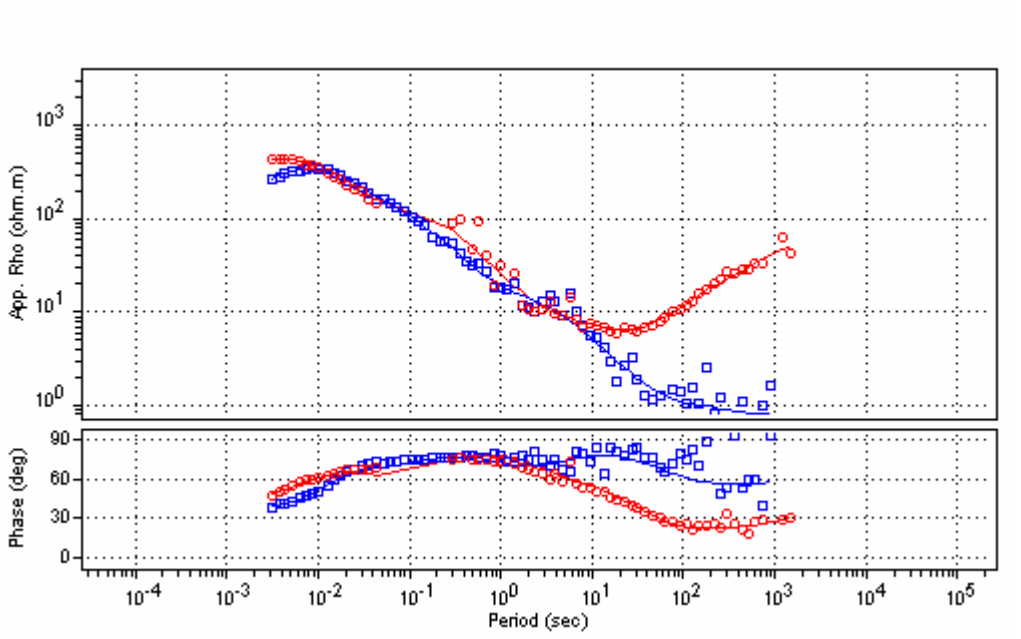

NTL030

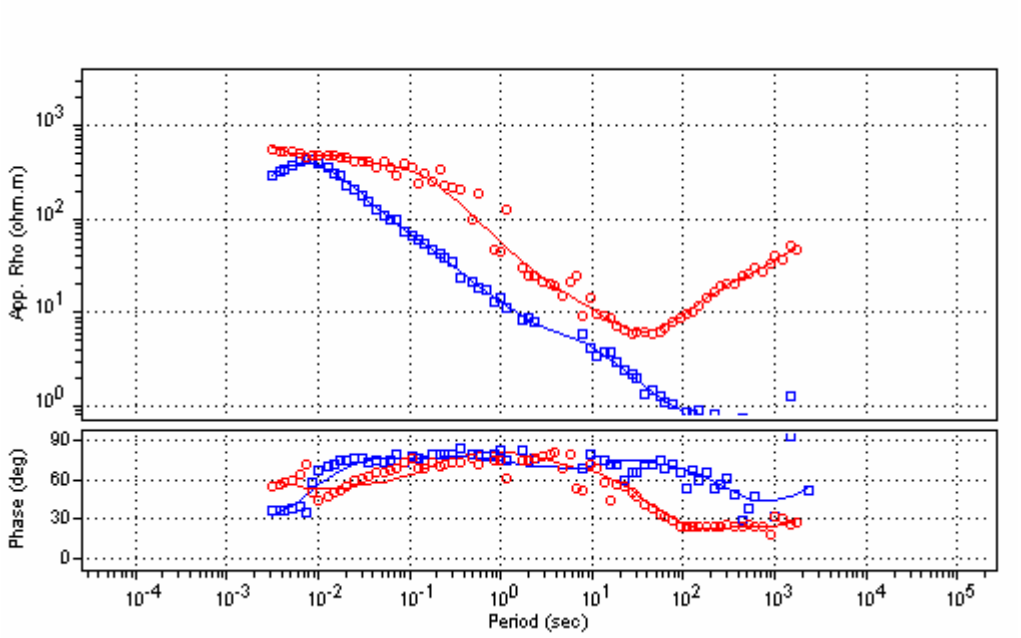

NTL031

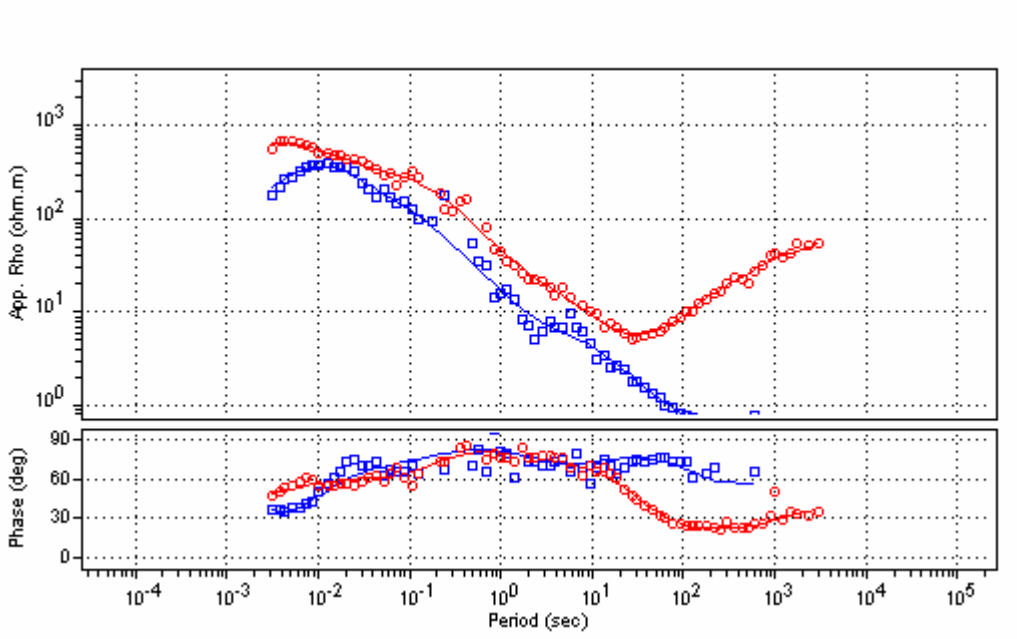

NTL032

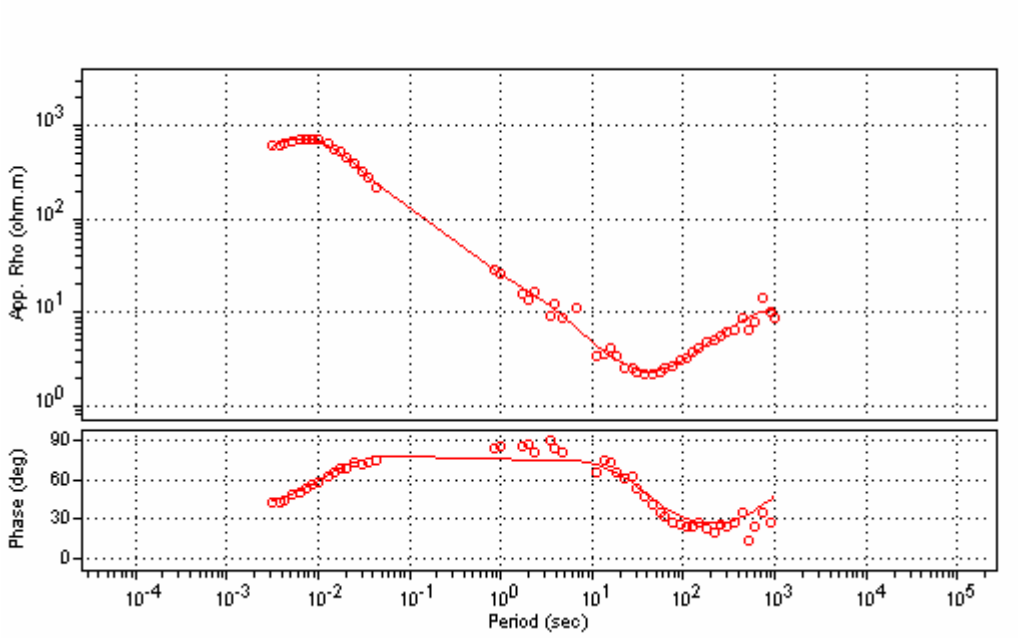

NTL033

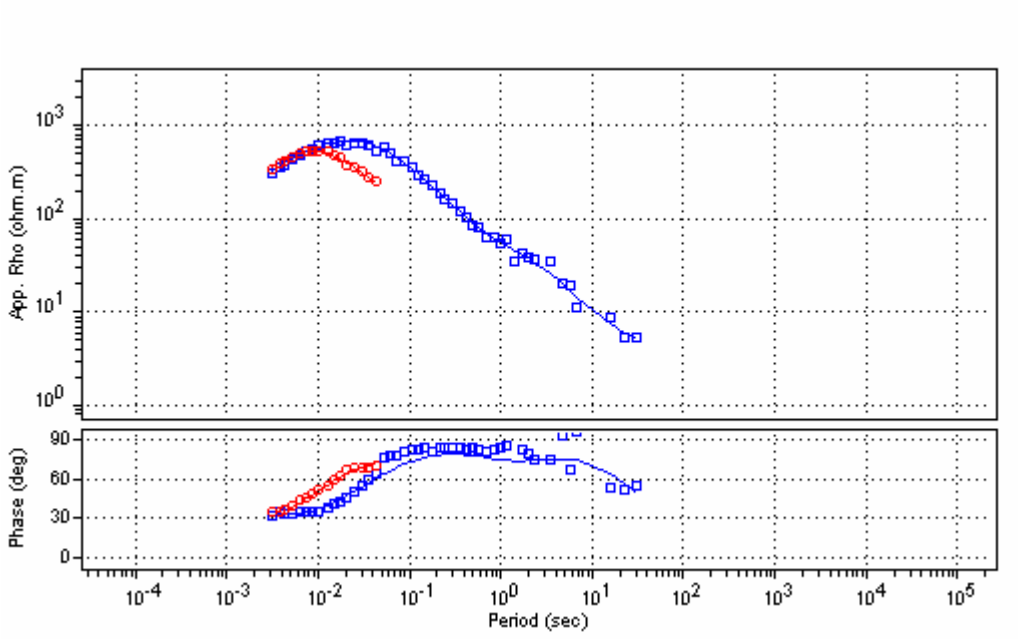

NTL034

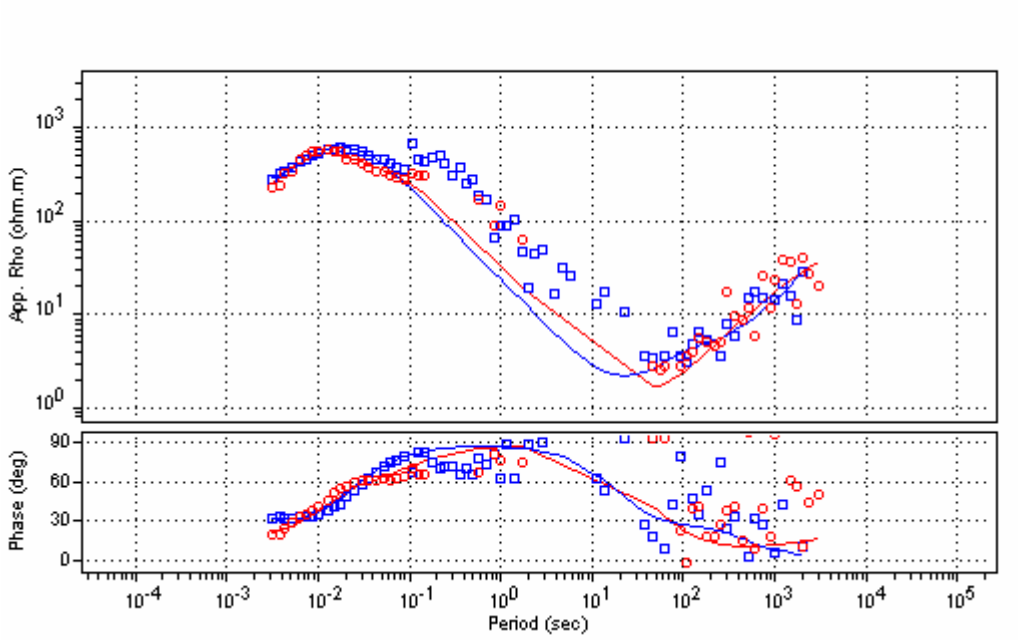

NTL035

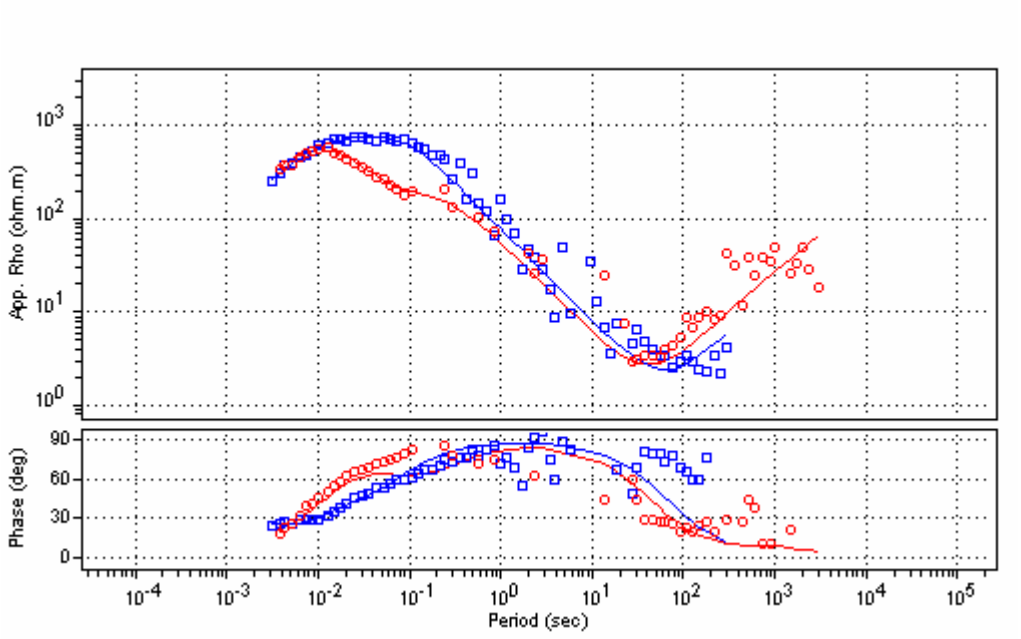

NTL036

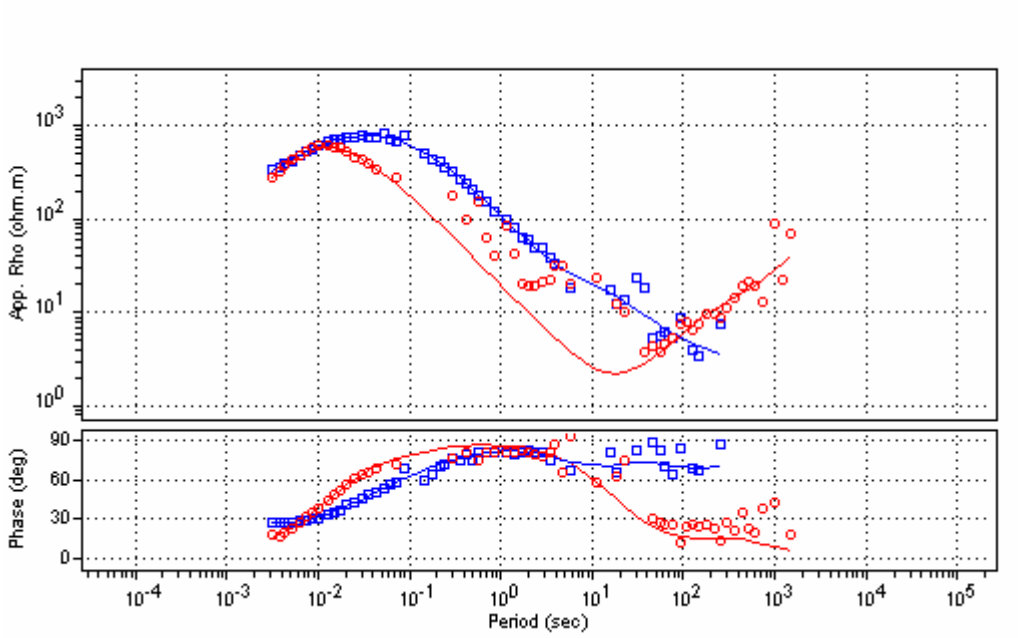

NTL037

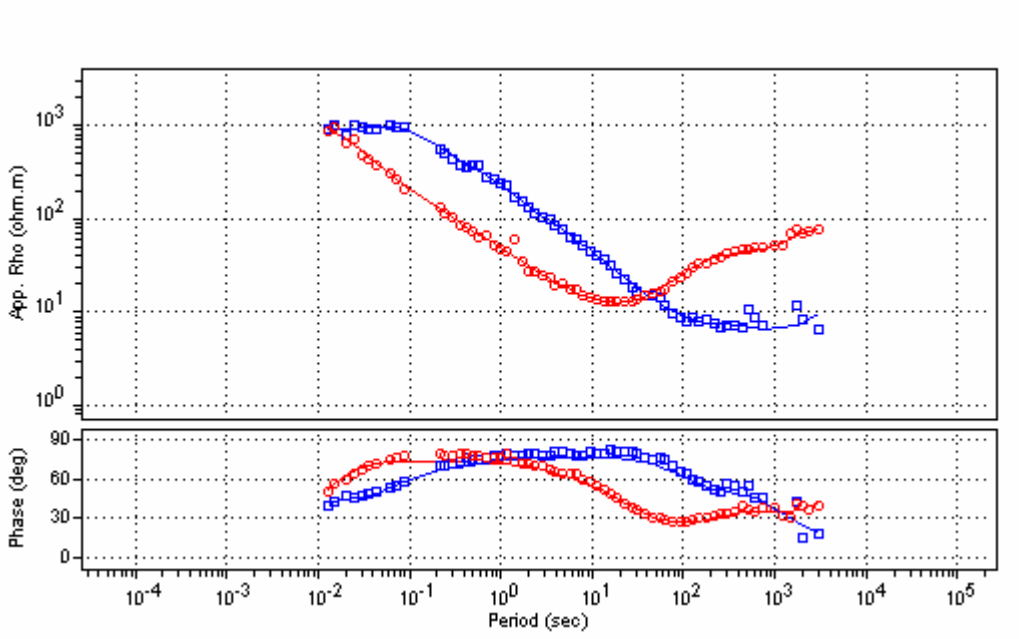

NTL038

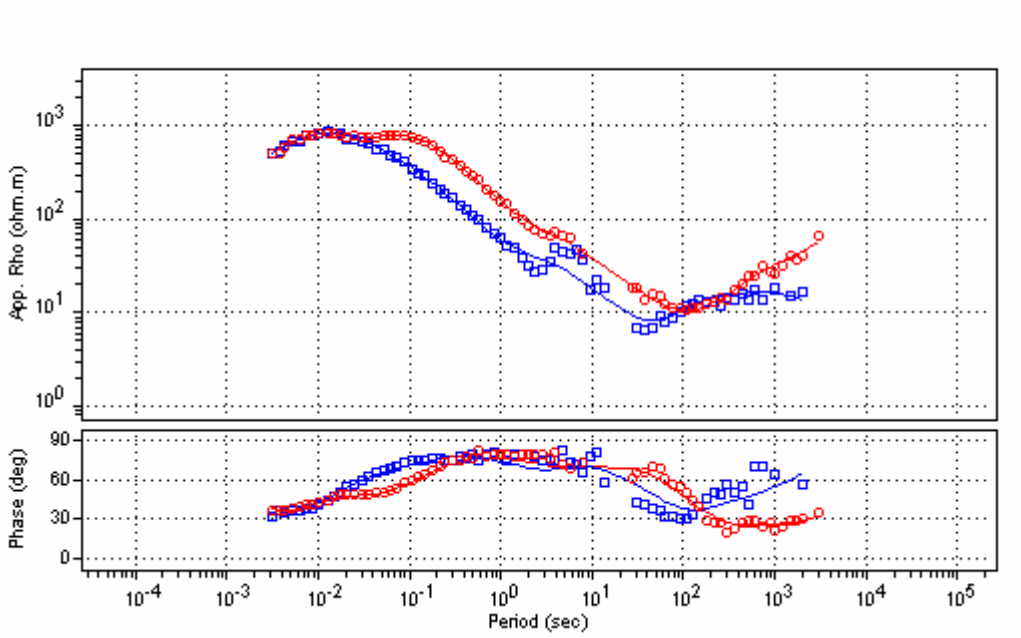

NTL040

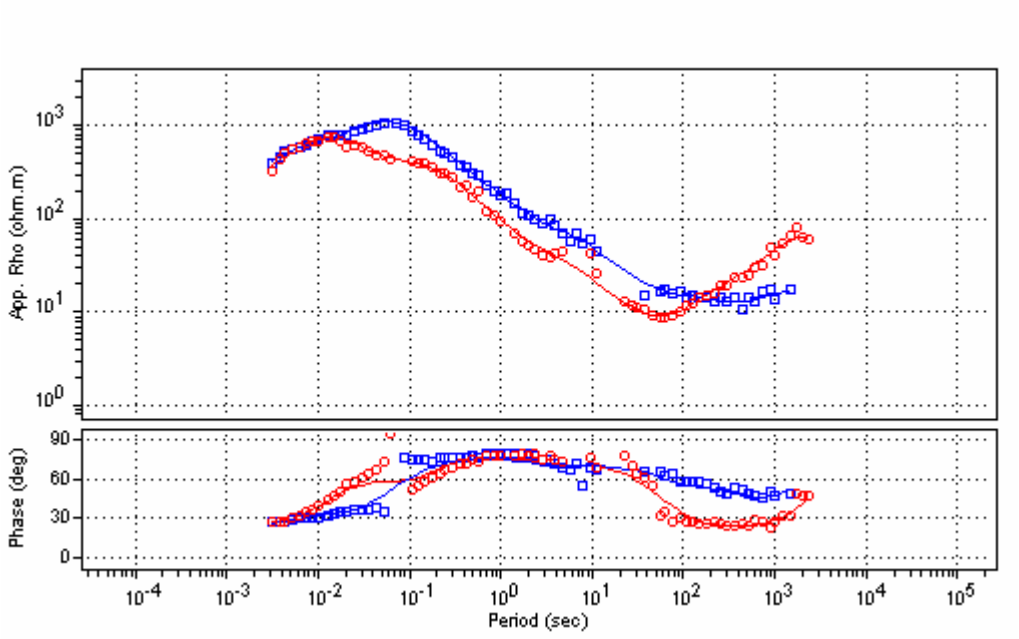

NTL041

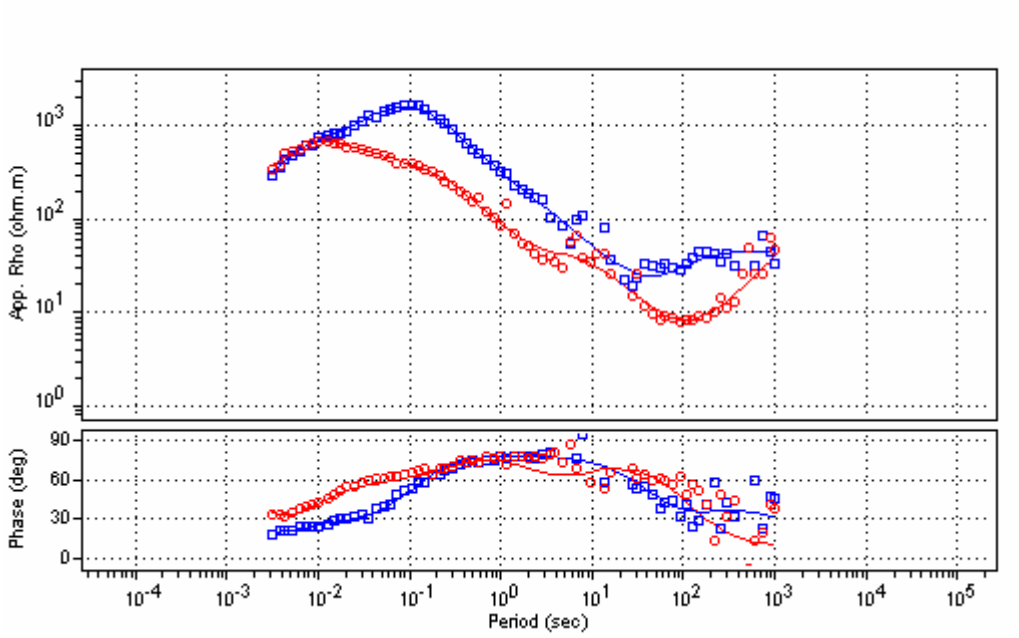

NTL042

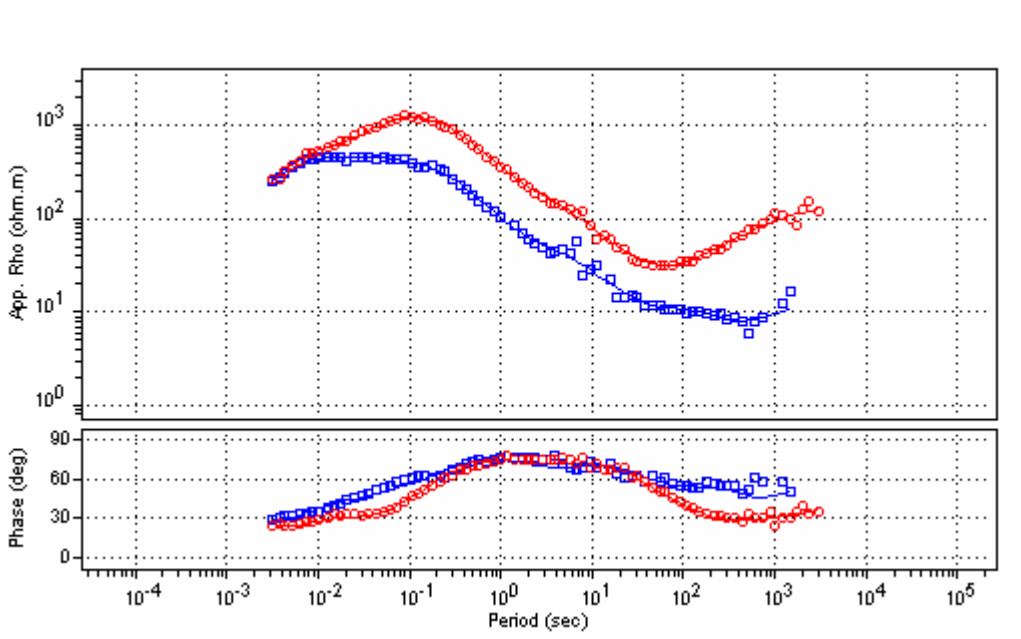
App. Rho (ohm.m)
10^3
10^2
10^1
10^0
Phase (deg)
90
60
30
0
10^{-4}
10^{-3}
10^{-2}
10^{-1}
10^0
10^1
10^2
10^3
10^4
10^5
Period (sec)

NTL043

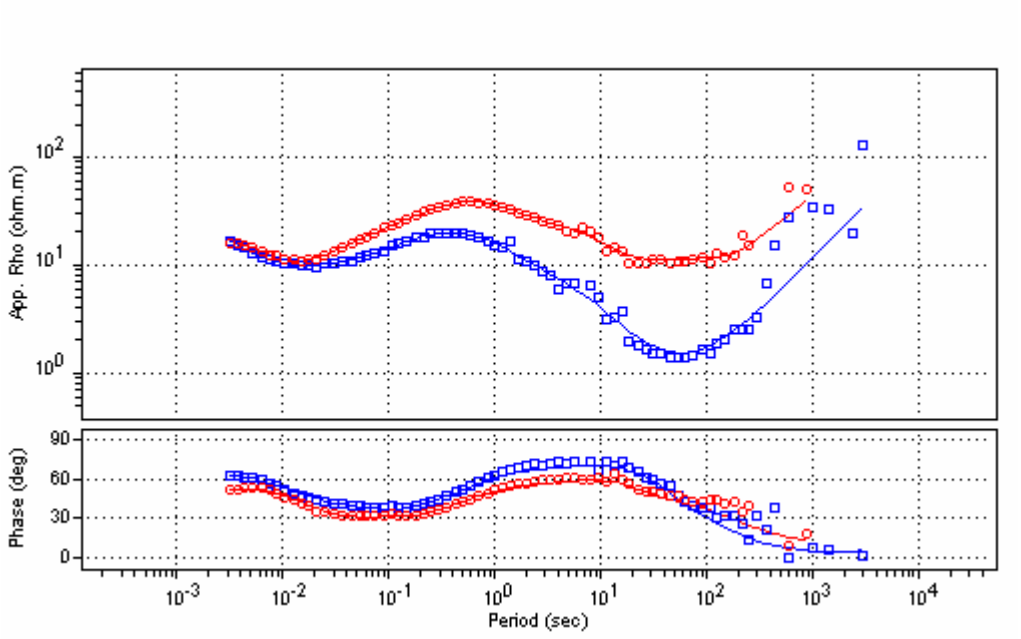

STL002

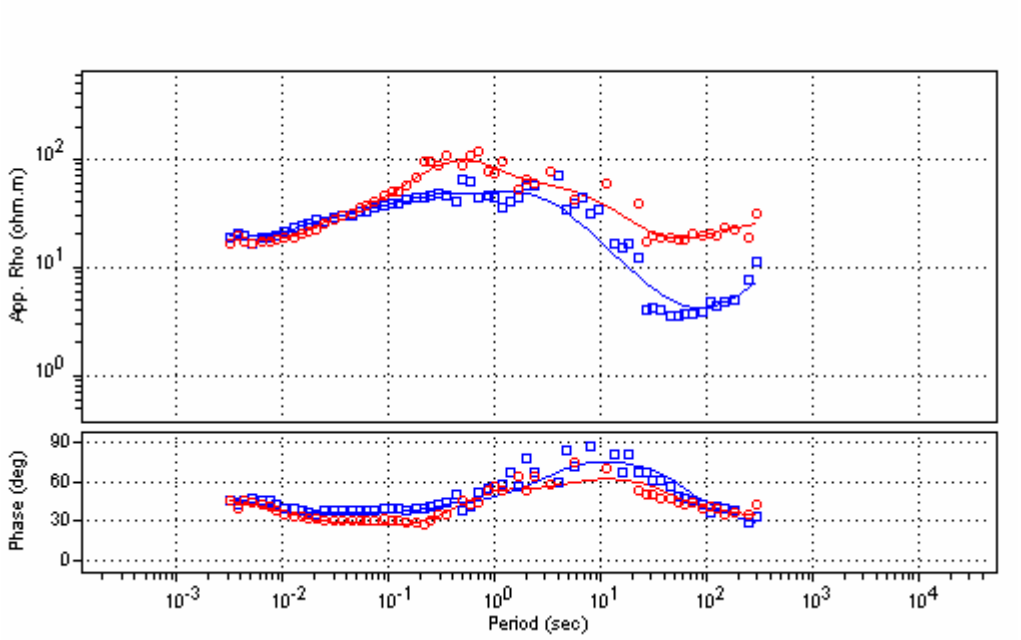

STL003

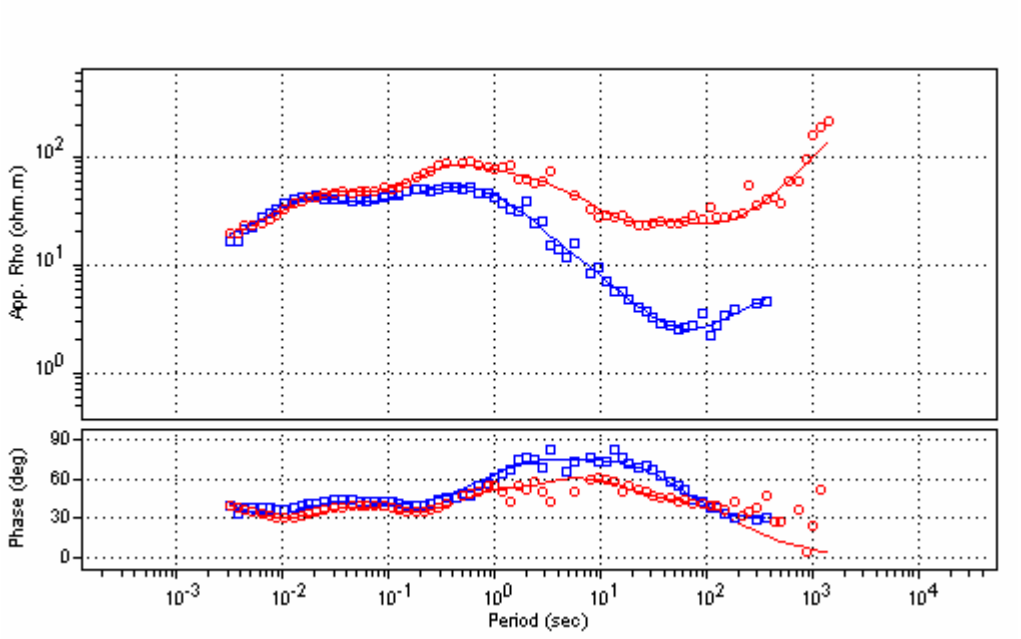

STL004

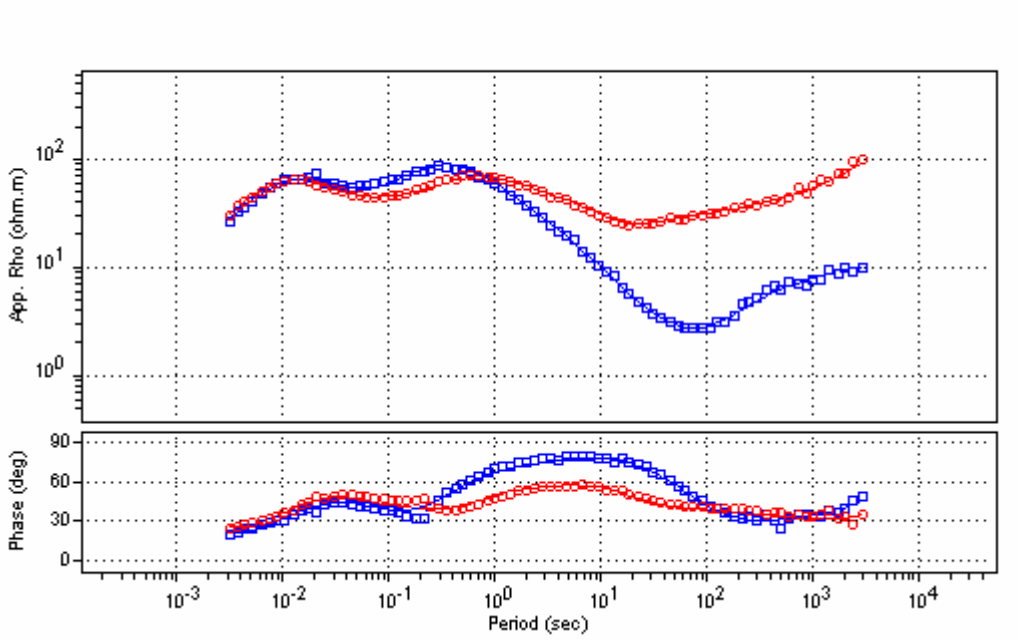

STL005

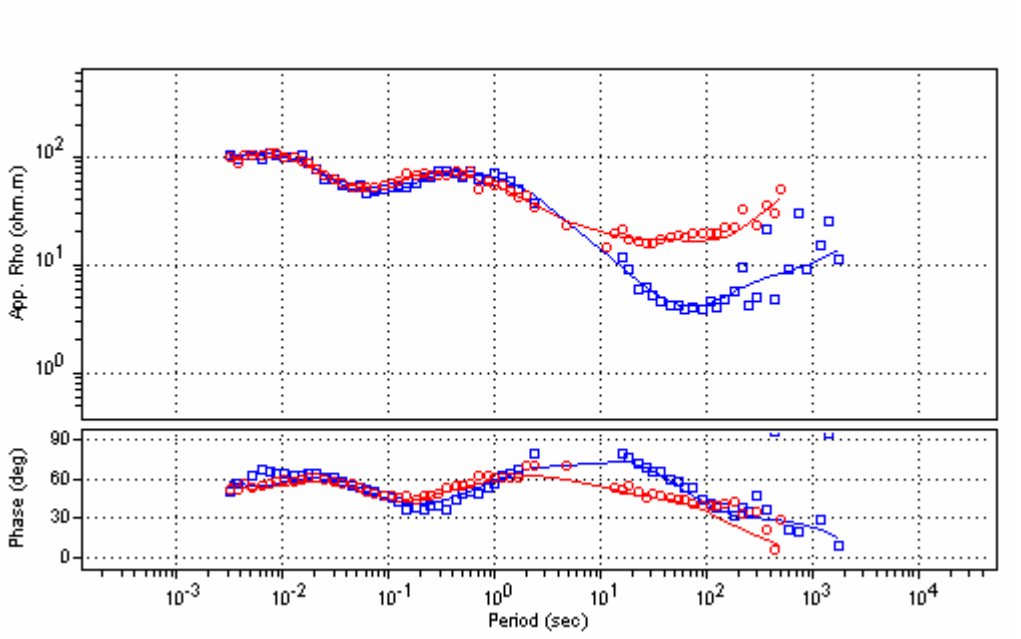

STL006

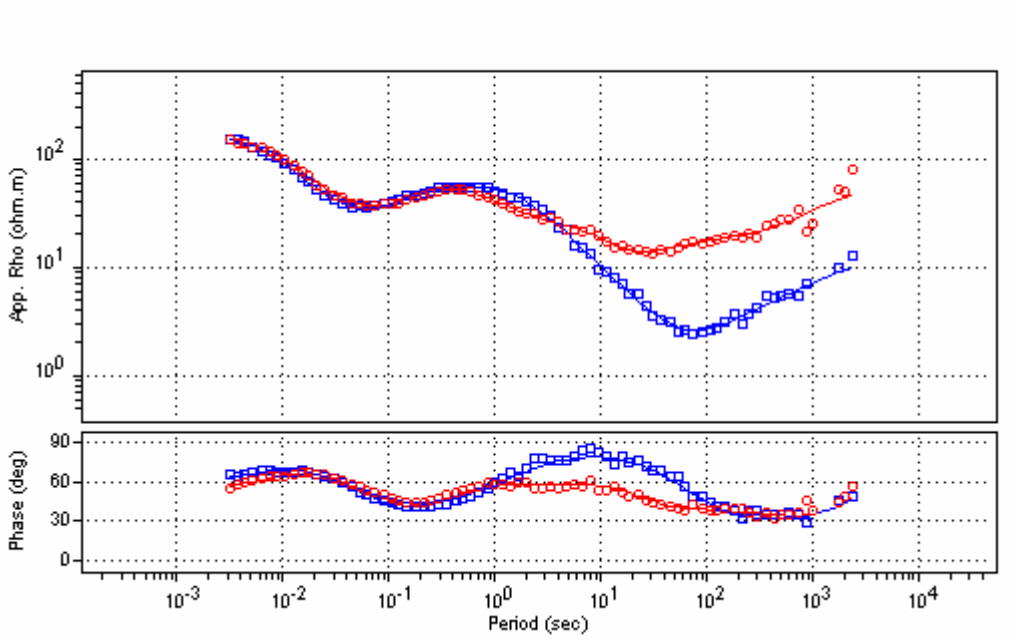

STL007

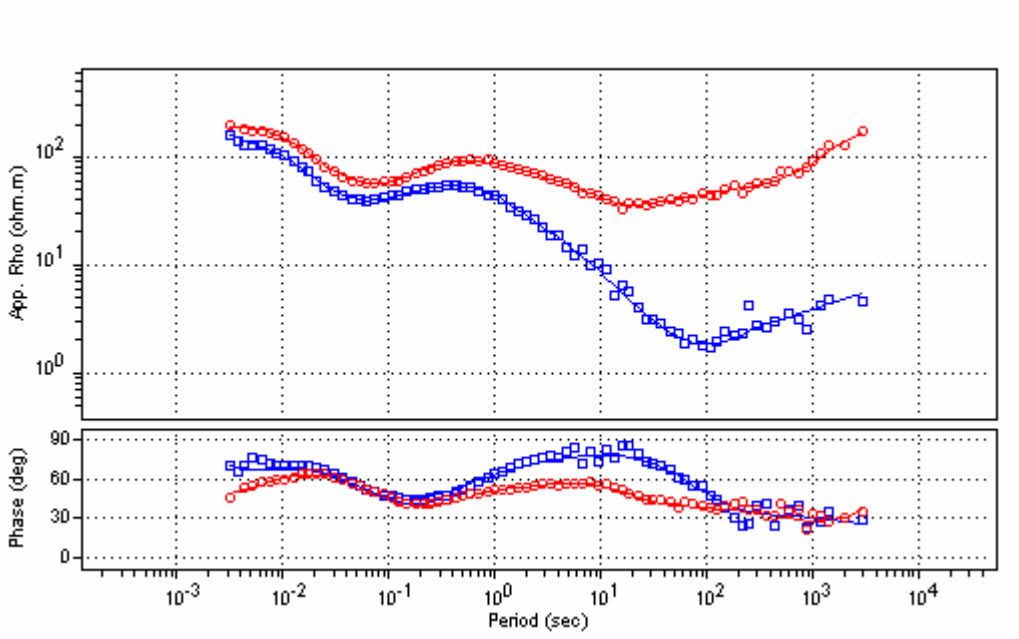

STL008

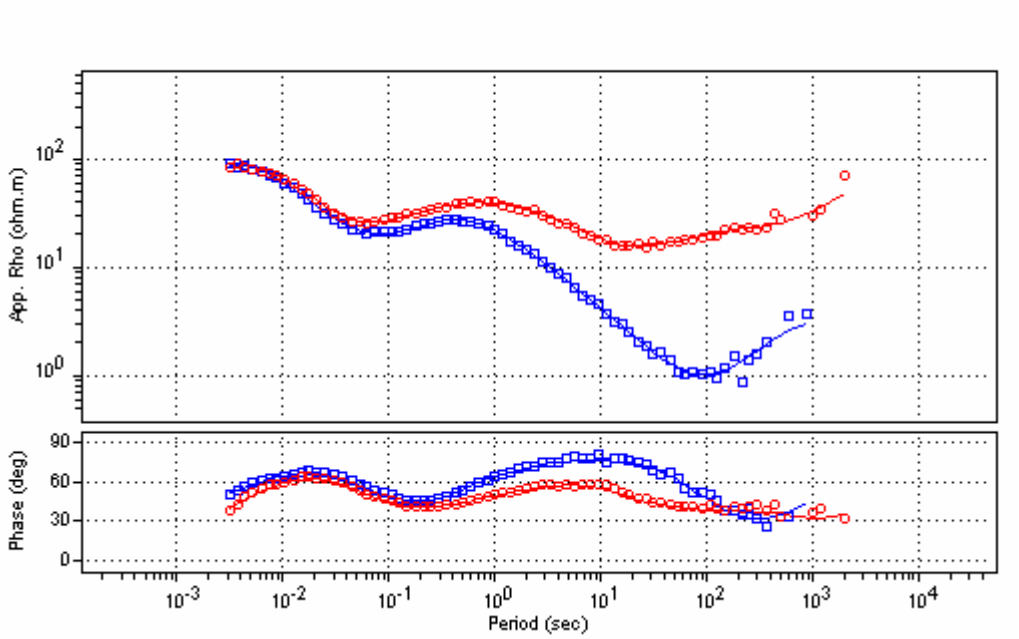

STL009

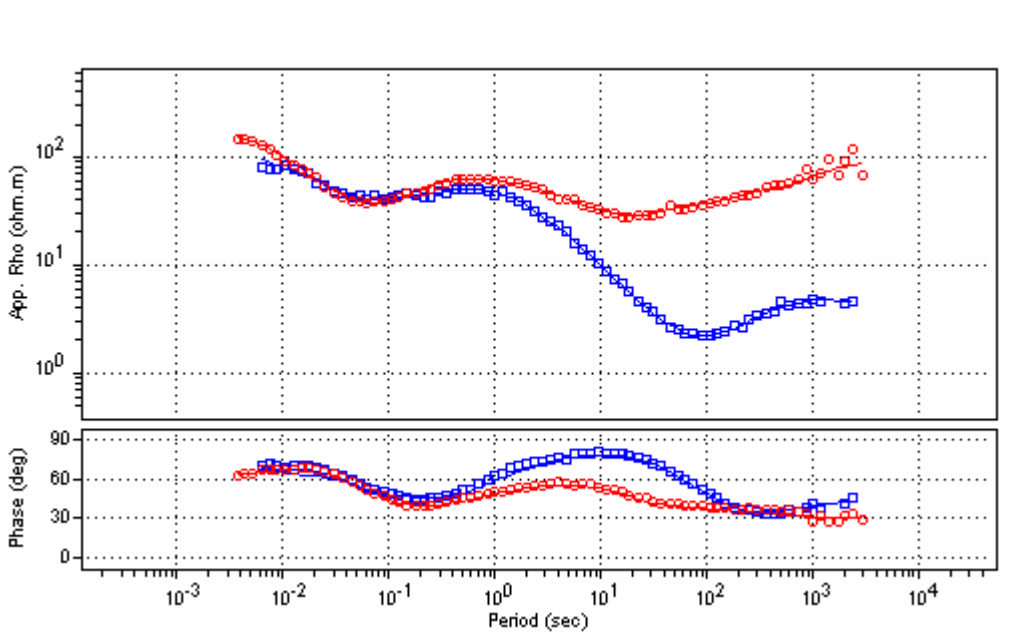

STL010

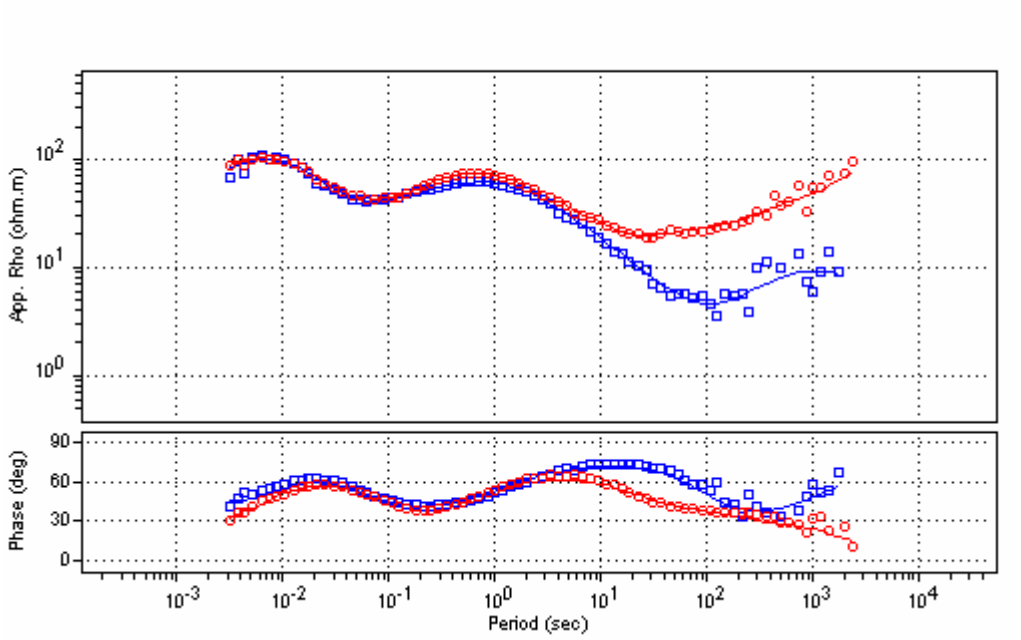

STL011

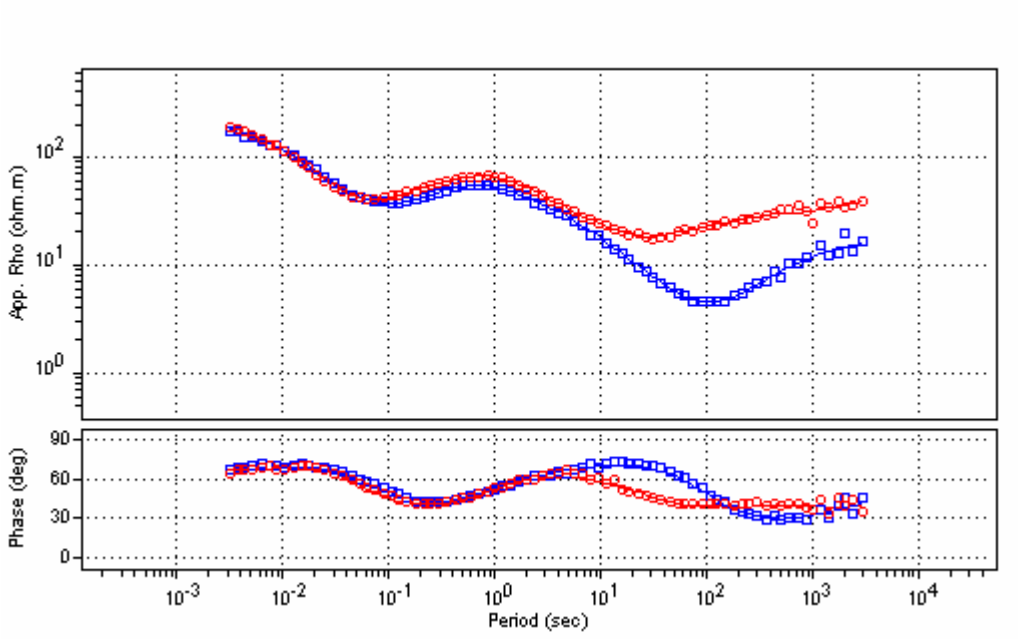

STL012

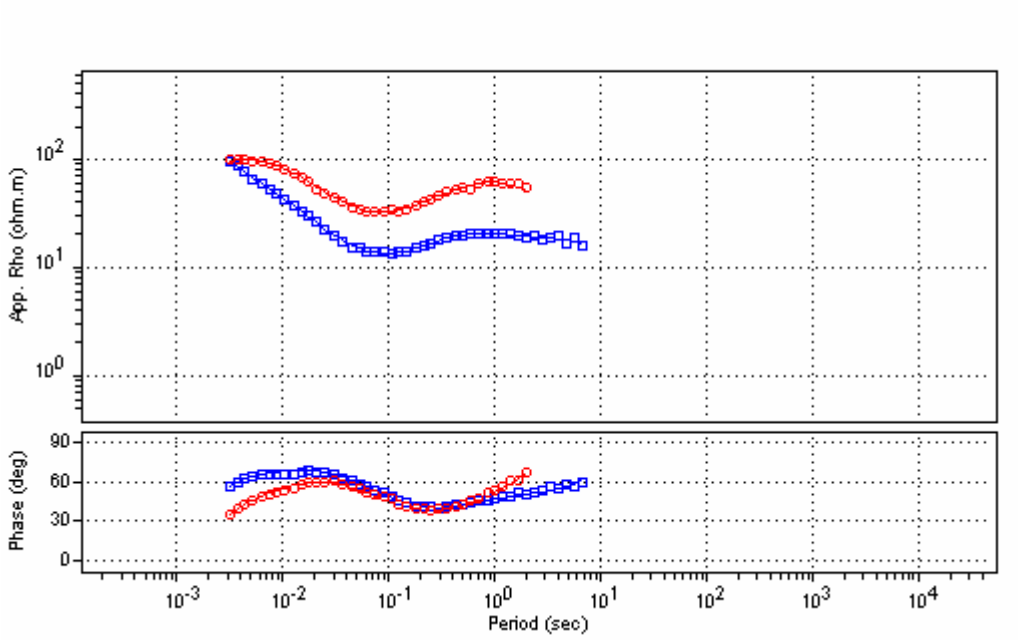

STL013

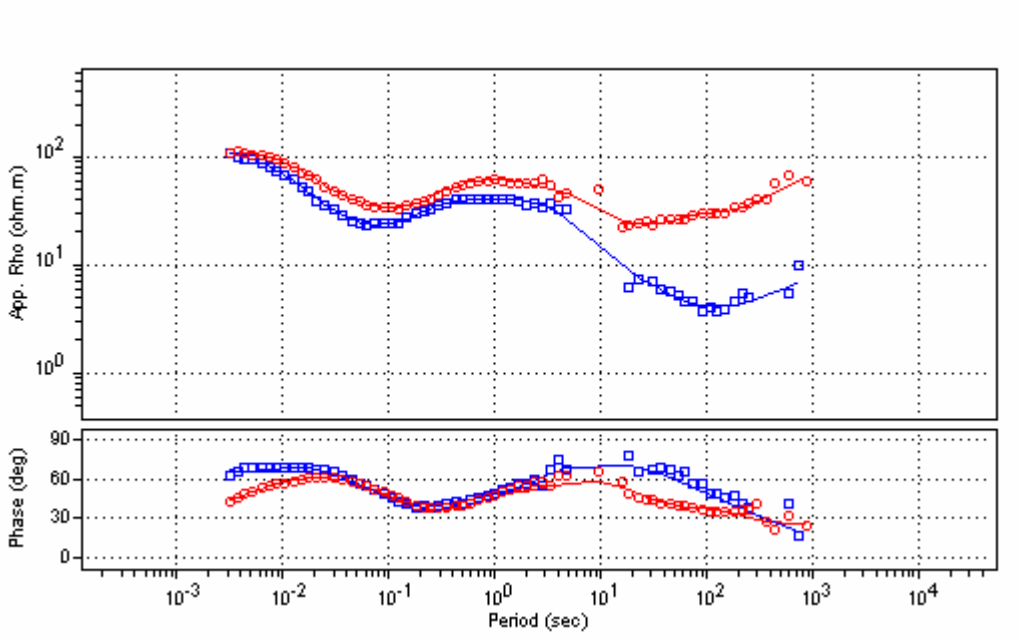

STL014

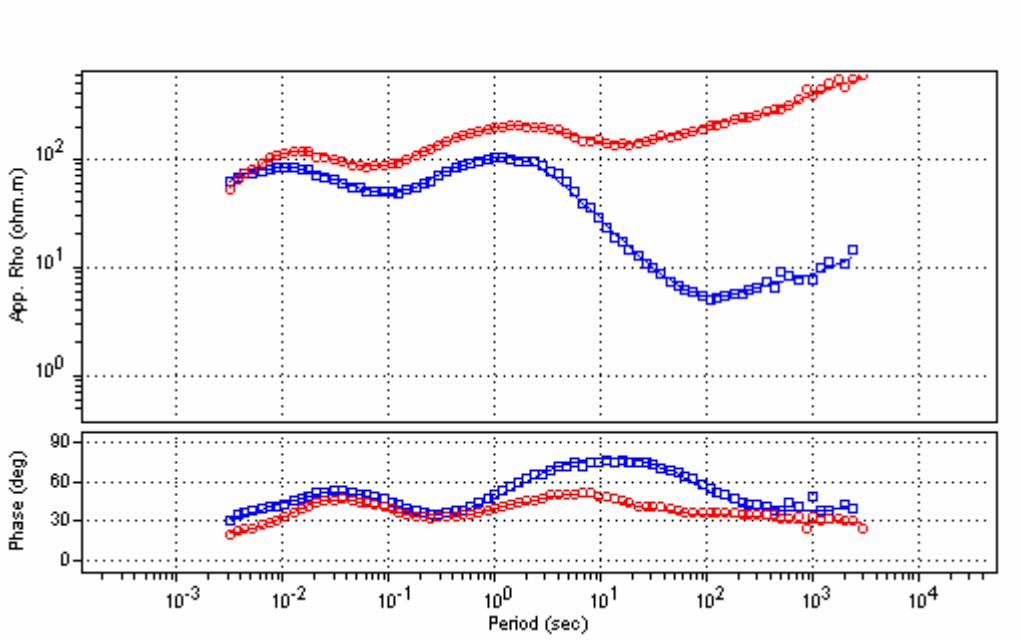

STL015

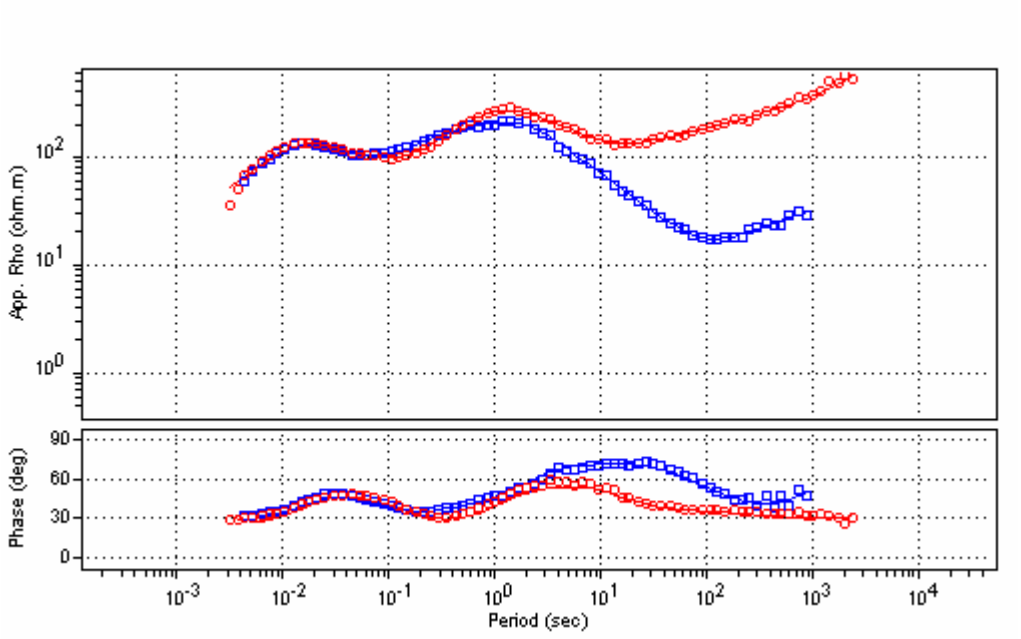

STL016

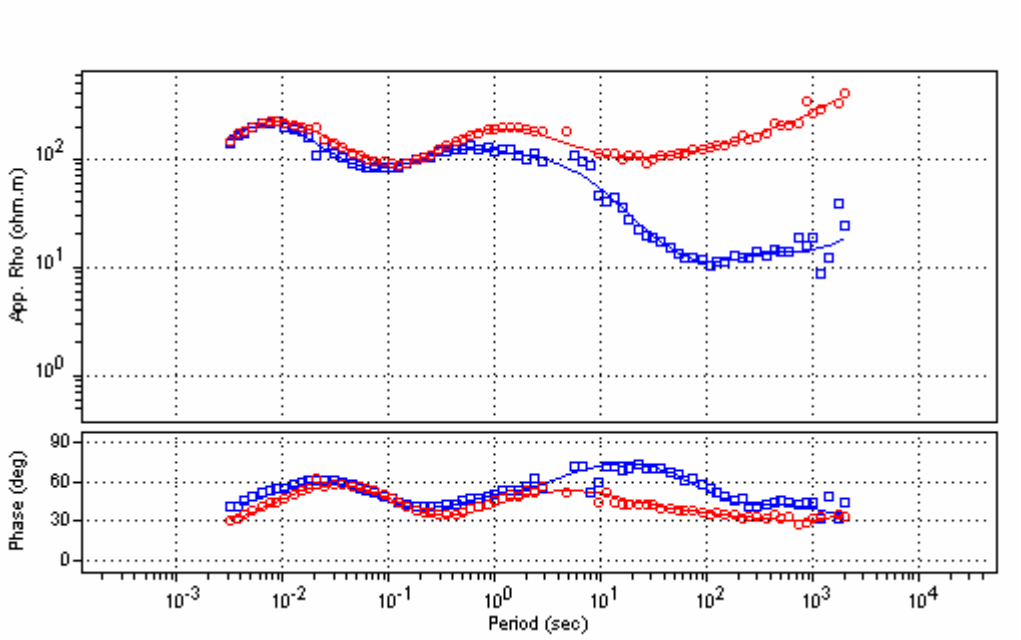

STL017

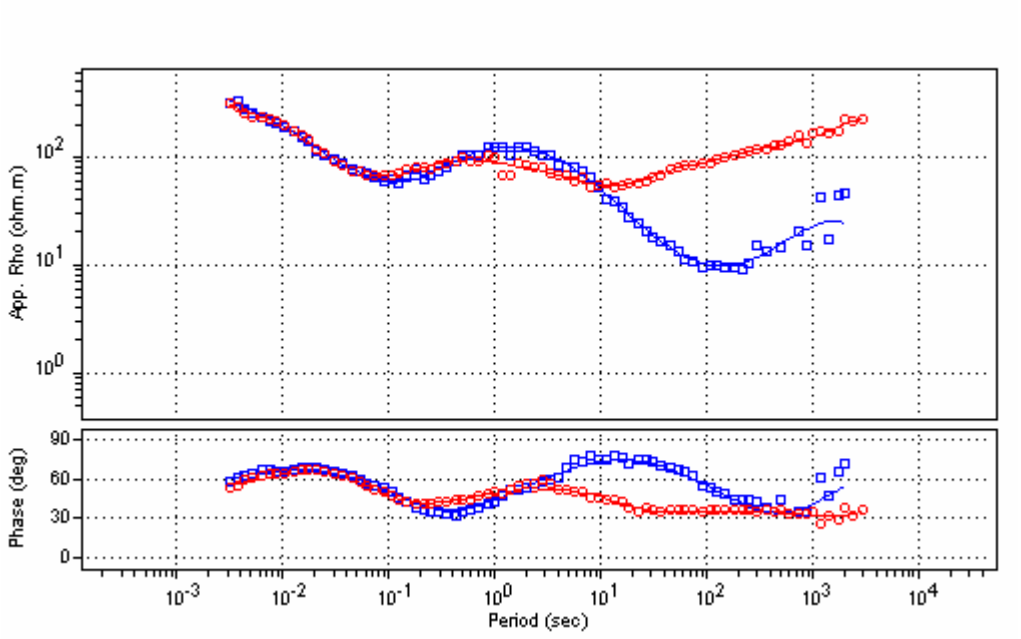

STL018

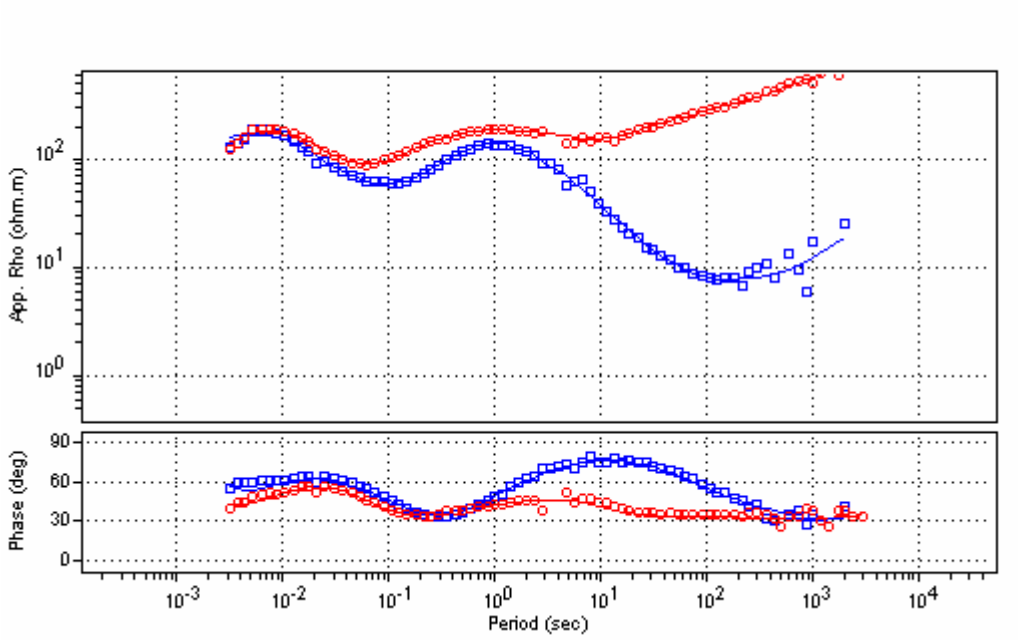

STL019

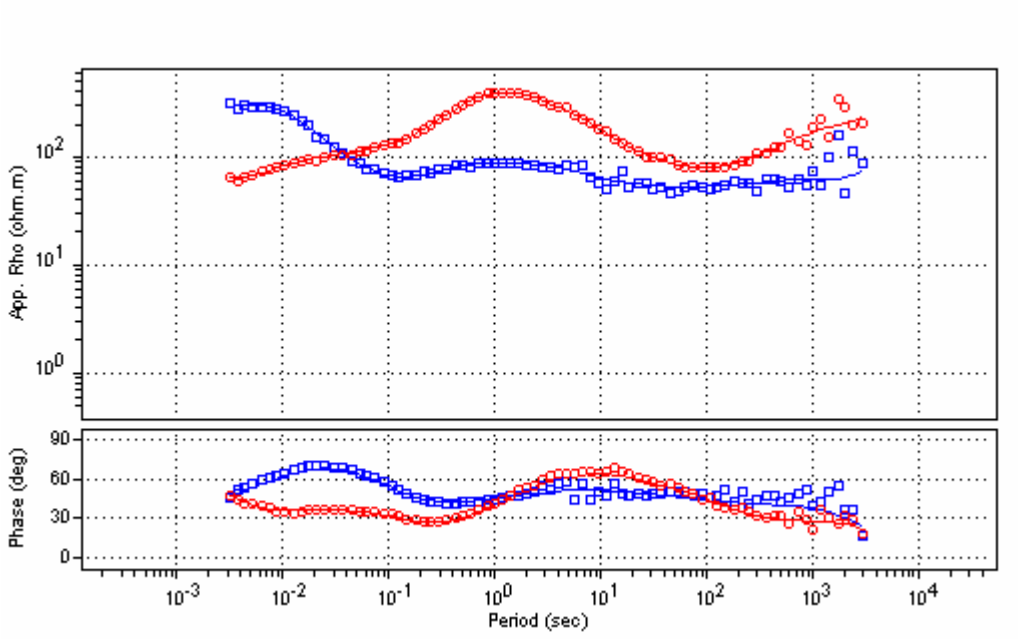

STL20

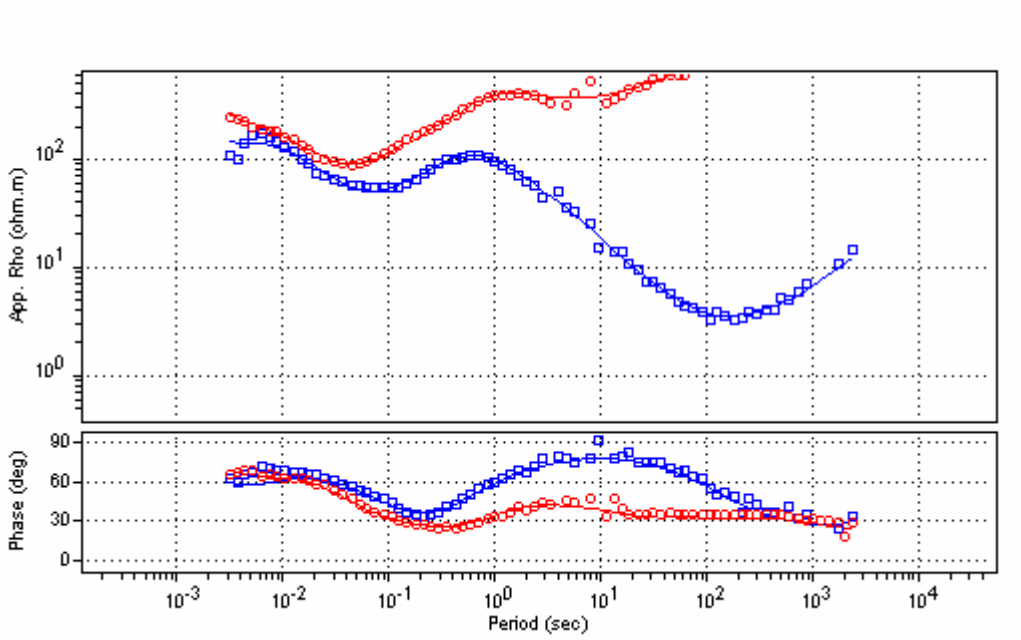

STL021

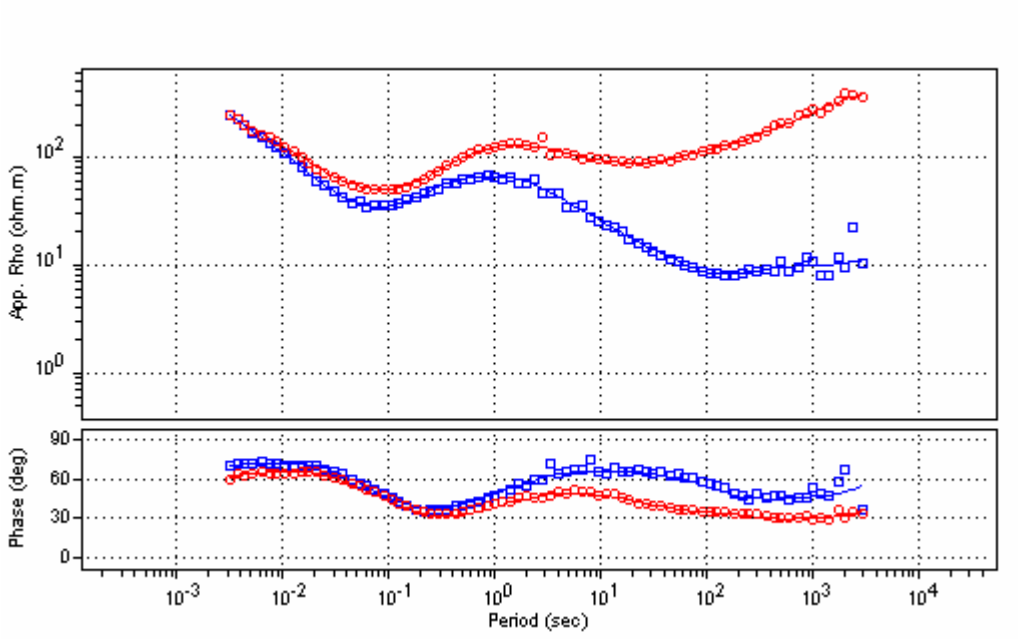

STL022

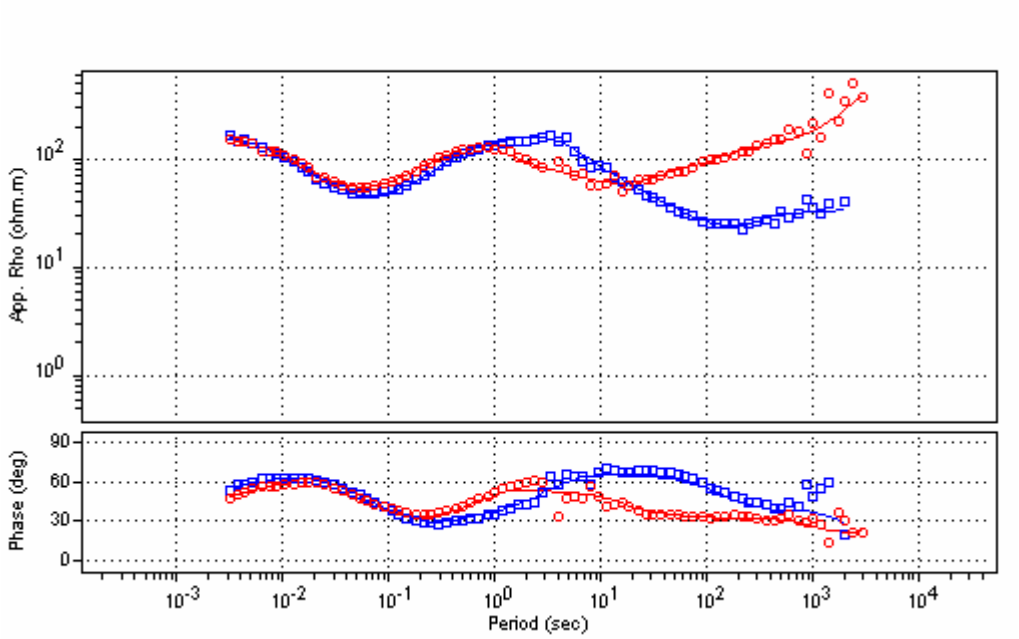

STL023

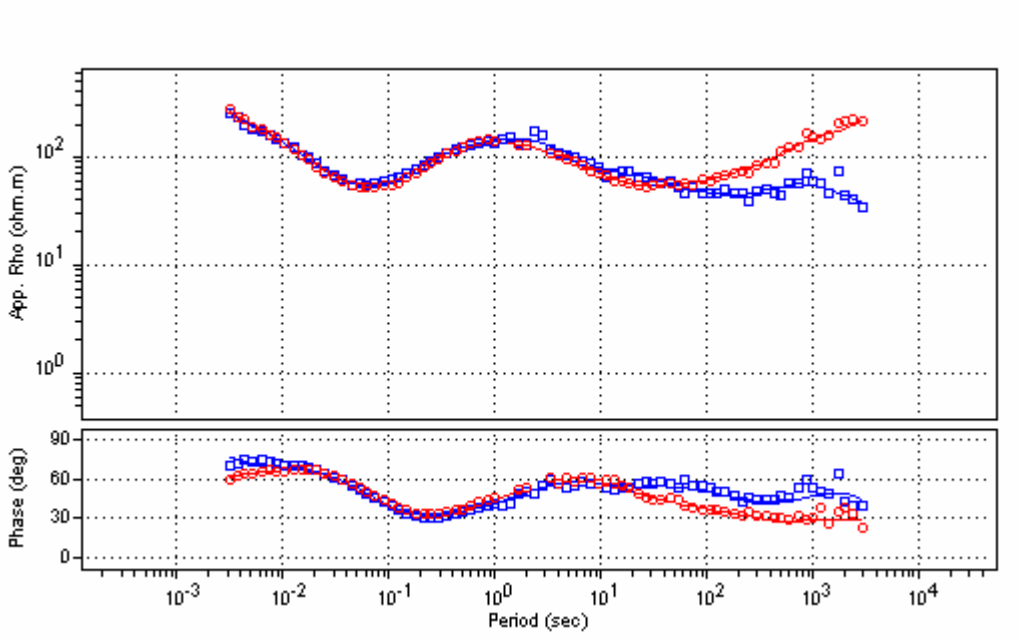

STL024

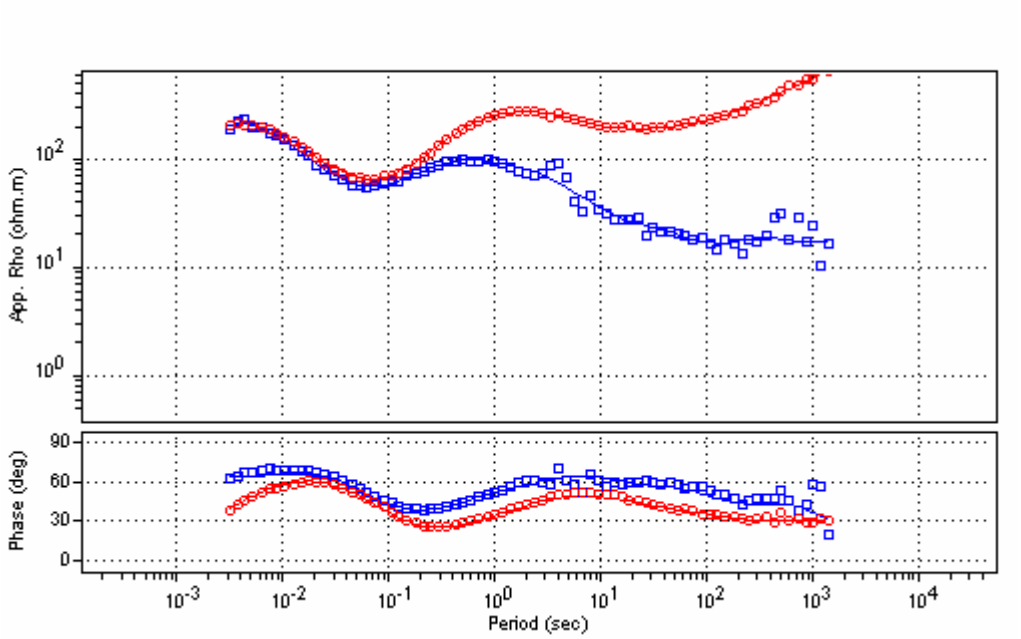

STL025

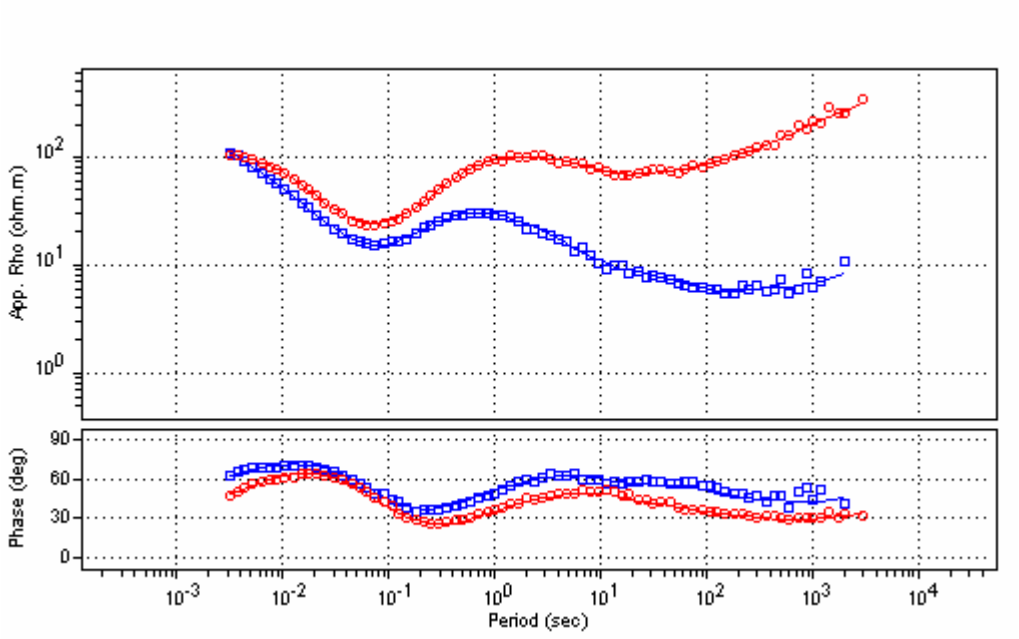

STL026

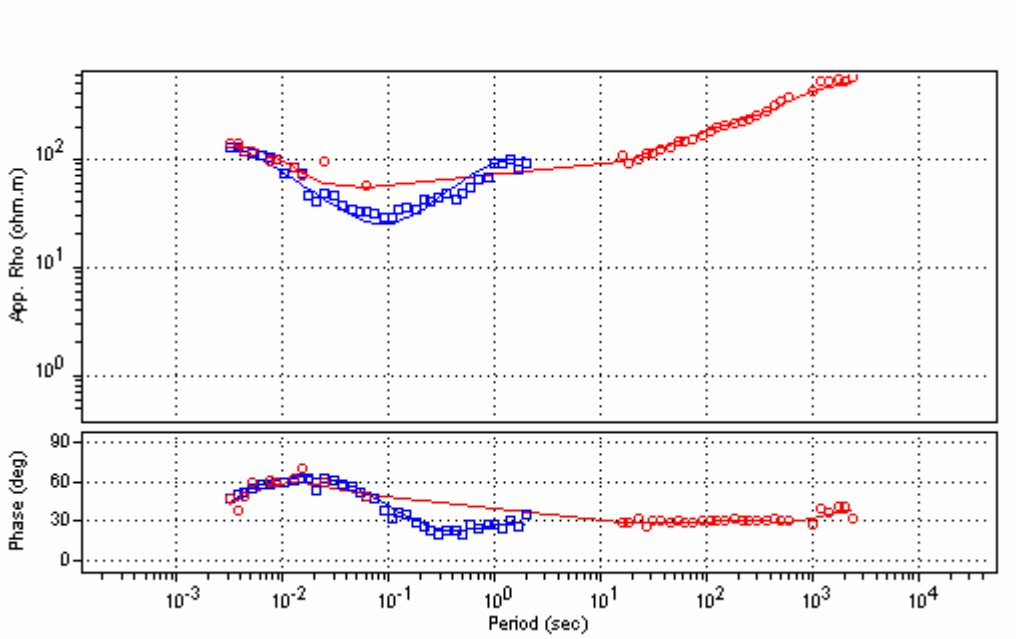

STL027

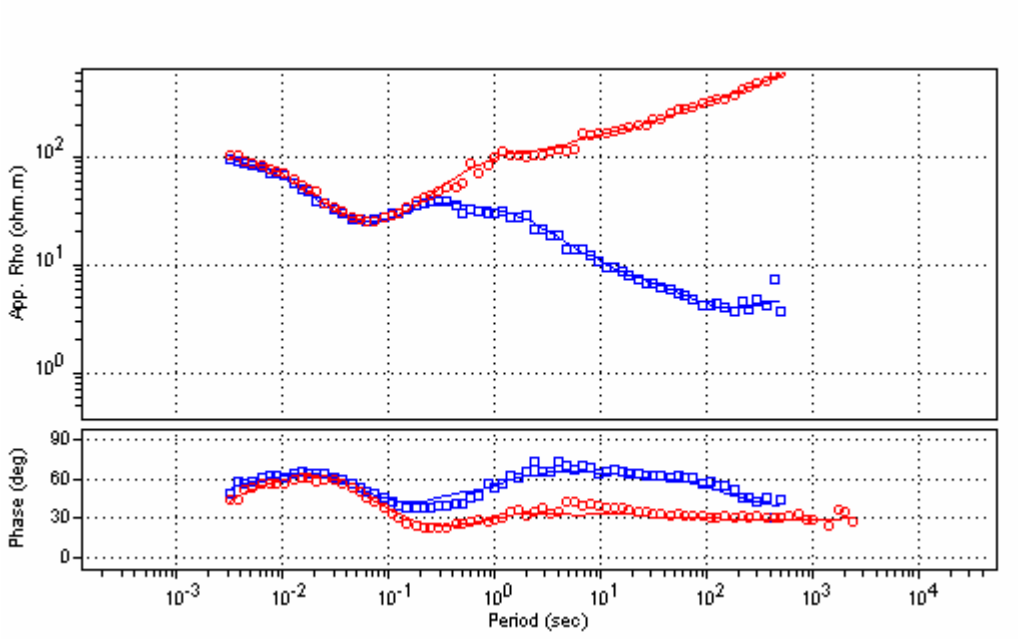

STL028

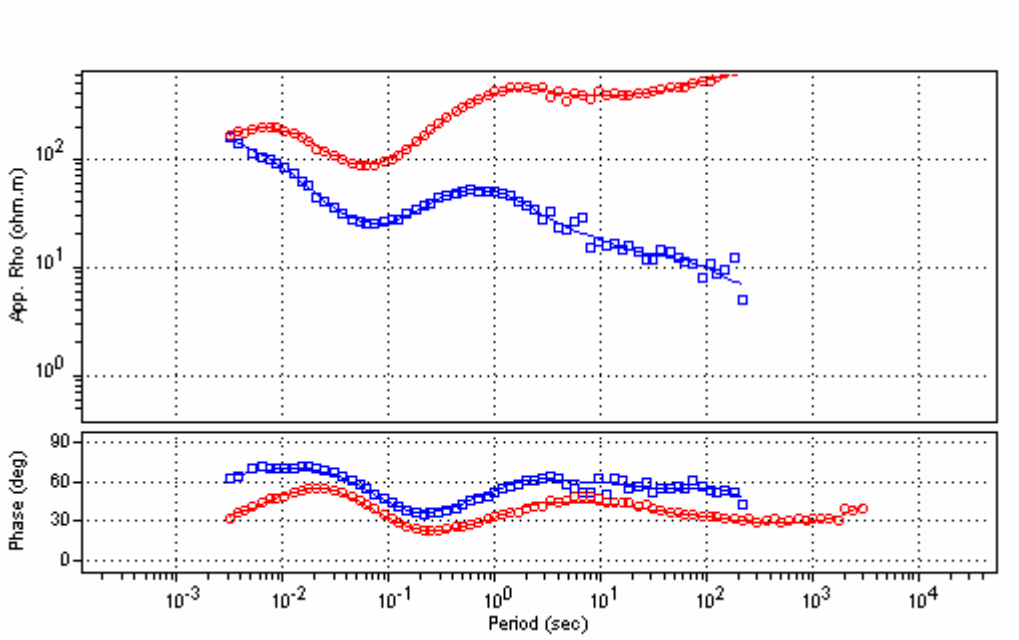

STL029

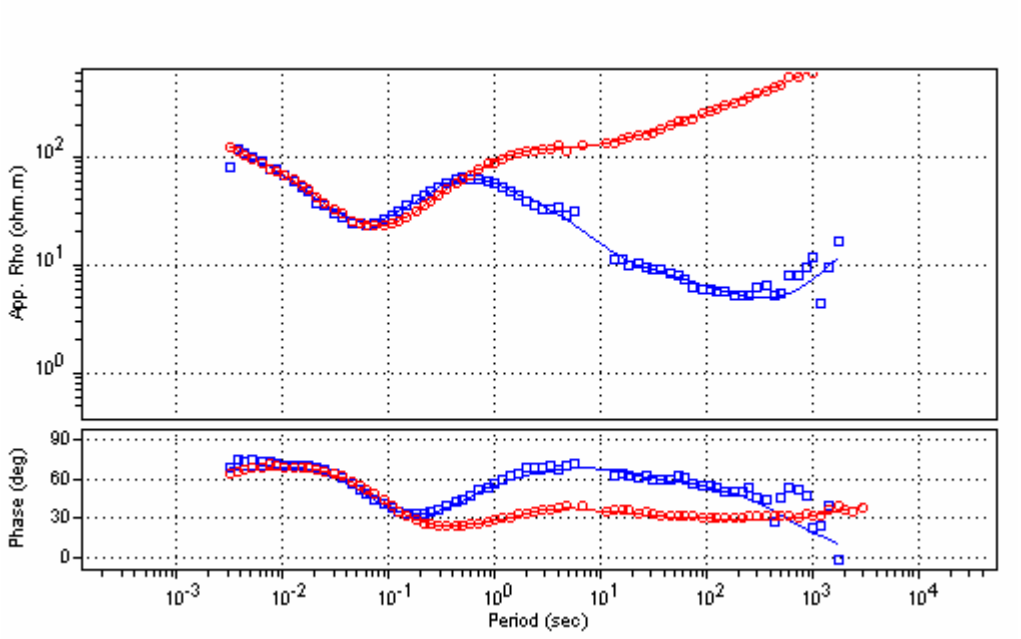

STL030

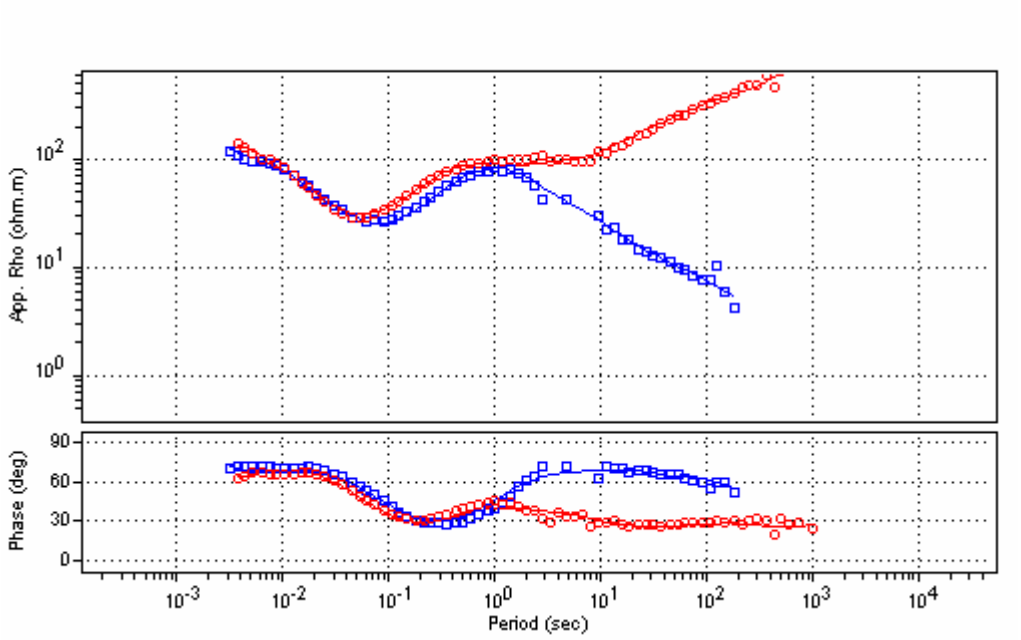

STL031

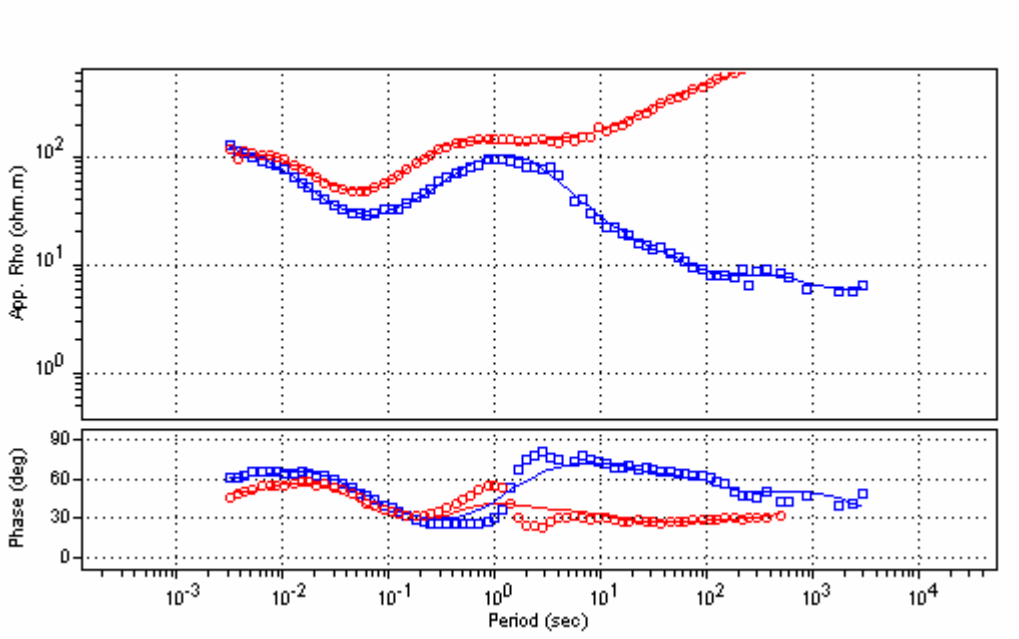

STL032

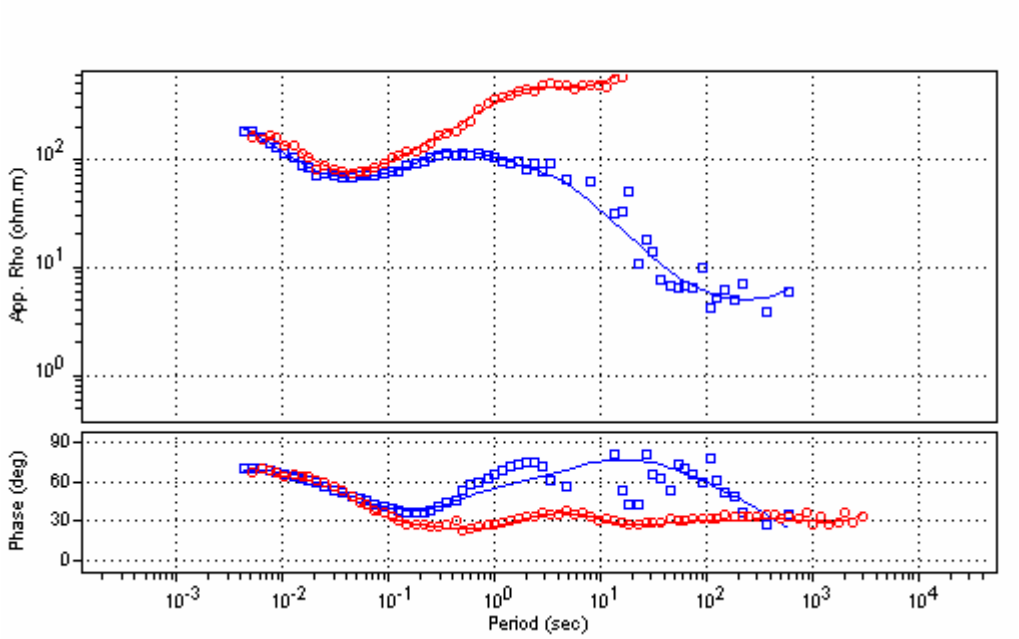

STL033

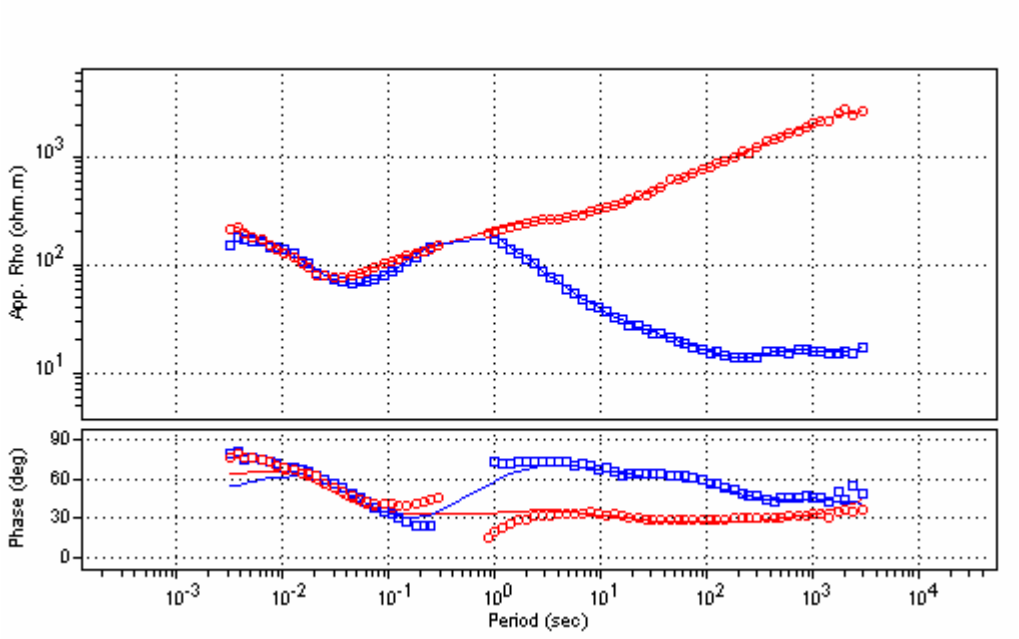

STL034

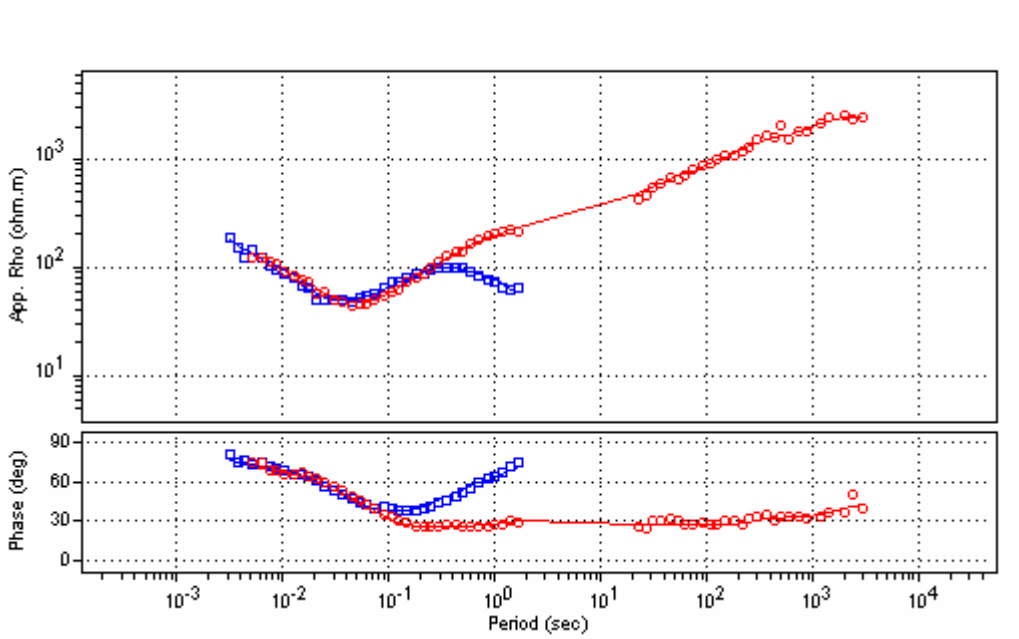

STL035

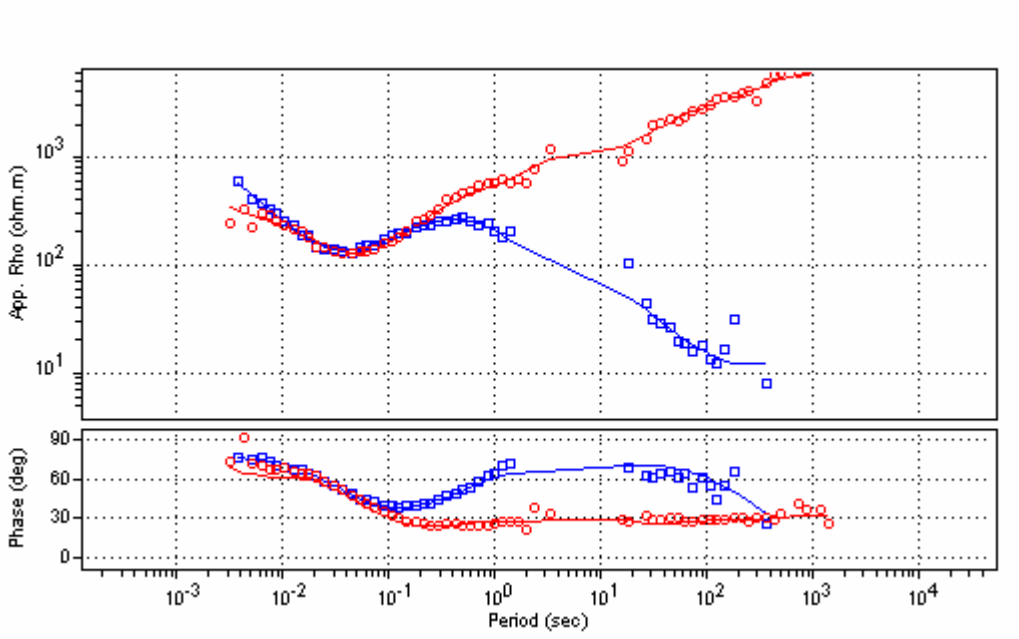

STL036

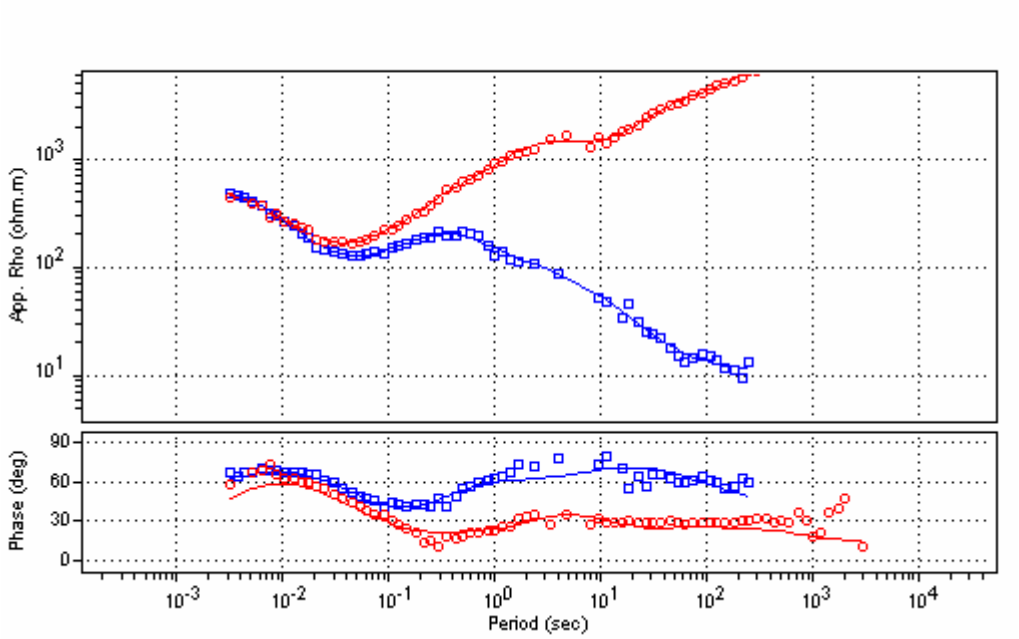

STL037

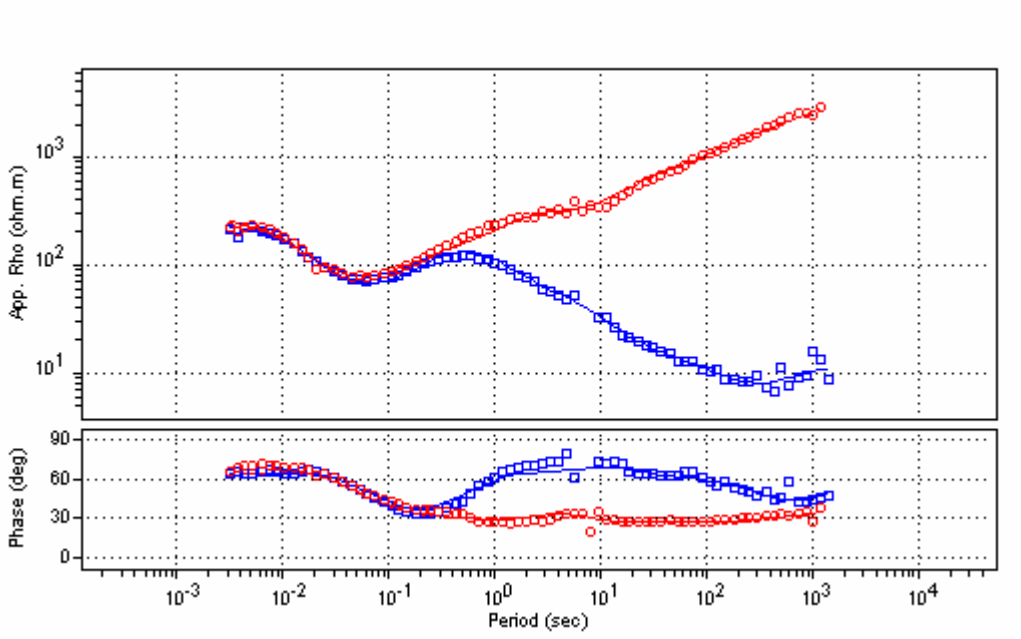

STL038

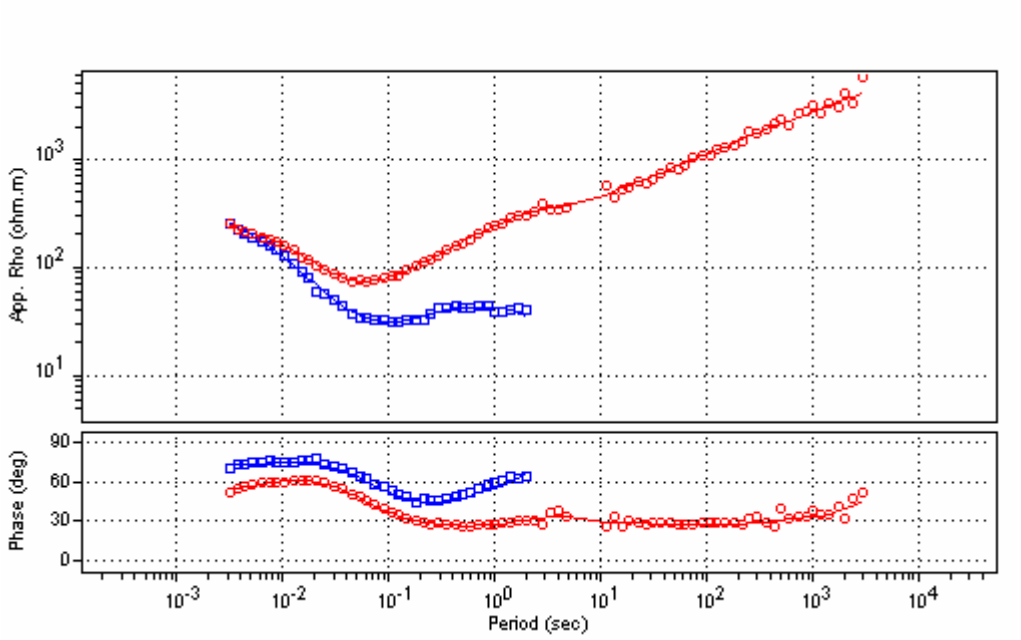

STL039

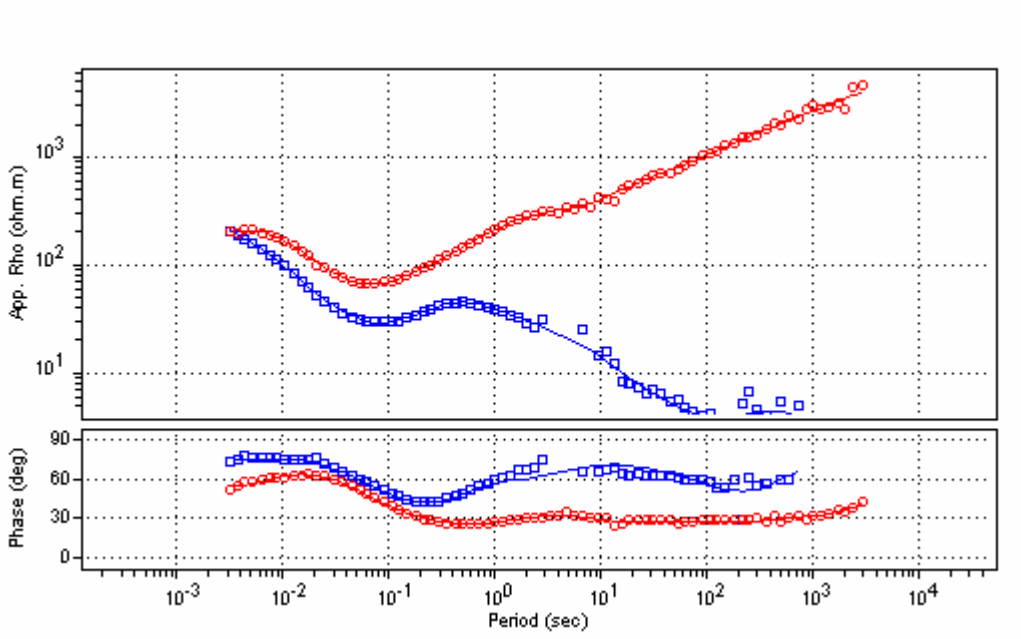

STL040

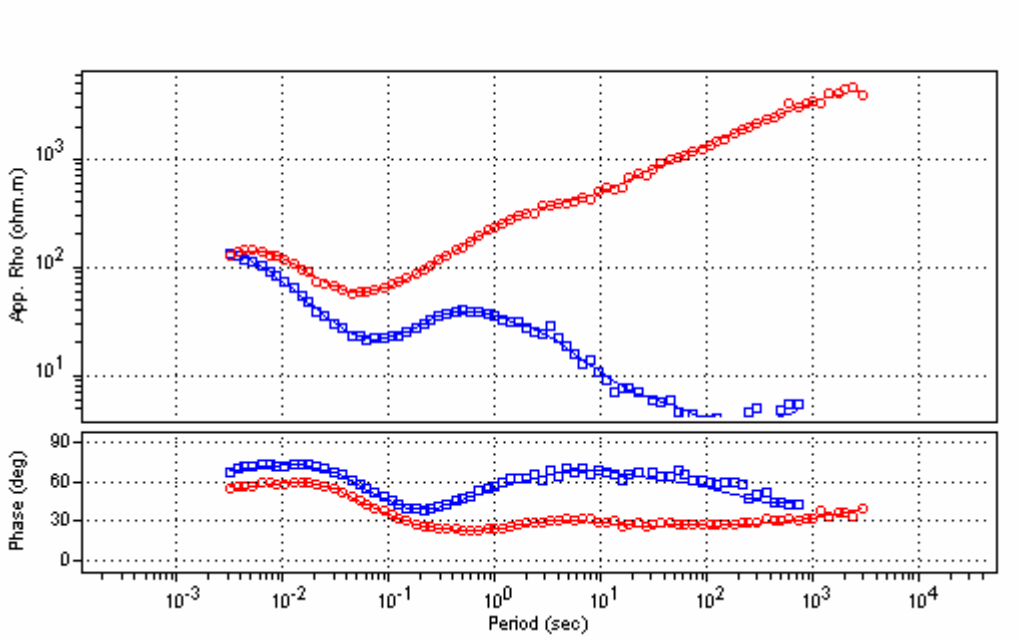

STL041

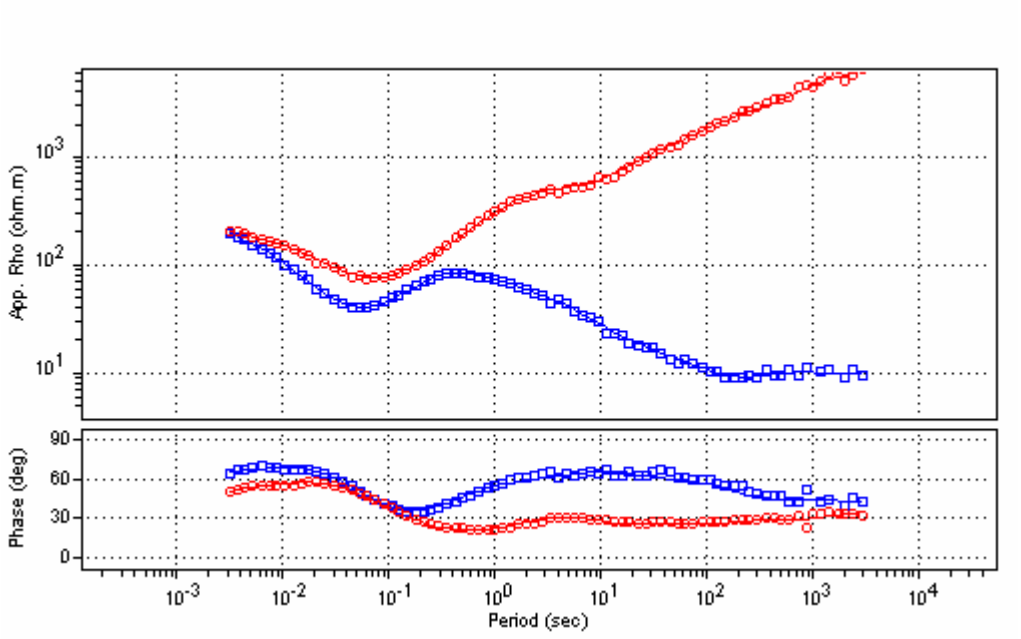

STL042

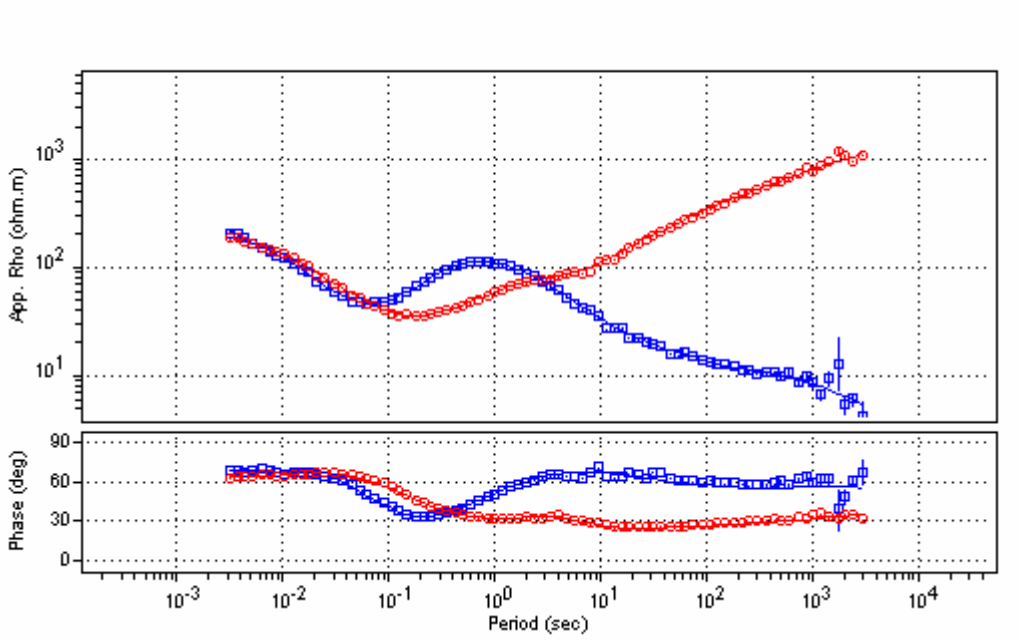

STL043

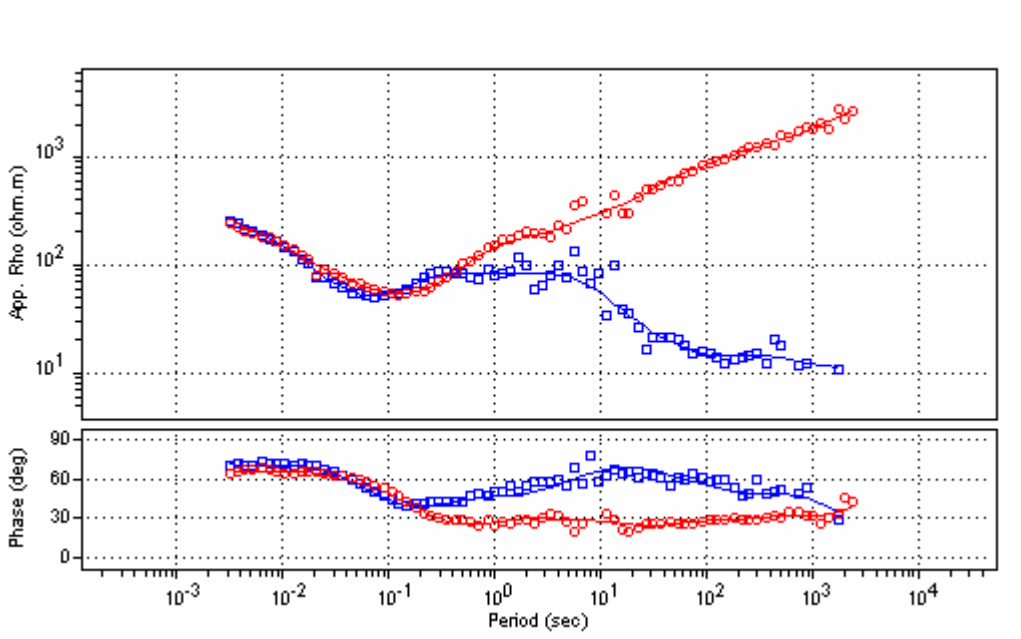

STL044

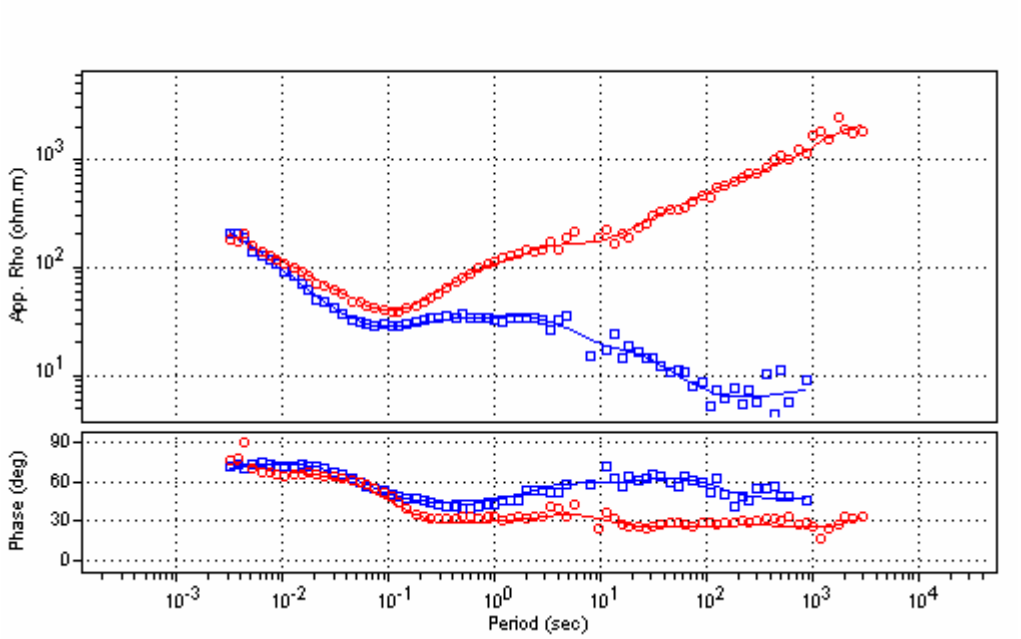

STL045

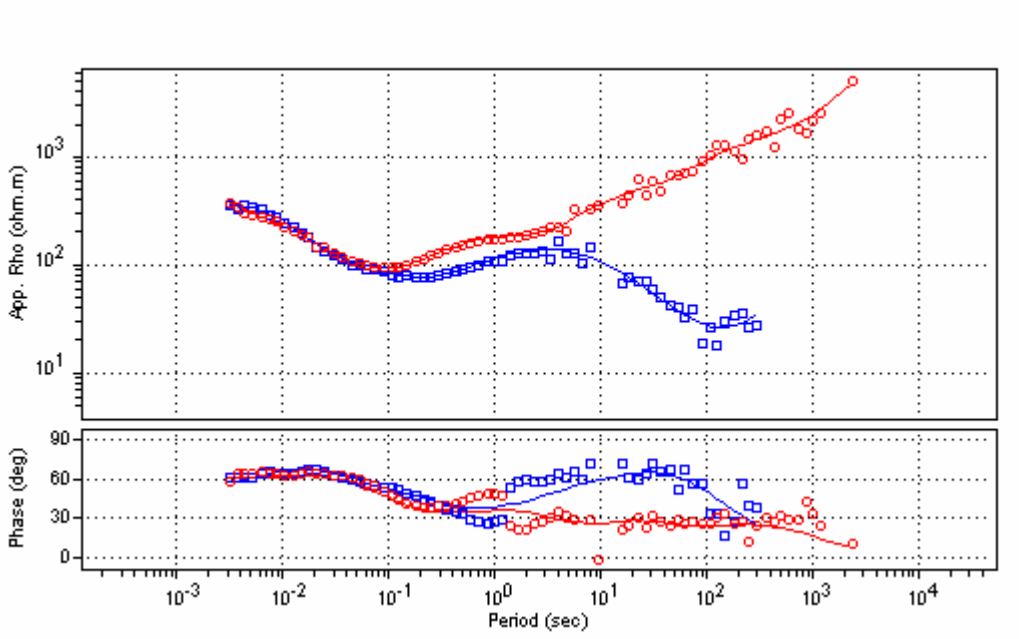

STL046

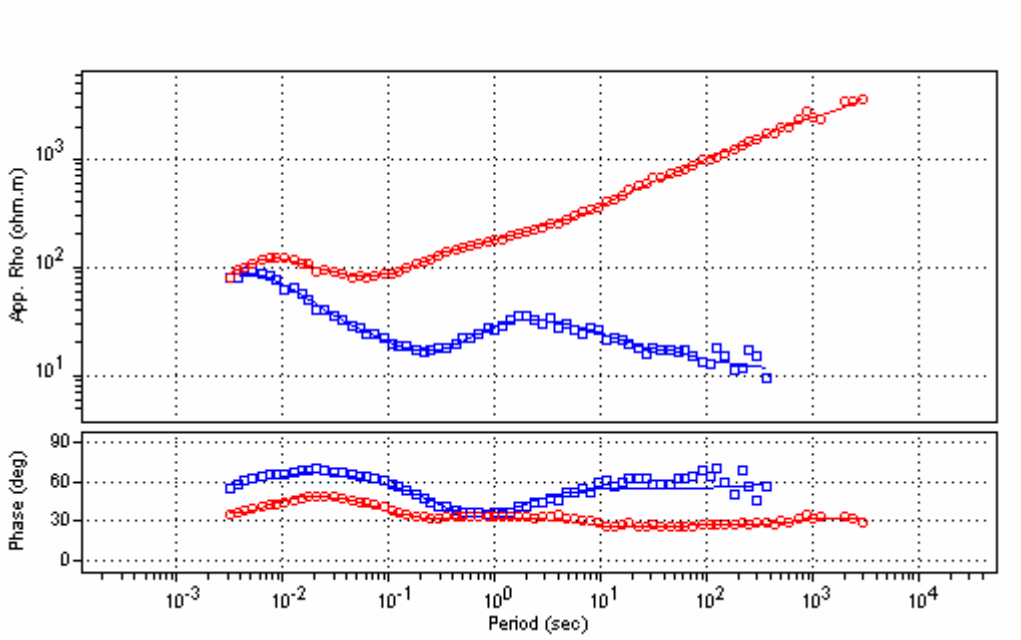

STL047

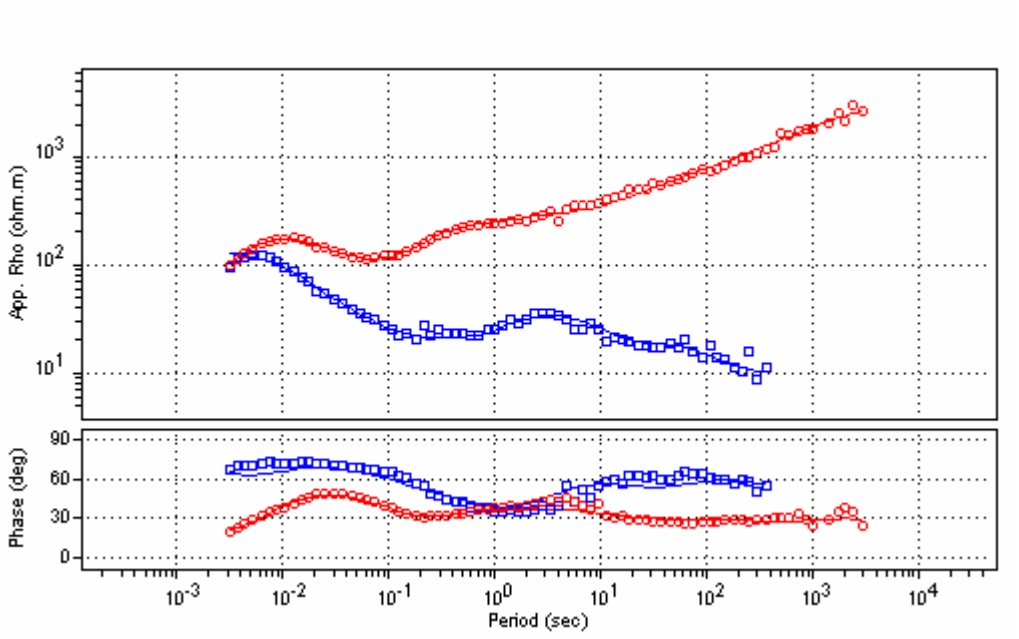

STL048

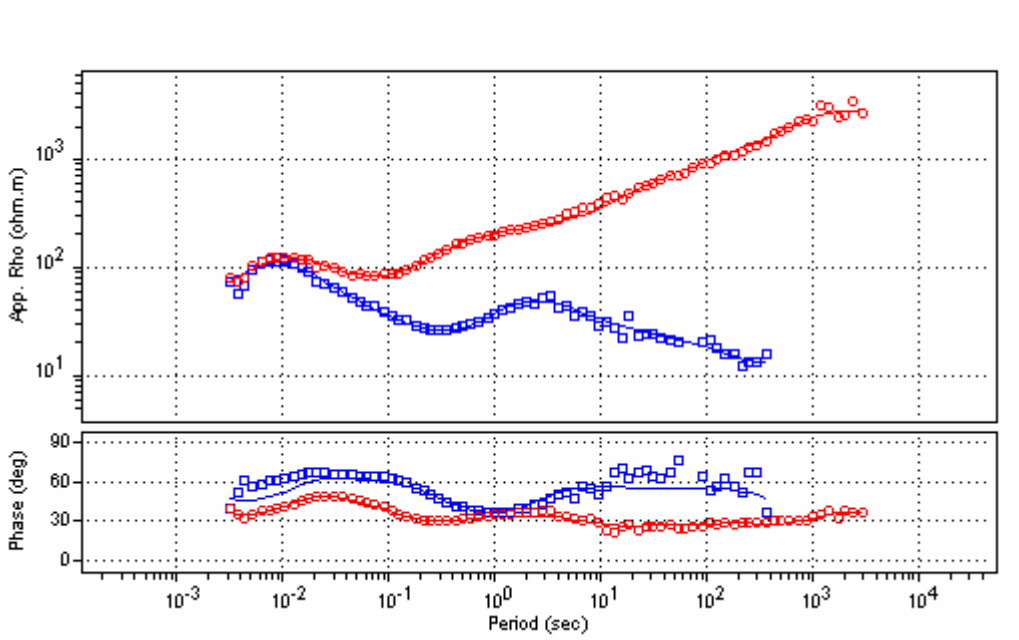

STL049

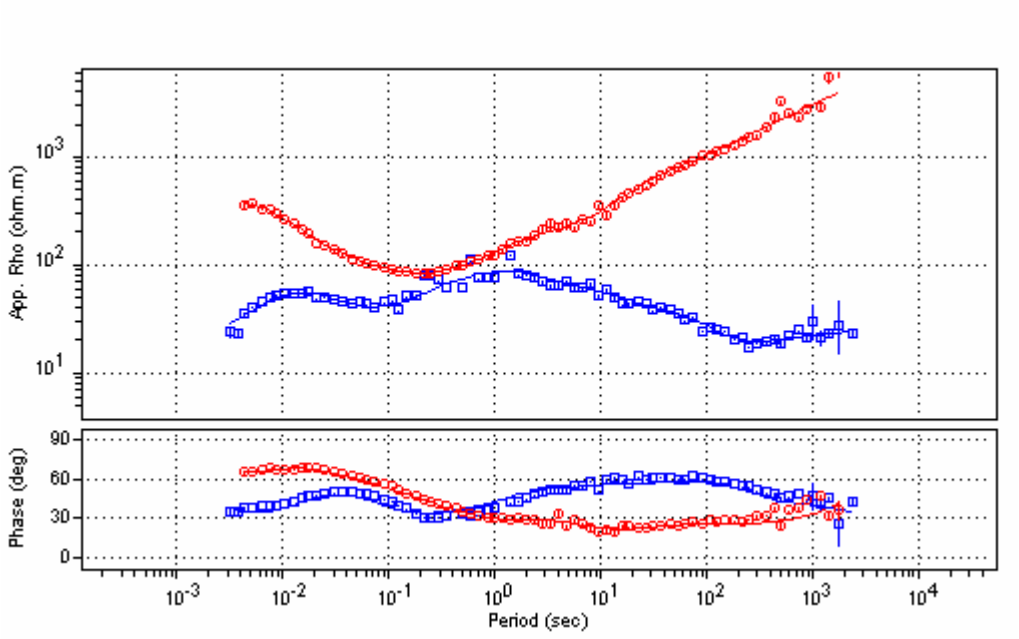

STL050

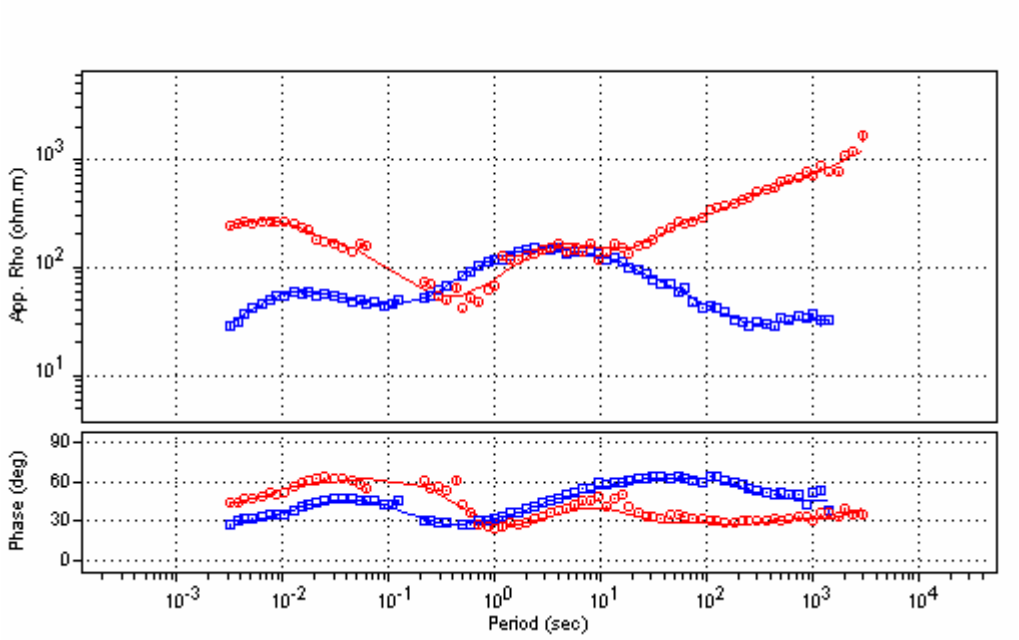

STL051

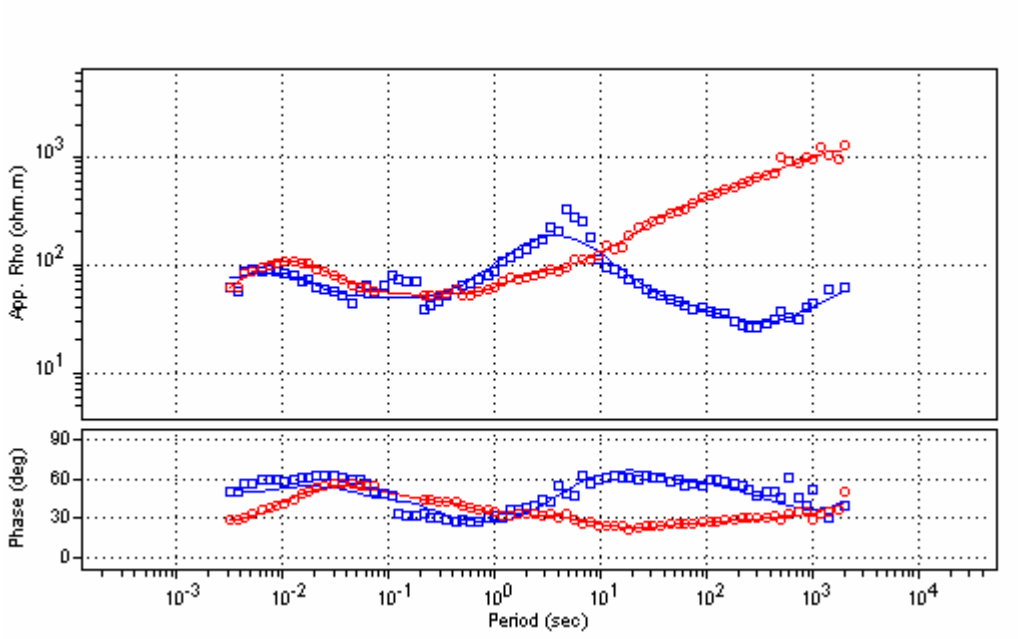

STL052

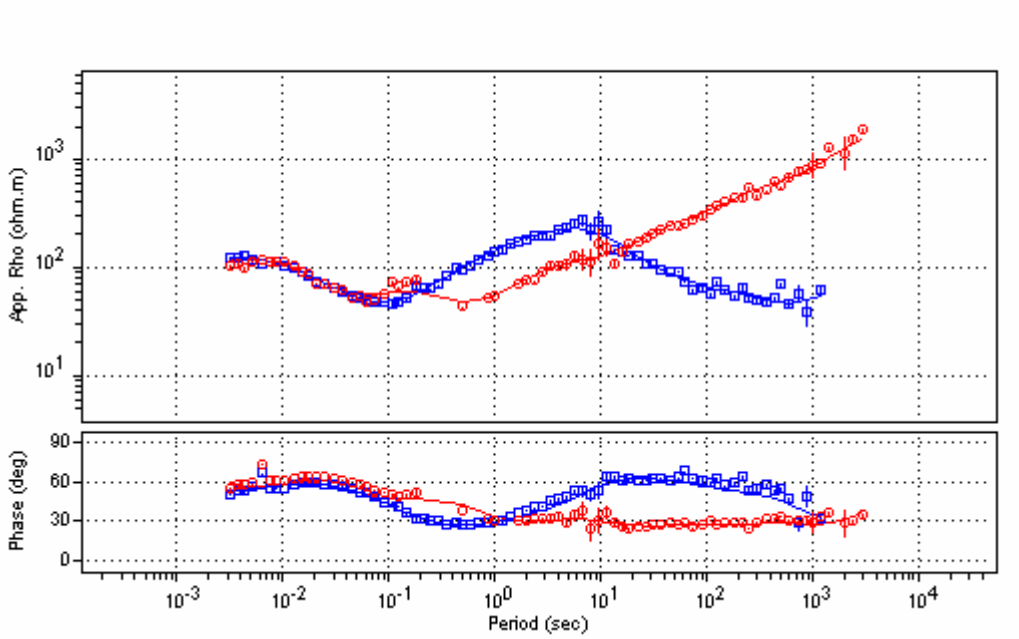

STL053

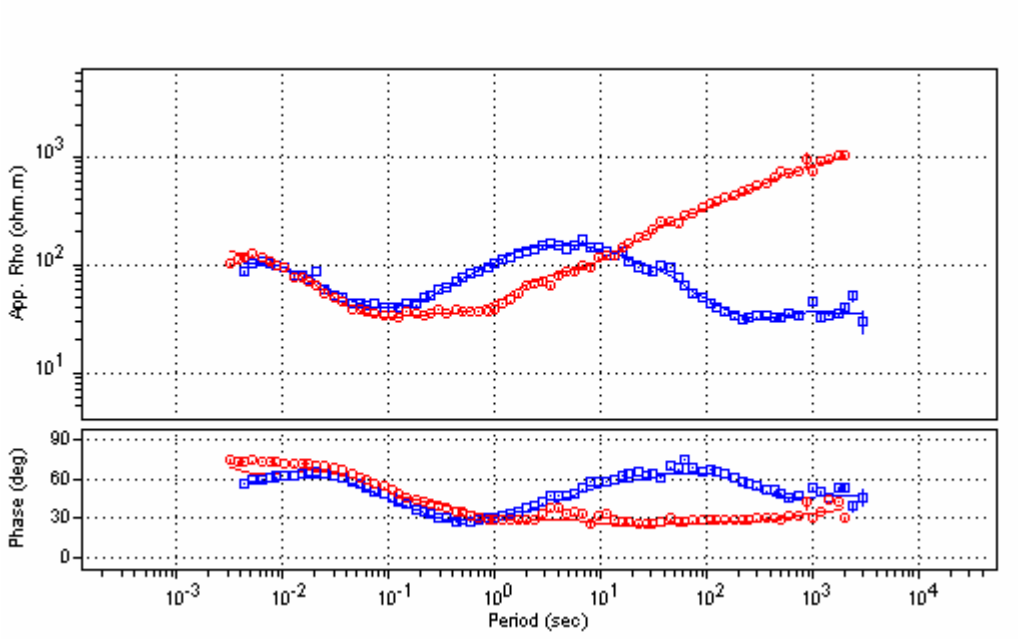

STL054

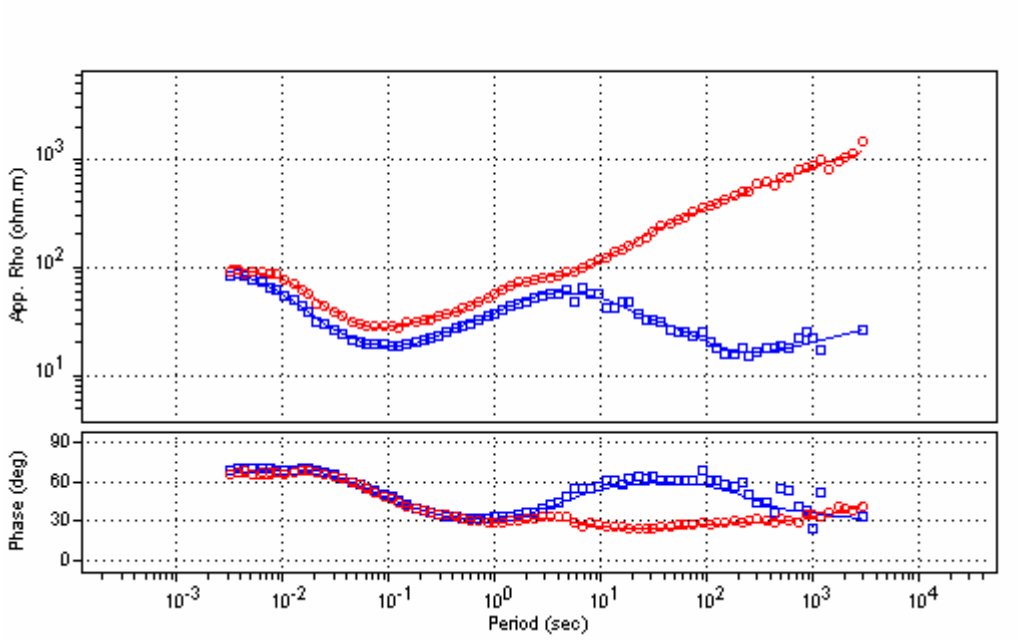

STL055

Appendix 2

Apparent resistivity and phase data obtained by 2D inversion of TE and TM data using the 1D-constrained a priori model. Symbols are experimental smoothed data, curves are computed data.